MINIMUM IMPULSE THREE-BODY TRAJECTORIES

by

LOUIS ANTHONY D'AMARIO

S. B., Rensselaer Polytechnic Institute (1968)
S. M., Massachusetts Institute of Technology (1970)

SUBMITTED IN PARTIAL FULFILLMENT
OF THE REQUIREMENTS FOR THE
DEGREE OF DOCTOR OF PHILOSOPHY
at the
MASSACHUSETTS INSTITUTE OF TECHNOLOGY
June, 1973

Signature of Author: _____
Department of Aeronautics and Astronautics, May 8, 1973

Certified by: _____
Thesis Supervisor

Certified by: _____
Thesis Supervisor

Certified by: _____
Thesis Supervisor

Certified by: _____
Thesis Supervisor

Accepted by: _____
Chairman, Departmental Graduate Committee

MINIMUM IMPULSE THREE-BODY TRAJECTORIES

by

Louis Anthony D'Amario

Submitted to the Department of Aeronautics and Astronautics on May 8, 1973 in partial fulfillment of the requirements for the Degree of Doctor of Philosophy.

Abstract

A rapid and accurate method of calculating optimal impulsive transfers in the restricted problem of three bodies has been developed. The technique combines a multi-conic method of trajectory integration with primer vector theory and an accelerated gradient method of trajectory optimization. A unique feature is that the state transition matrix and the primer vector are found analytically without additional integrations or differentiations. The method has been applied to the determination of optimal two- and three-impulse transfers between the L_2 libration point and circular orbits about both the Earth and the Moon.

A general error analysis of three multi-conic methods of three-body trajectory integration has been carried out. Single-step error functions for position and velocity have been derived as Taylor series in powers of the time step and also in integral form. These error functions are used to investigate the relative accuracy of the three methods in various regions of the Earth-Moon space and to provide a method of variable step-size control for the trajectory integration procedure. Numerical results are used to compare the multi-step performance of the methods for both large and small step sizes.

Thesis Supervisor: John J. Deyst, Jr., Sc. D.
Title: Associate Professor of Aeronautics and Astronautics

Thesis Supervisor: Theodore N. Edelbaum, S. M.
Title: Deputy Associate Director, Charles Stark Draper Laboratory

Thesis Supervisor: Robert G. Stern, Ph. D.
Title: Lecturer, Department of Aeronautics and Astronautics

Thesis Supervisor: James E. Potter, Ph. D.
Title: Associate Professor of Aeronautics and Astronautics

ACKNOWLEDGEMENT

The author would like first to thank Mr. Theodore Edelbaum for suggesting the topic of this thesis, for acting as the principal thesis advisor, and especially for always being available for many helpful discussions. His overall guidance throughout the period of the author's research was invaluable.

The author would also like to express his appreciation to the other members of his doctoral committee: to Professor John Deyst for serving as the chairman, and to Professor James Potter and Doctor Robert Stern for their many helpful suggestions and criticisms.

In addition the author wishes to thank Robert Farquhar and Vearl Huff for their support and active interest in this research, and David Jacobson, Jason Speyer, Saul Serben and especially Chung Pu for many helpful discussions.

Finally, thanks go to the author's fellow students, Harold Jones and Stephen Synnott, and to the author's roommate, Reginald Murphy, for providing much needed moral support, and also to Beth Hwoschinsky for typing the final copy of this thesis.

There were also many other people, too numerous to mention, at the Charles Stark Draper Laboratory, Inc. whose contributions deserve recognition. During his thesis research the author was a Research Assistant in the Control and Flight Dynamics Division of the Charles Stark Draper Laboratory, Inc.

This research was supported by DSR Project 56-40024, sponsored by the Goddard Space Flight Center, National Aeronautics and Space Administration through Grant NGR 22-009-207, Supplements 5 and 7.

The publication of this thesis does not constitute approval by the National Aeronautics and Space Administration of the findings or conclusions contained therein. It is published only for the exchange and stimulation of ideas.

TABLE OF CONTENTS

List of Symbols

a	gravitational parameter of the Moon
a	semi-major axis
a_n	coefficients in the power series for f (Equation D.10)
$\bar{a}$	thrust acceleration vector
A	gravitational parameter of the Earth
A	3x3 matrix defined by Equation (4.3)
b_n	coefficients in the power series for g (Equation D.11)
B, C, D,	3x3 matrices defined by Equations (3.71), (3.72), and (3.73)
c	exhaust velocity
δc	magnitude of the small impulse added to a reference two-impulse solution to form a three-impulse solution
$\bar{c}_f$	vector defined by Equation (7.18)
C	Jacobi constant
e	natural logarithm base
e	eccentricity
$\bar{e}$	error vector for Lambert problem iteration; defined by Equation (3.69)
f, f_t	functions associated with the solution to the two-body Kepler problem; defined by Equations (D.10) and (D.12)
g, g_t	functions associated with the solution to the two-body Kepler problem; defined by Equations (D.11) and (D.13)
$\bar{g}$	general gravitational acceleration vector
$\bar{g}_A$	geocentric two-body acceleration vector
$\bar{g}_a$	selenocentric two-body acceleration vector
$\delta\bar{g}_A$	geocentric disturbing acceleration vector
$\delta\bar{g}_a$	selenocentric disturbing acceleration vector
G	general gravity gradient matrix
h	step-size in a trajectory propagation
$\bar{h}$	angular momentum vector
H	Hamiltonian function

i	inclination
I	3x3 identify matrix
J	cost function
δJ	difference in cost between neighboring two- and three-impulse trajectories
δJ	variation in the cost produced by variations in Ω_f and θ_f
k	parameter defined by Equation (6.27) or (6.31)
m_o	initial mass of the spacecraft
Δm	fuel consumed during an impulsive transfer
n	number of steps in a trajectory propagation
P	3x3 matrix defined by Equation (3.70)
$\bar{r}$	selenocentric position vector of the spacecraft
$\dot{\bar{r}}$	selenocentric velocity vector of the spacecraft
$\bar{r}_{IaF}$, $\dot{\bar{r}}_{IaF}$	position and velocity vectors obtained by propagating the state vector at t_I along a selenocentric conic to t_F
$\delta\bar{r}$	general variation of the position vector
$\delta\bar{r}_m$	perturbation of the position vector at t_m on a two-impulse trajectory used to form a three-impulse trajectory
$\delta\bar{r}_J$, $\delta\bar{r}_J^*$	difference between the three-body selenocentric position vector and a particular selenocentric conic position vector at t_J as defined in Equations (6.45) and (6.68)
$\bar{R}$	geocentric position vector of the spacecraft
$\dot{\bar{R}}$	geocentric velocity vector of the spacecraft
$\bar{R}_{FAI}$, $\dot{\bar{R}}_{FAI}$	position and velocity vectors obtained by propagating the state vector at t_F backward in time to t_I along a geocentric conic
$\delta\bar{R}_J$, $\delta\bar{R}_J^*$	difference between the three-body geocentric position vector and a particular geocentric conic position vector at t_J as defined in Equations (6.44) and (6.57)

$\delta\bar{R}_S$	single-step final position error of the Stumpff-Weiss method
$\delta\bar{R}_{em}$	single-step final position error of the Earth-Moon method
$\delta\bar{R}_{me}$	single-step final position error of the Moon-Earth method
$\delta\dot{\bar{R}}_S$	single-step final velocity error of the Stumpff-Weiss method
$\delta\bar{R}_{FAI}$	single-step error in $\bar{R}_{FAI}$
$\delta\dot{\bar{R}}_{FAI}$	single-step error in $\dot{\bar{R}}_{FAI}$
$\delta\bar{r}_{FaI}$	single-step error in $\bar{r}_{FaI}$
$\delta\dot{\bar{r}}_{FaI}$	single-step error in $\dot{\bar{r}}_{FaI}$
t	time
t_o	initial time for a complete trajectory
t_I	initial time of one trajectory propagation step
t_f	final time of a complete trajectory
t_F	final time of one trajectory propagation step
t_n	time at the end of the nth step of a trajectory propagation procedure
$\bar{u}$	unit vector in the direction of the thrust acceleration vector
$\bar{u}_h$	unit vector in the direction of the angular momentum vector
$\bar{u}_n$	unit vector in the direction of the ascending node
$\bar{u}_r$	unit vector in the direction of $\bar{r}$
$\bar{u}_R$	unit vector in the direction of $\bar{R}$
$\bar{u}_z$	unit vector in the direction of the z-axis, i.e., normal to the Earth-Moon plane in the direction of the Moon's angular momentum vector
U	potential function for the three-body problem
$\bar{v}$	selenocentric velocity vector
$\Delta\bar{v}$	velocity impulse vector
$\Delta\bar{v}_o$	change in $\bar{v}_o$ from one iteration to the next of a Lambert problem solution
$\delta\bar{v}$	general variation of the velocity vector

V	magnitude of the velocity vector in rotating barycentric coordinates
x, y, z	components of a position vector
$\dot{x}, \dot{y}, \dot{z}$	components of a velocity vector
X, Y, Z	rotating barycentric coordinate system
X, Y, Z	coordinate system defined by Figure 19
X_1, Y_1, Z_1	geocentric rotating coordinate system defined in Section 6.3
X_2, Y_2, Z_2	selenocentric inertial coordinate system used on Figure 3
α	gravitational parameter of the Earth-Moon system
$\overline{\alpha}$	vector defined by Equation (6.24)
$\overline{\beta}$	vector defined by Equation (6.25)
γ	departure angle from L_2; defined on Figure 6
$\overline{\eta}$	unit vector in the direction of the impulse added to a two-impulse reference trajectory to form a three-impulse trajectory
θ	argument of latitude
λ_Ω	adjoint variable for Ω
λ_θ	adjoint variable for θ
$\overline{\lambda}$	primer vector (adjoint vector for velocity)
$\dot{\overline{\lambda}}$	derivative of the primer vector
μ	ratio of the mass of the Moon to the sum of the masses of the Earth and Moon
μ_i	arbitrary constants used in Equations (7.10) and (7.11)
$\overline{\mu}$	adjoint vector for position
$\overline{\rho}$	geocentric position vector of the Moon
$\dot{\overline{\rho}}$	geocentric velocity vector of the Moon
φ	arrival angle defined by Figure 6
$\varphi_{11}, \varphi_{12}, \varphi_{21}, \varphi_{22}$	3x3 partitions of the 6x6 state transition matrix defined in Equation (2.10)
Φ	general 6x6 state transition matrix

Φ_{2B}^{a}	state transition matrix for a selenocentric two-body (conic) trajectory
Φ_{2B}^{A}	state transition matrix for a geocentric two-body (conic) trajectory
Φ_{3B}	state transition matrix for a three-body trajectory
Φ_{L}	state transition matrix for a linear (field-free) trajectory
ψ	constraint function
Ω	longitude of the ascending node

CHAPTER 1
INTRODUCTION

1.1 Historical Background

Almost all of the work done on space trajectory optimization to date has been concerned with two-body trajectory optimization. Most of the more than three hundred references in the Gobetz and Doll survey of impulsive trajectories[1] are concerned with inverse square fields. In fact, the organization of their survey is based entirely on the two-body problem.

For the two-body problem, both the trajectory and its state transition matrix can be calculated analytically. In spite of this, the determination of optimal trajectories is far from easy. Although there are several special cases for which analytic solutions are known, it is generally necessary to use numerical methods to optimize two-body trajectories. Effective techniques have been developed by combining primer vector theory with accelerated gradient techniques[2, 3, 4].

For the three-body problem, both the trajectory and its state transition matrix must be calculated numerically. Some analytic approximations have been used to represent lunar and interplanetary trajectories. Among the approximations are the patched conic method[5], and the method of matched asymptotic expansions[6, 7, 8]. Unfortunately, these methods have inherent accuracy limitations and break down completely for some missions of interest, such as trajectories to the collinear libration points[9, 10, 11] of a three-body problem.

Even numerical integration of the state and the transition matrix for the three-body problem presents difficulties because of the singularities at the center of each body. These difficultkes can be overcome by various regularizations of the differential equations[12] or by making the time step a function of the potential[10, 13]. Unfortunately, numerical integration is time-consuming. As a large number of trajectories and state transition matrices must be calculated in the process of converging to an optimal

trajectory, the computer time with this approach can easily become prohibitive.

Recently, a new approach to the integration of the N-body problem has been tried. This approach was conceived independently by several investigations[14, 15, 16] and actually constitutes a class of closely related methods known as the "multi'conic" methods.

One of the most fruitful points of view is to regard them as large step numerical integration formulas. Instead of being based on series, as are most convential numerical integration formulas, these methods are based on two-body conics.

The oldest of these methods is the "N-body reference orbit" of Stumpff and Weiss[14]. The N-body reference orbit is an analytic approximation to the true three-body trajectory. In their approach, two-body conics of each body with respect to each of the other bodies are used to evaluate the N-body integrals of the differential equations of motion. All the conics are propagated forward in time from the initial state. The method also utilizes field-free trajectories which go backward in time. Stumpff and Weiss also derived expressions for the deviations of the position and velocity of the N-body reference orbit from the true trajectory for a single time step. The position deviations are shown to be proportional to the fourth power of the time step and the velocity deviations to the third power. By using sufficiently small steps, these deviation errors can be kept so small that they can be neglected. The sufficiently small step size for acceptable truncation errors is still much larger than for conventional numerical integration. It is also possible to integrate numerically the differential equations for the deviations from the N-body reference orbit, as in an Encke method, and use large steps in the numerical integration. Stumpff and Weiss have shown that when only a single trajectory is being calculated, as in an initial value problem, it is more efficient to use larger steps and integrate the deviations. Weiss later showed[17] that if the deviations are neglected, then, since the position and velocity can be calculated analytically, the state transition matrix

along the N-body reference orbit may also be obtained analytically. This represents a very substantial savings in time since the state transition matrix is normally found by an integration of the six-by-six matrix of variational equations or by a numerical differentiation which requires the calculation of seven trajectories.

The other two methods were developed subsequently to calculate trajectories in the Earth-Moon space. Wilson[15] developed his method for the three-body problem and derived two alternate ways to calculate the trajectory depending upon whether the spacecraft is moving from the Earth to the Moon or vice-versa. The two-body conics used in this method are propagated from different starting points and are connected by linear field-free trajectories. In the N-body reference orbit of Stumpff and Weiss, the conics and the linear trajectories all start from the same point and thus are used in a parallel fashion, whereas in Wilson's method they are used in a sequential fashion each one starting where the previous one ended. Wilson did not show how the state transition matrix could be calculated nor did he derive expressions for the deviations from the actual three-body trajectory. Wilson then simplifies his basic method into what he calls the "pseudostate theory" which has better accuracy then the patched conic method with nearly the same computational effort. The multi-conic method of Byrnes and Hooper[16], which was conceived independently, is in effect an extension of Wilson's method to account for the effects of Earth oblateness and a fourth body, the Sun. However, both these effects are included in a linear manner. Both Wilson's method and the method of Byrnes and Hooper are designed for Earth-to-Moon trajectories and need some modification for other applications.

The most recent publication along these lines is a paper by Fang[18] in which the deviations of the Stumpff-Weiss N-body reference orbit are calculated as a Taylor series in powers of the time step under the assumption that the trajectory remains close to one of the bodies. The number of terms used in the Taylor series and the size of the time step are adjusted to maintain a maximum allowable error per step in position or velocity.

This thesis is the first attempt known to the author to apply the multi-conic approach to three-body trajectory optimization.

1.2 Thesis Objective

The objective of this thesis is to apply multi-conic methods of trajectory calculation, primer vector theory, and an accelerated gradient method of functional minimization to the determination of minimum impulse trajectories for the restricted problem of three bodies, and to perform an error analysis of these multi-conic methods in order to gain insights into their performance.

1.3 Synopsis

In Chapter 2 the trajectory optimization problem is described and the role of the primer vector in its solution is illustrated. It is shown that the primer vector can be calculated from a knowledge of the state transition matrix and that the primer vector is a useful tool for determining not only the optimality of a given trajectory, but also the way the cost of a non-optimal trajectory can be lowered. This Chapter is used primarily to introduce the primer vector and contains no new results.

In Chapter 3 it is shown that the N-body reference orbit of Stumpff and Weiss (specialized to three bodies) and Wilson's method are closely related members of a family of three-body trajectory integration formulas. Also, analytic expressions for the state transition matrix are derived for each method. Previously there existed no such expressions for Wilson's method. The usage of the multi-conic methods for the solution of initial and boundary value problems is described.

In Chapter 4, a multi-conic method similar to Wilson's, primer vector theory, and an accelerated gradient method of functional minimization are combined to provide a rapid and efficient method of calculating optimal three-impulse, three-body trajectories. The method readily extends to any number of impulses or bodies.

In Chapter 5 some results are presented for trajectories from the L_2 libration point on the far side of the Moon to circular orbits about both the Earth and the Moon.

In Chapter 6 a general error analysis of the multi-conic family of trajectory integration methods is performed, and expressions for the deviations of the approximations from the actual three-body trajectory for a single time step are developed, first as Taylor series in powers of the time step and then as a set of integrals. The first representation is used to find contours of constant errors in the Earth-Moon space, to find boundaries on which the error of any two methods are equal, and to provide a method of internal step-size control

In Chapter 7 the trajectory optimization method of Chapter 4 is modified to allow for a different set of end-point constraints by using transversality conditions on the primer vector.

In Chapter 8 the major conclusions drawn from the results of this thesis are summarized, and some suggestions for future research are listed.

CHAPTER 2
THE TRAJECTORY OPTIMIZATION PROBLEM

2.1 Necessary Conditions for an Optimal Transfer

In order to solve the classic trajectory optimization problem, the optimal number, location, direction, and magnitude of the velocity impulses must be determined such that the spacecraft transfers from a given initial position and velocity to a given final position and velocity in a fixed transfer time while minimizing the fuel consumption. The purpose of this section is to provide a heuristic derivation of the necessary conditions for an optimal transfer through application of the Maximum Principle. A rigorous derivation using the calculus of variations was performed by Lawden[19].

For a rocket engine having constant exhaust velocity but unbounded thrust magnitude, the amount of fuel consumed during a transfer is given by

$$\Delta m = m_o (1 - e^{-J/c}) \tag{2.1}$$

where m_o is the initial mass of the spacecraft, c is the exhaust velocity of the rocket, and

$$J = \int_{t_o}^{t_f} |\bar{a}| \, dt \tag{2.2}$$

where $\bar{a}$ is the thrust acceleration vector. The quantity J is known as the characteristic velocity. Minimizing J will minimize the fuel consumption since the fuel consumption is a monotonic function of J. The trajectory optimization problem may therefore be stated as an optimal control problem in which J is the cost function and the thrust acceleration vector, $\bar{a}$, is the control variable.

The state equations may be written as

$$\dot{\bar{r}} = \bar{v} \tag{2.3}$$

$$\dot{\bar{v}} = \bar{g}\,(\bar{r},\ t) + \bar{a} \tag{2.4}$$

where $\bar{r}$ and $\bar{v}$ are the position and velocity vectors, respectively, $\bar{g}$ is the gravitational acceleration vector, and $\bar{a}$ is the thrust acceleration vector. The Hamiltonian for this optimal control problem is

$$H = (\bar{\lambda}^T \bar{u} - 1)\, a + \bar{\mu}^T \bar{v} + \bar{\lambda}^T \bar{g} \tag{2.5}$$

where $\bar{\mu}$ is the adjoint vector for position, $\bar{\lambda}$ is the adjoint vector for velocity, and $\bar{u}$ is a unit vector in the direction of the thrust. The differential equations for the adjoint vectors are

$$\dot{\bar{\mu}} = - G \bar{\lambda} \tag{2.6}$$

$$\dot{\bar{\lambda}} = - \bar{\mu} \tag{2.7}$$

where $G = \partial \bar{g} / \partial \bar{r}$ is the gravity gradient matrix. According to the Maximum Principle, the Hamiltonian is maximized over all possible directions of the control by choosing

$$\bar{u} = \frac{\bar{\lambda}}{\lambda} \tag{2.8}$$

Furthermore, for $\lambda<1$ the Hamiltonian is maximized by choosing $a = 0$, and for $\lambda>1$ the Hamiltonian is maximized by choosing a to be infinite. An infinite a can be handled as a mathematical concept because it occurs only in the form of an impulse and therefore produces a finite change in velocity. Thus for an optimal trajectory, whenever $\lambda<1$, the spacecraft coasts, and whenever $\lambda=1$ instantaneously, an impulse occurs in the direction of $\bar{\lambda}$. Singular arcs for which $\lambda=1$ for a finite time are not considered.

These necessary conditions for the optimality of an impulsive trajectory were first formulated by Lawden[19] and are stated in terms

of $\bar{\lambda}$, the adjoint vector for velocity, which Lawden calls the "primer vector". The four necessary conditions are:

1. the primer vector and its first derivative are everywhere continuous;
2. whenever an impulse occurs, the primer vector is aligned with the impulse and has unit magnitude;
3. the primer vector magnitude may not exceed unity on a coasting arc;
4. the time derivative of the primer vector magnitude is zero at all interior junction points separating coasting arcs.

Figure 1 shows some typical time histories of the primer vector magnitude. Figure 1(a) shows a primer history for an optimal two-impulse trajectory. This primer history satisfies all the necessary conditions. Figures 1(b) and (c) show non-optimal two-impulse primer histories for which the primer magnitude rises above unity during coast. Figure 1(d) shows a non-optimal three-impulse primer history. The derivative of the primer magnitude at the interior impulse point is not continuous. Figure 1(e) shows an optimal three-impulse primer history which satisfies all the necessary conditions.

2.2 Calculation of the Primer Vector

The differential equations of the adjoint vectors, Equations (2.6) and (2.7), may be combined to yield

$$\ddot{\bar{\lambda}} = G\bar{\lambda} \tag{2.9}$$

Hence, the primer vector satisfies the same differential equations as do small variations in the state from a reference solution. The transition matrix for $(\bar{\lambda}, \dot{\bar{\lambda}})$ will therefore be identical to the state transition matrix. If the state transition matrix is defined as

$$\Phi(t, t_o) = \begin{bmatrix} \varphi_{11}(t, t_o) & \varphi_{12}(t, t_o) \\ \varphi_{21}(t, t_o) & \varphi_{22}(t, t_o) \end{bmatrix} \tag{2.10}$$

FIG. 1 TYPICAL PRIMER VECTOR HISTORIES

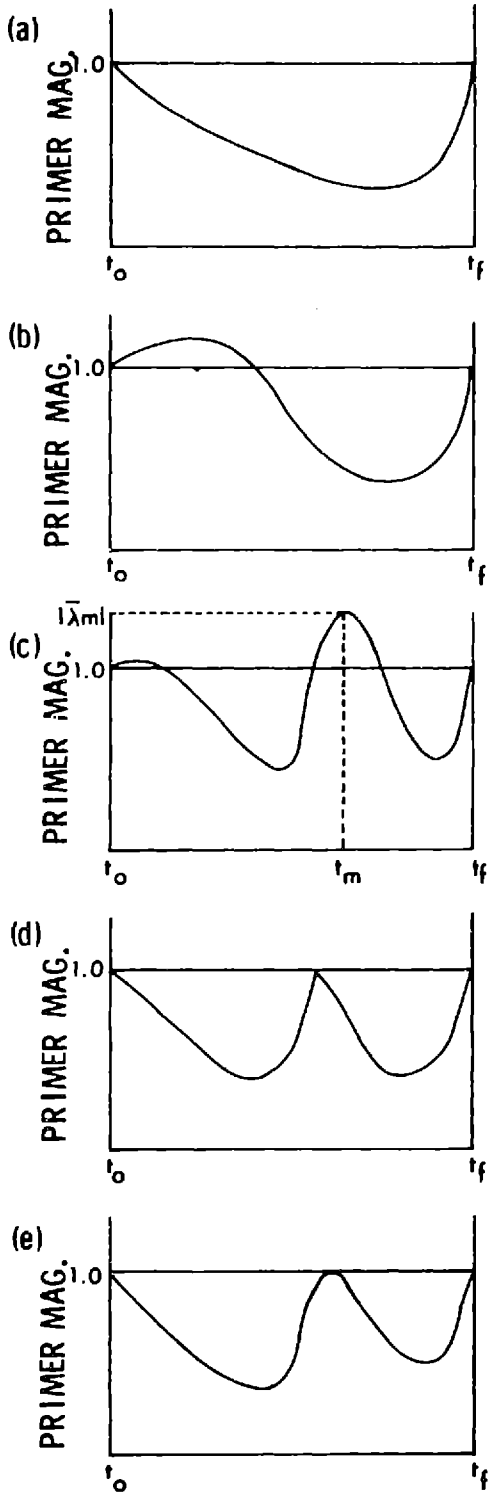

OPTIMAL TWO-IMPULSE PRIMER HISTORY

NON-OPTIMAL TWO-IMPULSE PRIMER HISTORY

NON-OPTIMAL TWO-IMPULSE PRIMER HISTORY

NON-OPTIMAL THREE-IMPULSE PRIMER HISTORY

OPTIMAL THREE-IMPULSE PRIMER HISTORY

then it follows that

$$\bar{\lambda}(t) = \varphi_{11}(t, t_o)\,\bar{\lambda}_0 + \varphi_{12}(t, t_o)\,\dot{\bar{\lambda}}_0 \tag{2.11}$$

$$\dot{\bar{\lambda}}(t) = \varphi_{21}(t, t_o)\,\bar{\lambda}_0 + \varphi_{22}(t, t_o)\,\dot{\bar{\lambda}}_0 \tag{2.12}$$

In order to generate a time history of the primer vector and its derivative, $\bar{\lambda}_0$, $\dot{\bar{\lambda}}_0$, and $\Phi(t, t_o)$ must be known. According to the necessary conditions, on any two-impulse trajectory (or any two-impulse segment of an n-impulse trajectory) the primer vector must have unit magnitude and point in the direction of the impulse at both impulse points. It follows that the primer vector must have the following boundary conditions:

$$\bar{\lambda}(t_o) = \bar{\lambda}_0 = \frac{\Delta\bar{v}_o}{|\Delta\bar{v}_o|} \tag{2.13}$$

$$\bar{\lambda}(t_f) = \bar{\lambda}_f = \frac{\Delta\bar{v}_f}{|\Delta\bar{v}_f|} \tag{2.14}$$

where $\Delta\bar{v}_o$ and $\Delta\bar{v}_f$ are the impulses at the initial and final times respectively. Evaluating Equation (2.11) at the final time, the initial value of the primer derivative is obtained as

$$\dot{\bar{\lambda}}_0 = \varphi_{12}^{-1}(t_f, t_o)\left[\bar{\lambda}_f - \varphi_{11}(t_f, t_o)\,\bar{\lambda}_0\right] \tag{2.15}$$

Therefore, with $\bar{\lambda}_0$ given by Equation (2.13), $\dot{\bar{\lambda}}_0$ given by Equation (2.15), and $\Phi(t, t_o)$ obtained from the trajectory calculation, a primer history can be generated for each two-impulse segment according to Equations (2.11) and (2.12)

2.3 Improvement of Non-Optimal Transfers

If the primer history of a given trajectory does not satisfy the necessary conditions, then that trajectory is not locally optimal. However, Lion and Handelsman have shown[2] that primer histories of non-optimal

transfers are very useful in that they show how the cost of these non-optimal transfers can be improved. Trajectories with primer histories like that of Figure 1(b) can be improved by an initial coast. That is, if the magnitude of the primer vector rises above unity immediately after the initial impulse, the cost can be reduced by delaying the first impulse until some time after t_o. Similarly if the magnitude of the primer vector is above unity immediately prior to the final impulse, the cost can be reduced by a final coast. It was also shown that if the primer magnitude exceeded unity between the impulses as in Figure 1(c), the trajectory can be improved by adding a third impulse. Furthermore, the greatest reduction in cost occurs when the impulse is added at the time when the primer magnitude is maximum, i.e., at t_m, and in the direction of the primer vector at that time, i.e., in the direction of $\overline{\lambda}_m$. The actual trajectory optimization algorithm, which improves non-optimal trajectories by adding impulses and converging to a local minimum of the cost, will be thoroughly discussed in Chapter 4. The important points of this Chapter are that, first, primer vector theory is useful not only for determining the optimality of a trajectory but also for improving a non-optimal trajectory, and, secondly, a primer history may be generated from known boundary conditions and a knowledge of the state transition matrix.

Before the actual trajectory optimization method is described in Chapter 4, the multi-conic method of trajectory calculation is introduced in Chapter 3.

CHAPTER 3
MULTI-CONIC TRAJECTORY PROPAGATION

3.1 Calculation of Position and Velocity

The model for the Earth-Moon system used in this study is that of the restricted problem of three bodies. The third body, the spacecraft, is assumed to have a negligible mass so that it is affected by, but does not affect, the motion of the other two bodies. The two massive bodies, the Earth and Moon, move in circular orbits about their common barycenter. The multi-conic approximation will provide a solution to this problem useful as a state vector propagation algorithm which is much faster than numerical integration of the equations of motion yet is of comparable accuracy. In effect the multi-conic approximation is a numerical integration technique which uses very large step sizes and yields very good accuracy. The multi-conic approximation spans the range between the extremely fast but relatively inaccurate patched conic methods and the slow but very accurate numerical integration techniques. The multi-conic methods derived in this Section will be valid for any three-body system in which the mass of one of the bodies is negligible.

The geometry of the three-body problem is illustrated in Figure 2. If the only forces acting are the central force fields of the Earth and the Moon, and the mass of the spacecraft is negligible, the accelerations are

$$\ddot{\bar{R}} = -A\frac{\bar{R}}{R^3} - a\frac{\bar{r}}{r^3} - a\frac{\bar{\rho}}{\rho^3} \tag{3.1}$$

$$\ddot{\bar{r}} = -a\frac{\bar{r}}{r^3} - A\frac{\bar{R}}{R^3} + A\frac{\bar{\rho}}{\rho^3} \tag{3.2}$$

$$\ddot{\bar{\rho}} = -\alpha\frac{\bar{\rho}}{\rho^3} \tag{3.3}$$

where A and a are the gravitational parameters of the Earth and Moon respectively and $\alpha = A + a$. The positions and velocities of the three bodies at any time t_J are related by

Fig. 2
GEOMETRY OF THE RESTRICTED THREE-BODY PROBLEM

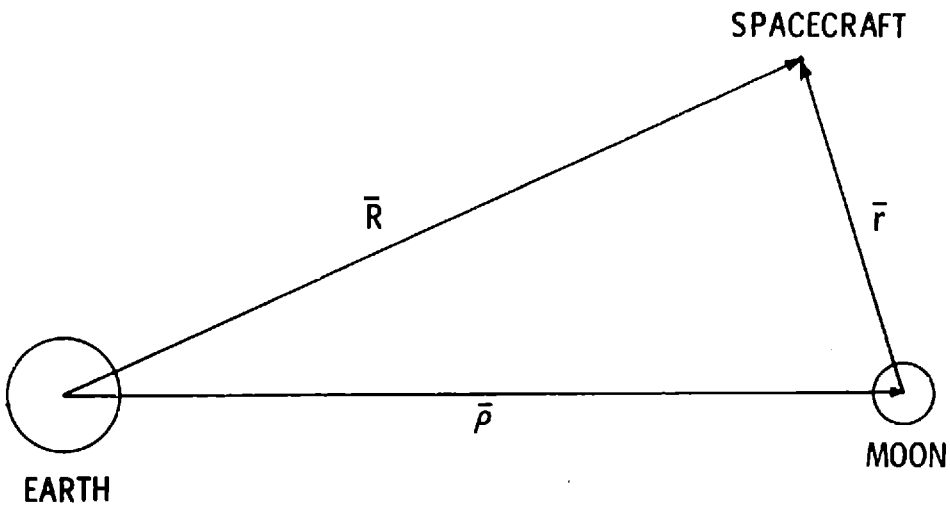

$$\bar{R}_J = \bar{r}_J + \bar{\rho}_J \tag{3.4}$$

$$\dot{\bar{R}}_J = \dot{\bar{r}}_J + \dot{\bar{\rho}}_J \tag{3.5}$$

Given the state vector (position and velocity) at some time t_I, the state vector at some later time t_F is desired. This is the initial value problem.

Integrating Equations (3.1) and (3.3) once, the following relationships between the velocity vectors at t_I and t_F is obtained:

$$\dot{\bar{R}}_F - \dot{\bar{R}}_I = -A\int_I^F \frac{\bar{R}_J}{R_J^3}\,dt_J - a\int_I^F \frac{\bar{r}_J}{r_J^3}\,dt_J - a\int_I^F \frac{\bar{\rho}_J}{\rho_J^3}\,dt_J \tag{3.6}$$

$$\dot{\bar{\rho}}_F - \dot{\bar{\rho}}_I = -\alpha\int_I^F \frac{\bar{\rho}_J}{\rho_J^3}\,dt_J \tag{3.7}$$

Integrating once more yeilds the relationships between the position vectors:

$$\bar{R}_F - \bar{R}_I = h\dot{\bar{R}}_I - A\int_I^F\int_I^K \frac{\bar{R}_J}{R_J^3}\,dt_J dt_K - a\int_I^F\int_I^K \frac{\bar{r}_J}{r_J^3}\,dt_J dt_K - a\int_I^F\int_I^K \frac{\bar{\rho}_J}{\rho_J^3}\,dt_J dt_K \tag{3.8}$$

$$\bar{\rho}_F - \bar{\rho}_I = h\dot{\bar{\rho}}_I - \alpha\int_I^F\int_I^K \frac{\bar{\rho}_J}{\rho_J^3}\,dt_J dt_K \tag{3.9}$$

where $h=t_F-t_I$. Only the integrals in Equations (3.7) and (3.9) can be evaluated in closed form since they represent the purely conic (two-body) motion of the Moon. The solutions may be written as

$$\dot{\bar{\rho}}_F - \dot{\bar{\rho}}_I = \dot{\bar{\rho}}_{I\alpha F} - \dot{\bar{\rho}}_I = \dot{\bar{\rho}}_F - \dot{\bar{\rho}}_{F\alpha I} \tag{3.10}$$

$$\bar{\rho}_F - \bar{\rho}_I = \bar{\rho}_{I\alpha F} - \bar{\rho}_I = \bar{\rho}_F - \bar{\rho}_{F\alpha I} \tag{3.11}$$

The compound subscript denotes a vector resulting from the conic propagation of some initial state vector. For example, $\dot{\bar{\rho}}_{I\alpha F}$ is the

velocity vector obtained by propagating the initial state vector t_I, $\bar{\rho}_I$, $\dot{\bar{\rho}}_I$ along a conic trajectory to t_F using α as the gravitational parameter.

The integrals involving $\bar{R}_J$ and $\bar{r}_J$ in Equations (3.6) and (3.8) cannot be evaluated exactly because the three-body position vector of the spacecraft is of course unknown. However, a conic approximation propagated from a suitable starting point could be used enabling the integrals to be evaluated. Assume that the spacecraft is moving away from the Moon and towards the Earth. As a first step in the solution, a selenocentric conic approximation propagated from the point I, which is closer to the Moon than the point F, is used for $\bar{r}_J$: $\bar{r}_J \cong \bar{r}_{IaJ}$. The integrals involving $\bar{r}_J$ in Equations (3.6) and (3.8) become

$$-a\int_I^F \frac{\bar{r}_J}{r_J^3}\,dt_J \cong -a\int_I^F \frac{\bar{r}_{IaJ}}{r_{IaJ}^3}\,dt_J = \dot{\bar{r}}_{IaF} - \dot{\bar{r}}_I \tag{3.12}$$

$$-a\int_I^F\int_I^K \frac{\bar{r}_J}{r_J^3}\,dt_J dt_K \cong -a\int_I^F\int_I^K \frac{\bar{r}_{IaJ}}{r_{IaJ}^3}\,dt_J dt_K = \bar{r}_{IaF} - \bar{r}_I - h\dot{\bar{r}}_I \tag{3.13}$$

The next step is to use for $\bar{R}_J$ a geocentric conic approximation propagated from point F, which is closer to the Earth than point I. Substituting $\bar{R}_{FAJ}$ for $\bar{R}_J$, the integrals involving $\bar{R}_J$ in Equations (3.6) and (3.8) become

$$-A\int_I^F \frac{\bar{R}_J}{R_J^3}\,dt_J \cong -A\int_I^F \frac{\bar{R}_{FAJ}}{R_{FAJ}^3}\,dt_J = \dot{\bar{R}}_F - \dot{\bar{R}}_{FAI} \tag{3.14}$$

$$-A\int_I^F\int_I^K \frac{\bar{R}_J}{R_J^3}\,dt_J dt_K \cong -A\int_I^F\int_I^K \frac{\bar{R}_{FAJ}}{R_{FAJ}^3}\,dt_J dt_K = \bar{R}_F - \bar{R}_{FAI} - h\dot{\bar{R}}_{FAI} \tag{3.15}$$

Finally Equations (3.7) and (3.9) are rearranged to yield

$$- a \int_I^F \frac{\bar{\rho}_J}{\rho_J^3} dt_J = \mu \left(\dot{\bar{\rho}}_F - \dot{\bar{\rho}}_I\right) \tag{3.16}$$

$$- a \int_I^F \int_I^K \frac{\bar{\rho}_J}{\rho_J^3} dt_J dt_K = \mu \left(\bar{\rho}_F - \bar{\rho}_I - h\dot{\bar{\rho}}_I\right) \tag{3.17}$$

where

$$\mu = \frac{a}{A + a} \cong \frac{1}{82.3} \tag{3.18}$$

Now substituting Equations (3.12), (3.14), and (3.16) into Equation (3.6) and using Equation (3.5) results in

$$\dot{\bar{R}}_{FAI} \cong \dot{\bar{r}}_{IaF} + \dot{\bar{\rho}}_I + \mu \left(\dot{\bar{\rho}}_F - \dot{\bar{\rho}}_I\right) \tag{3.19}$$

and substituting Equations (3.13), (3.15), and (3.17) into Equation (3.8) and using Equations (3.4), (3.5), and (3.19) yields

$$\bar{R}_{FAI} \cong \bar{r}_{IaF} + \bar{\rho}_I - h\dot{\bar{r}}_{IaF} + \mu \left(\bar{\rho}_F - \bar{\rho}_I - h\dot{\bar{\rho}}_F\right) \tag{3.20}$$

What has been obtained in the approximate expressions for $\bar{R}_{FAI}$ and $\dot{\bar{R}}_{FAI}$ are approximations to the position and velocity which would be a result of propagating the unknown but desired $\bar{R}_F$ and $\dot{\bar{R}}_F$ backward in time to t_I along a geocentric conic. In other words, Equations (3.19) and (3.20) give formulas for the particular geocentric position and velocity which, if propagated forward in time by an amoung $h = t_F - t_I$ along a gencentric conic, would yeild a position and velocity close to that which would result from propagating $\bar{R}_I$, $\dot{\bar{R}}_I$ forward in time to t_F along the actual three-body trajectory. The process of propagating $\bar{R}_{FAI}$ and $\dot{\bar{R}}_{FAI}$ forward on a two-body conic tc obtain the estimates of $\bar{R}_F$ and $\dot{\bar{R}}_F$ may be written as

$$\bar{R}_F = \left[\bar{R}_{FAI}\right]_{AF} \tag{3.21a}$$

$$\dot{\bar{R}}_F = \left[\dot{\bar{R}}_{FAI}\right]_{AF} \qquad (3.21b)$$

If it had been assumed instead that the spacecraft were moving away from the Earth and towards the Moon and if Equation (3.2) had been integrated twice using the alternate substitutions $\bar{R}_J \cong \bar{R}_{IAJ}$ and $\bar{r}_J \cong \bar{r}_{FaJ}$ to evaluate the unknown integrals, a different set of formulas, this time for $\bar{r}_{FaI}$ and $\dot{\bar{r}}_{FaI}$ would have been obtained. An easier way to derive these formulas is to solve for $\bar{r}_{IaF}$ and $\dot{\bar{r}}_{IaF}$ in Equations (3.19) and (3.20) and interchange the subscripts I and F:

$$\dot{\bar{r}}_{FaI} \cong \dot{\bar{R}}_{IAF} - \dot{\bar{\rho}}_F + \mu\,(\dot{\bar{\rho}}_F - \dot{\bar{\rho}}_I) \qquad (3.22)$$

$$\bar{r}_{FaI} \cong \bar{R}_{IAF} - \bar{\rho}_F - h(\dot{\bar{R}}_{IAF} - \dot{\bar{\rho}}_F) + \mu\,(\bar{\rho}_F - \bar{\rho}_I - h\dot{\bar{\rho}}_F) \qquad (3.23)$$

The position and velocity given by the above formulas have a similar interpretation: if they are propagated forward in time by an amount h along a selenocentric conic, estimates of the three-body final position and velocity are obtained for the case of Earth-to-Moon motion.

A one-step Earth-to-Moon multi-conic approximation to a trajectory from the L_2 libration point to the Moon is shown in Figure 3. The actual procedure used to generate the multi-conic approximation illustrated in Figure 3 is given below (the points a, b, c, d, e refer to Figure 3):

1. from the given initial state at point a, propagate a geocentric conic forward in time by an amoung $h = t_F - t_I$ to point b;
2. transform the position and velocity vectors at point b to the selenocentric frame;
3. from point b, propagate the position vector linearly backward along the velocity vector by an amount h to point c (field-free trajectory);
4. modify the position and velocity vectors (point c to point d) to account for the indirect effect of the Moon's motion (terms involving μ);
5. from point d, propagate a selenocentric conic forward in time by an amount h to point e to obtain estimates of the three-body final position and velocity.

Fig. 3 TRUE TRAJECTORY AND 1 STEP MULTI-CONIC APPROXIMATION

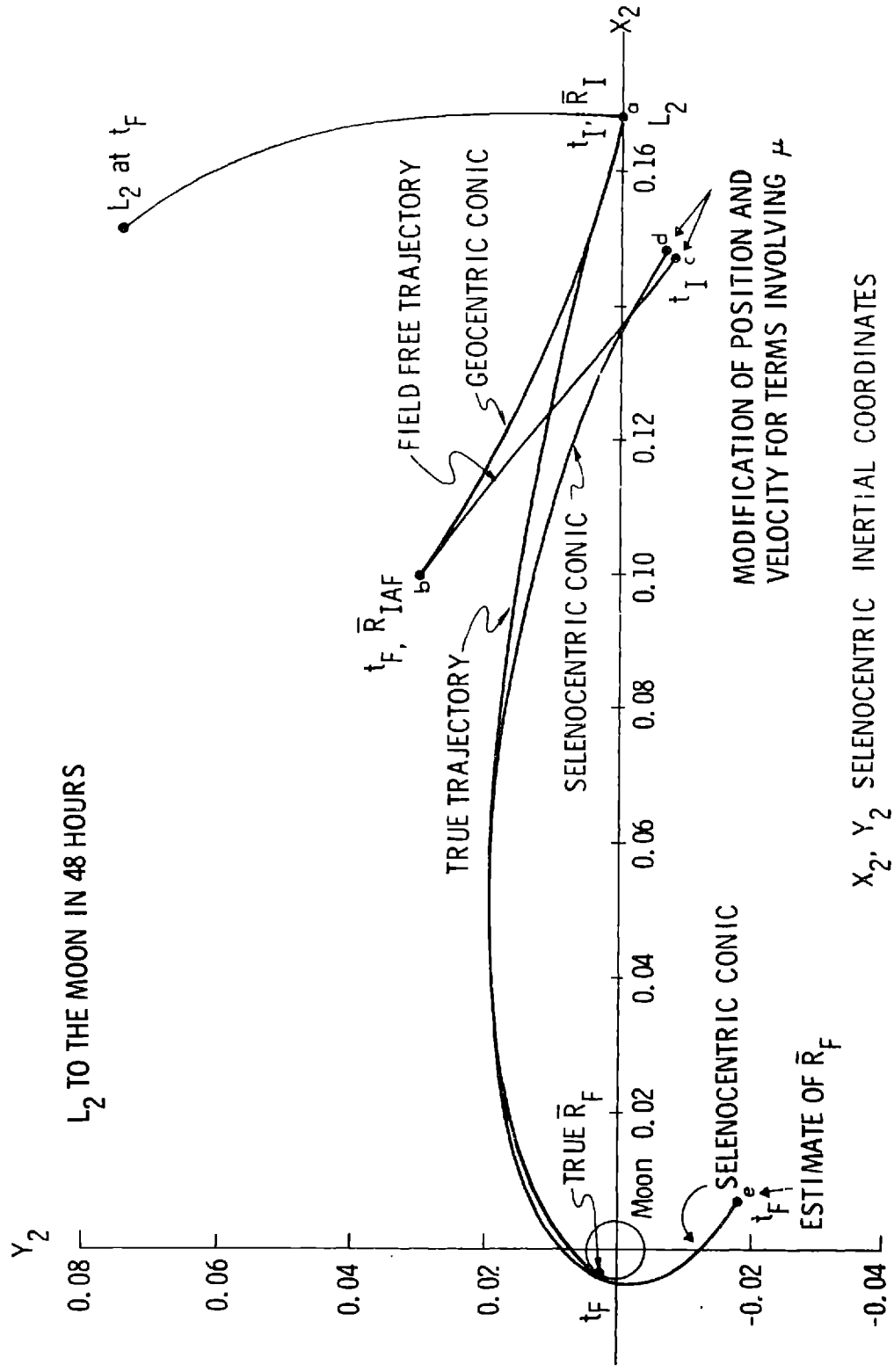

Steps 1 through 4 explain in words the operations defined by Equations (3.22) and (3.23) for Earth-to-Moon motion. Equations (3.19) and (3.20) result in a similar set of sequential procedures to arrive at the final position and velocity for Moon-to-Earth motion.

Thus far two alternative sets of approximations have been made in order to integrate the three-body differential equations of motion. The first alternative was to assume that

$$\bar{R}_J \cong \bar{R}_{FAJ} \tag{3.24}$$

$$\bar{r}_J \cong \bar{r}_{IaJ} \tag{3.25}$$

and the second alternative was to assume that

$$\bar{R}_J \cong \bar{R}_{IAJ} \tag{3.26}$$

$$\bar{r}_J \cong \bar{r}_{FaJ} \tag{3.27}$$

The first set of assumptions enabled the derivation of a multi-conic method of calculating three-body trajectories suitable for Moon to Earth type trajectories, and the second for Earth to Moon type trajectories. These two methods were first derived by Wilson[15]. There is a third alternative set of assumptions, namely that

$$\bar{R}_J \cong \bar{R}_{IAJ} \tag{3.28}$$

$$\bar{r}_J \cong \bar{r}_{IaJ} \tag{3.29}$$

One might use these approximations if one had no knowledge of which way the spacecraft were moving or if the spacecraft's motion did not satisfy either of the other two assumptions.

In any case, if one uses the approximations given by Equations (3.28) and (3.29) to evaluate the unknown integrals involving $\bar{R}_J$ and $\bar{r}_J$ in Equations

(3.6) and (3.8), the following results are obtained:

$$-A\int_I^F \frac{\bar{R}_J}{R_J^3}\,dt_J \cong -A\int_I^F \frac{\bar{R}_{IAJ}}{R_{IAJ}^3}\,dt_J = \dot{\bar{R}}_{IAF} - \dot{\bar{R}}_I \tag{3.30}$$

$$-a\int_I^F \frac{\bar{r}_J}{r_J^3}\,dt_J \cong -a\int_I^F \frac{\bar{r}_{IaJ}}{r_{IaJ}^3}\,dt_J = \dot{\bar{r}}_{IaF} - \dot{\bar{r}}_I \tag{3.31}$$

$$-A\int_I^F\int_I^K \frac{\bar{R}_J}{R_J^3}\,dt_J dt_K \cong -A\int_I^F\int_I^K \frac{\bar{R}_{IAJ}}{R_{IAJ}^3}\,dt_J dt_K = \bar{R}_{IAF} - \bar{R}_I - h\dot{\bar{R}}_I \tag{3.32}$$

$$-a\int_I^F\int_I^K \frac{\bar{r}_J}{r_J^3}\,dt_J dt_K \cong -a\int_I^F\int_I^K \frac{\bar{r}_{IaJ}}{r_{IaJ}^3}\,dt_J dt_K = \bar{r}_{IaF} - \bar{r}_I - h\dot{\bar{r}}_I \tag{3.33}$$

Equations (3.16) and (3.17) still apply, of course, for the integrals of $\bar{\rho}_J$. Now substituting Equations (3.30), (3.31), and (3.16) into Equation (3.6) yeilds

$$\dot{\bar{R}}_F = \dot{\bar{R}}_{IAF} + \dot{\bar{r}}_{IaF} - \dot{\bar{r}}_I + \mu\,(\dot{\bar{\rho}}_F - \dot{\bar{\rho}}_I) \tag{3.34}$$

and substituting Equations (3.32), (3.33) and (3.17) into Equation (3.8) yeilds

$$\bar{R}_F = \bar{R}_{IAF} + \bar{r}_{IaF} - \bar{r}_I - h\dot{\bar{r}}_I + \mu\,(\bar{\rho}_F - \bar{\rho}_I - h\dot{\bar{\rho}}_I) \tag{3.35}$$

Unlike the other two methods, the third method yeilds formulas for the final position and velocity directly rather than indirectly in terms of a state to be subsequently propagated along a conic. Notice that for all three methods two conics and a field-free trajectory are used. However, for both the Earth to Moon and Moon to Earth method, they are propagated sequentially and hence from different starting points. For the last method both conics and the field-free trajectory are propagated from the same starting point, the initial state, and they are utilized in a parallel fashion.

The third multi-conic method is equivalent to the Stumpff-Weiss N-body reference orbit[14] specialized to the restricted problem of three bodies. If the terms involving μ in the equations of the other two methods are eliminated, the resulting relations constitute Wilson's pseudostate theory[15]. Therefore, it is true that Wilson's two methods and the Stumpff-Weiss method are all related members of a multi-conic family of trajectory propagation techniques. Henceforth, these three multi-conic methods will be denoted the Moon-Earth method (Equations (3.19) and (3.20)), the Earth-Moon method (Equations (3.22) and (3.23)), and the Stumpff-Weiss method (Equations (3.34) and (3.35)). The fact that Wilson's two methods and the Stumpff-Weiss method can be obtained from the same derivation is not surprising but nonetheless satisfying.

The trajectory initial value problem may be stated as follows: given the initial position and velocity at time t_o, what will be the position and velocity at some later time t_f? The total time interval is divided into smaller segments (t_I, t_F), and any one of the multi-conic methods may be applied successively over these steps to update the position and velocity. Some sort of switching logic is needed to determine which of the multi-conic methods to use for each step. The switching technique used in this study will be explained in Chapter 4. Furthermore, for the purpose of this study, it was assumed that the conic of the Moon's orbit about the Earth is a circle; that is, the Earth and the Moon both move in circular orbits about their common barycentric. The geocentric position and velocity of the Moon are therefore known functions of time. For example, if a coordinate system is chosen such that the Moon is on the x-axis at the initial time t_o, the xy plane is the plane of the Moon's orbit, and the z-axis points in the direction of the Moon's angular momentum vector, then the geocentric position and velocity needed in the above equations are given by

$$\bar{\rho}_J = \rho \begin{bmatrix} \cos (t_J - t_o) \\ \sin (t_J - t_o) \\ 0 \end{bmatrix} \tag{3.36}$$

$$\dot{\bar{\rho}}_J = \sqrt{\frac{\alpha}{\rho}} \begin{bmatrix} -\sin(t_J - t_o) \\ \cos(t_J - t_o) \\ 0 \end{bmatrix} \tag{3.37}$$

where ρ is the radius of the Moon's orbit about the Earth.

Each step in the multi-conic trajectory propagation methods requires the solution of two two-body Kepler problems. The total solution to the initial value problem therefore requires the solution of 2n Kepler problems where n is the number of steps in the propagation. A rigorous error analysis of the multi-conic methods will be deferred until Chapter 6. But it may be stated here that, for a 48 hour trajectory from L_2 to the Moon, step sizes of the order of 2-3 hours produce results accurate to about .1 feet/sec. in velocity and about .2 miles in position, while a step size of the order of 6 hours produces results accurate to about 2-3 feet/sec. in velocity and 2-3 miles in position, certainly good enough for mission studies. The above errors are the errors in the final position and velocity upon arrival at the Moon. Step sizes over 6 hours but less than 30 hours are useful for obtaining an intuitive feeling for the actual trajectory.

3.2 Calculation of the State Transition Matrix

A great advantage of the multi-conic method is that in addition to the position and velocity at the final time, the state transition matrix may also be found with no additional integrations or differentiations. For the Earth-Moon or Moon-Earth method, each step of the propagation is itself a five-part sequential procedure as illustrated above. In referring to this five-part procedure it should be fairly obvious that the operations defined by steps 2 and 4 do not make any contributions to the state transition matrix, so that to obtain the state transition matrix for the entire five-step sequence, the state transition matrices of steps 1, 3, and 5 need only be multiplied sequentially. Steps 1 and 5 are two-body conics which are solutions to Kepler's problem, and from each Kepler problem solution the state transition matrix for that particular two-body conic is readily obtained.

Let $\Phi_{2B}(t_F, t_I)$ denote a two-body state transition matrix, $\Phi_{3B}(t_F, t_I)$ a three-body state transition matrix, and $\Phi_L(t_F, t_I)$ the transition matrix along a linear trajectory. Since $\bar{R} = \bar{r} + \bar{\rho}$ and there are no variations in $\bar{\rho}$, then a small variation in $\bar{R}$ is identically equal to a small variation in $\bar{r}$, and the state transition matrix may be defined as

$$\Phi(t_F, t_I) = \begin{bmatrix} \frac{\partial \bar{R}_F}{\partial \bar{R}_I} & \frac{\partial \bar{R}_F}{\partial \dot{\bar{R}}_I} \\ \frac{\partial \dot{\bar{R}}_F}{\partial \bar{R}_I} & \frac{\partial \dot{\bar{R}}_F}{\partial \dot{\bar{R}}_I} \end{bmatrix} = \begin{bmatrix} \frac{\partial \bar{r}_F}{\partial \bar{r}_I} & \frac{\partial \bar{r}_F}{\partial \dot{\bar{r}}_I} \\ \frac{\partial \dot{\bar{r}}_F}{\partial \bar{r}_I} & \frac{\partial \dot{\bar{r}}_F}{\partial \dot{\bar{r}}_I} \end{bmatrix} \tag{3.38}$$

Along the linear trajectory (which occurs in the selenocentric coordinate system for both the Earth-Moon and Moon-Earth methods), position and velocity at the final time are given by

$$\bar{r}_F = \bar{r}_I + h\dot{\bar{r}}_I \tag{3.39}$$

$$\dot{\bar{r}}_F = \dot{\bar{r}}_I \tag{3.40}$$

and hence

$$\Phi_L(t_F, t_I) = \begin{bmatrix} I & hI \\ 0 & I \end{bmatrix} \tag{3.41}$$

The three-body state transition matrix may be calculated from

$$\Phi_{3B}(t_F, t_I) = \Phi_{2B}^{(2)}(t_F, t_I)\ \Phi_L(t_I, t_F)\ \Phi_{2B}^{(1)}(t_F, t_I) \tag{3.42}$$

where the superscript (1) refers to the conic of the first step in the above five step procedure and (2) refers to the second conic (step 5). The product of the last two matrices on the right hand side of Equation (3.42) causes

the position derivatives of $\Phi_{2B}^{(1)}(t_F, t_I)$ to be backdated along the corresponding velocity derivatives by an amount h. For example, for the Earth-Moon case $\Phi_{2B}^{(1)}(t_F, t_I)$ would be equal to

$$\begin{bmatrix} \frac{\partial \bar{R}_{IAF}}{\partial \bar{R}_I} & \frac{\partial \bar{R}_{IAF}}{\partial \dot{\bar{R}}_I} \\ \frac{\partial \dot{\bar{R}}_{IAF}}{\partial \bar{R}_I} & \frac{\partial \dot{\bar{R}}_{IAF}}{\partial \dot{\bar{R}}_I} \end{bmatrix} \tag{3.43}$$

and premultiplying by $\Phi_L(t_I, t_F)$ would yield

$$\begin{bmatrix} \frac{\partial}{\partial \bar{R}_I}(\bar{R}_{IAF}-h\dot{\bar{R}}_{IAF}) & \frac{\partial}{\partial \dot{\bar{R}}_I}(\bar{R}_{IAF}-h\dot{\bar{R}}_{IAF}) \\ \frac{\partial \dot{\bar{R}}_{IAF}}{\partial \bar{R}_I} & \frac{\partial \dot{\bar{R}}_{IAF}}{\partial \dot{\bar{R}}_I} \end{bmatrix} \tag{3.44}$$

Thus an analogous procedure may be stated for calculating the three-body state transition matrix for each step in the propagation:

1. from the first two-body conic obtain the two-body state transition matrix;
2. backdate the position derivatives along the corresponding velocity derivatives by an amount $h = t_F - t_I$;
3. premultiply by the two-body state transition matrix of the second conic.

The state transition matrix for the whole trajectory is found by sequentially multiplying the state transition matrices for each step.

The state transition matrix for the Stumpff-Weiss method is most easily found by directly taking derivatives of the final position and velocity with respect to the initial conditions according to the definition of the state transition matrix in Equation (3.38).

The final position and velocity for the Stumpff-Weiss method are given fiven by Equations (3.34) and (3.35):

$$\dot{\bar{R}}_F = \dot{\bar{R}}_{IAF} + \dot{\bar{r}}_{IaF} - \dot{\bar{r}}_I + \mu\,(\dot{\bar{\rho}}_F - \dot{\bar{\rho}}_I) \tag{3.45}$$

$$\bar{R}_F = \bar{R}_{IAF} + \bar{r}_{IaF} - \bar{r}_I - h\dot{\bar{r}}_I + \mu\,(\bar{\rho}_F - \bar{\rho}_I - h\dot{\bar{\rho}}_I) \tag{3.46}$$

The derivatives of the final position and velocity with respect to the initial conditions are

$$\frac{\partial \dot{\bar{R}}_F}{\partial \bar{R}_I} = \frac{\partial \dot{\bar{R}}_{IAF}}{\partial \bar{R}_I} + \frac{\partial \dot{\bar{r}}_{IaF}}{\partial \bar{R}_I} \tag{3.47}$$

$$\frac{\partial \dot{\bar{R}}_F}{\partial \dot{\bar{R}}_I} = \frac{\partial \dot{\bar{R}}_{IAF}}{\partial \dot{\bar{R}}_I} + \frac{\partial \dot{\bar{r}}_{IaF}}{\partial \dot{\bar{R}}_I} - \frac{\partial \dot{\bar{r}}_I}{\partial \dot{\bar{R}}_I} \tag{3.48}$$

$$\frac{\partial \bar{R}_F}{\partial \bar{R}_I} = \frac{\partial \bar{R}_{IAF}}{\partial \bar{R}_I} + \frac{\partial \bar{r}_{IaF}}{\partial \bar{R}_I} - \frac{\partial \bar{r}_I}{\partial \bar{R}_I} \tag{3.49}$$

$$\frac{\partial \bar{R}_F}{\partial \dot{\bar{R}}_I} = \frac{\partial \bar{R}_{IAF}}{\partial \dot{\bar{R}}_I} + \frac{\partial \bar{r}_{IaF}}{\partial \dot{\bar{R}}_I} - h\frac{\partial \dot{\bar{r}}_I}{\partial \dot{\bar{R}}_I} \tag{3.50}$$

Since $\bar{\rho}$ is unaffected by the deviations in the state of the spacecraft, from Equations (3.4) and (3.5) it is true that

$$\frac{\partial}{\partial \bar{R}_I} = \frac{\partial}{\partial \bar{r}_I} \tag{3.51}$$

$$\frac{\partial}{\partial \dot{\bar{R}}_I} = \frac{\partial}{\partial \dot{\bar{r}}_I} \tag{3.52}$$

Therefore Equations (3.47) to (3.50) can be written as

$$\frac{\partial \dot{\bar{R}}_F}{\partial \bar{R}_I} = \frac{\partial \dot{\bar{R}}_{IAF}}{\partial \bar{R}_I} + \frac{\partial \dot{\bar{r}}_{IaF}}{\partial \bar{r}_I} \tag{3.53}$$

$$\frac{\partial \dot{\bar{R}}_F}{\partial \dot{\bar{R}}_I} = \frac{\partial \dot{\bar{R}}_{IAF}}{\partial \dot{\bar{R}}_I} + \frac{\partial \dot{\bar{r}}_{IaF}}{\partial \dot{\bar{r}}_I} - I \tag{3.54}$$

$$\frac{\partial \bar{R}_F}{\partial \bar{R}_I} = \frac{\partial \bar{R}_{IAF}}{\partial \bar{R}_I} + \frac{\partial \bar{r}_{IaF}}{\partial \bar{r}_I} - I \tag{3.55}$$

$$\frac{\partial \bar{R}_F}{\partial \dot{\bar{R}}_I} = \frac{\partial \bar{R}_{IAF}}{\partial \dot{\bar{R}}_I} + \frac{\partial \bar{r}_{IAF}}{\partial \dot{\bar{r}}_I} - hI \tag{3.56}$$

where I is a 3x3 identity matrix. The three-body state transition matrix can therefore be calculated as

$$\Phi_{3B}(t_F, t_I) = \Phi_{2B}^{A}(t_F, t_I) + \Phi_{2B}^{a}(t_F, t_I) - \Phi_L(t_F, t_I) \tag{3.57}$$

where $\Phi_{2B}^{A}(t_F, t_I)$ is the two-body state transition matrix from the geocentric conic, $\Phi_{2B}^{a}(t_F, t_I)$ comes from the selenocentric conic and $\Phi_L(t_F, t_I)$ is defined in Equation (3.41).

Once again, to obtain the state transition matrix for the whole trajectory, the state transition matrices for each step are multiplied sequentially. Notice that the per-step state transition matrix for the Earth-Moon or Moon-Earth method is calculated by a multiplicative process (Equation (3.42)) while for the Stumpff-Weiss method it is calculated by an additive process (Equation (3.57)). The reason for this behavior is that the trajectory calculation for either the Earth-Moon or Moon-Earth method is a sequential procedure with each new trajectory segment starting from the state at which the previous one ended. On the other hand, for the Stumpff-Weiss method all trajectory segments start at the initial point and are added together to obtain the three-body estimate.

3.3 Boundary Value Problems

The previous two Sections dealt with the solution of the trajectory propagation problem for the restricted problem of three bodies by means of multi-conic methods. That problem may be thought of as the three-body initial value (Kepler) problem. This Section considers the two-point boundary value problem of finding the initial velocity to fit a trajectory between given initial and final positions in a given time of flight This problem is the three-body Lambert problem. The multi-conic method is ideally suited to solving this problem since, as was noted in the previous Section, the solution to the initial value problem furnishes, in addition to the position and velocity at the final time, also the state transition matrix containing the partials of position and velocity at the final time with respect to the initial conditions. Typically the boundary value problem is solved by iterating on the unknown initial velocity to reduce the position error at the final time to zero. Since analytic partials are available, a Newton-Raphson method is attractive and is used in this study.

With the state transition matrix expressed as in Equation (2.10), the deviations in position and velocity at the final time are related to the deviations at the initial time by

$$\delta\bar{r}_f = \varphi_{11}\,\delta\bar{r}_o + \varphi_{12}\,\delta\bar{v}_o \tag{3.58}$$

$$\delta\bar{v}_f = \varphi_{21}\,\delta\bar{r}_o + \varphi_{22}\,\delta\bar{v}_o \tag{3.59}$$

Since $\bar{r}_o$ is fixed in the boundary value problem, i.e., $\delta\bar{r}_o = 0$, the final position and velocity before and after a change in $\bar{v}_o$ are related by

$$\bar{r}_{f_{n+1}} = \bar{r}_{f_n} + \varphi_{12}\,\Delta\bar{v}_{o_n} \tag{3.60}$$

$$\bar{v}_{f_{n+1}} = \bar{v}_{f_n} + \varphi_{22}\,\Delta\bar{v}_{o_n} \tag{3.61}$$

where

is the difference between the initial velocity which comes from the solution to the Lambert problem and the given initial velocity of the boundary conditions; the final impulse is the difference between the final desired velocity of the boundary conditions and the velocity of arrival on the trajectory which came from the solution to the Lambert problem. The initial velocity of the Lambert solution becomes the velocity immediately after the initial impulse, and the velocity of arrival of the Lambert solution is the velocity immediately before the final impulse. The Lambert solution satisfies the position constraints at the end points, and the impulses satisfy the velocity constraints.

Now, let us look at the modified Lambert problem which arises when the boundary conditions at the final time are not given in terms of a desired position. For instance, it might be desirable to specify that the desired end conditions are defined by a circular orbit of given altitude and inclination. If the destination body is the Moon, the inclination is chosen to be that of the orbit defined by the final position and velocity and is relative to the plane of the Moon's orbit about the Earth. In this case, the magnitude of the final position and velocity vectors and their dot and cross products are important, and not the actual components of the vectors. For, in order to achieve a circular orbit of given altitude and inclination, the following four quantities must be specified: r_f, v_f, $\dot{r}_f$, i. The quantity $\dot{r}_f$ is the radial velocity at the final time; $\dot{r}_f$ must be zero. The inclination is i. Once r_f is specified, v_f is fixed by the requirement that the orbit be circular. If we decide that the impulse at the final time will adjust only the magnitude of the velocity and will not affect its direction, then we are specifying that the circular orbit be entered tangentially with no change in inclination. The circular orbit is entered tangentially because such a maneuver will minimize the final impulse since the greatest change in the energy of an orbit is accomplished by an impulse along the velocity vector. Since the final impulse will affect only the magnitude of the velocity, the solution to the modified Lambert problem must insure that the correct position magnitude and inclination and a zero radial velocity have been achieved prior to the final impulse. The modified Lambert problem must therefore fit a trajectory between a given initial position and the following end

$$\Delta\bar{v}_{o_n} = \bar{v}_{o_{n+1}} - \bar{v}_{o_n} \tag{3.62}$$

The quantity $\bar{v}_{o_n}$ is the initial velocity on the nth iteration; $\bar{v}_{o_{n+1}}$ is the initial velocity on the $n+1^{st}$ iteration; $\bar{r}_{f_n}$ and $\bar{v}_{f_n}$ are the final position and velocity of the trajectory defined by $\bar{r}_o$ and $\bar{v}_{o_n}$. The desired end condition is

$$\bar{r}_{f_{n+1}} = \bar{r}_f \tag{3.63}$$

where $\bar{r}_f$ is the desired final position. Substituting Equation (3.60) into Equation (3.63) and solving for $\Delta\bar{v}_{o_n}$ leads to a formula for updating the initial velocity:

$$\bar{v}_{o_{n+1}} = \bar{v}_{o_n} + \varphi_{12}^{-1}(\bar{r}_f - \bar{r}_{f_n}) \tag{3.64}$$

The matrix φ_{12} is the upper right hand 3x3 submatrix of the 6x6 state transition matrix associated with the trajectory defined by $\bar{r}_o$ and $\bar{v}_{o_n}$. The iteration is halted when the final position has converged to within some acceptable tolerance.

The boundary value problem described above is the usual Lambert problem. Given the initial and final positions and a time of flight, a trajectory satisfying these boundary conditions is found by iterating on the initial velocity. The velocity which the spacecraft has at the initial time is, in general, not equal to that which is required to reach the final position. Also, the velocity which is desired at the final time is, in general, not equal to the velocity of arrival on the trajectory which has been fitted between the initial and final positions. Therefore, velocity impulses are required at the initial and final times to achieve the velocities desired at those points. Thus, if the state is fully specified at the initial and final times, a two-impulse trajectory satisfying these boundary conditions may be found as follows: solve the Lambert problem to fit a trajectory between the given initial and final positions; the initial impulse

conditions:

$$|\bar{r}_{f_{n+1}}| = r_f \tag{3.65}$$

$$\bar{r}_{f_{n+1}}^T \bar{v}_{f_{n+1}} = 0 \tag{3.66}$$

$$\bar{u}_z^T \frac{\bar{h}_{n+1}}{h_{n+1}} = \cos i \tag{3.67}$$

The quantity r_f is the desired final position magnitude; $\bar{u}_z$ is a unit vector in the direction of the Moon's angular momentum vector; $\bar{h}_{n+1} = \bar{r}_{f_{n+1}} \times \bar{v}_{f_{n+1}}$ is the angular momentum vector of the spacecraft; i is the desired inclination. The requirement that $\bar{r}_{f_{n+1}}^T \bar{v}_{f_{n+1}} = 0$ insures that the radial velocity is zero. There are three components of $\bar{v}_o$ to adjust in solving the modified Lambert problem and three end conditions to satisfy.

When Equations (3.60) and (3.61) are substituted into Equations (3.65), (3.66), and (3.67), and terms of second or higher order in $\Delta\bar{v}_{o_n}$ are neglected, three scalar equations involving the three unknown components of $\Delta\bar{v}_{o_n}$ are obtained. These three scalar equations which are derived in Appendix A, may be combined into the following vector equation:

$$P\,\Delta\bar{v}_{o_n} = \bar{e}_n \tag{3.68}$$

where

$$\bar{e}_n = \begin{bmatrix} r_f - r_{f_n} \\ -\bar{r}_{f_n}^T \bar{v}_{f_n} \\ \cos i - \cos i_n \end{bmatrix} \tag{3.69}$$

$$P = B\,\varphi_{22} + C\,\varphi_{12} \tag{3.70}$$

$$B = \begin{bmatrix} 0 \\ \overline{r}_{f_n}^{\,T} \\ \frac{1}{h_n^{\,3}}\,\overline{u}_z^{\,T}\,D\,(\overline{r}_{f_n}\,x) \end{bmatrix} \tag{3.71}$$

$$C = \begin{bmatrix} \frac{1}{r_{f_n}}\,\overline{r}_{f_n}^{\,T} \\ \overline{v}_{f_n}^{\,T} \\ -\frac{1}{h_n^{\,3}}\,\overline{u}_z^{\,T}\,D\,(\overline{v}_{f_n}\,x) \end{bmatrix} \tag{3.72}$$

$$D = h_n^{\,2}\,I - \overline{h}_n\,\overline{h}_n^{\,T} \tag{3.73}$$

$$(\overline{r}_{f_n}\,x) = \begin{bmatrix} 0 & -z_{f_n} & y_{f_n} \\ z_{f_n} & 0 & -x_{f_n} \\ -y_{f_n} & x_{f_n} & 0 \end{bmatrix} \tag{3.74}$$

$$(\overline{v}_{f_n}\,x) = \begin{bmatrix} 0 & -\dot{z}_{f_n} & \dot{y}_{f_n} \\ \dot{z}_{f_n} & 0 & -\dot{x}_{f_n} \\ -\dot{y}_{f_n} & \dot{x}_{f_n} & 0 \end{bmatrix} \tag{3.75}$$

$$\bar{r}_{f_n} = \begin{bmatrix} x_{f_n} \\ y_{f_n} \\ z_{f_n} \end{bmatrix} \tag{3.76}$$

$$\bar{v}_{f_n} = \begin{bmatrix} \dot{x}_{f_n} \\ \dot{y}_{f_n} \\ \dot{z}_{f_n} \end{bmatrix} \tag{3.77}$$

The solution to Equation (3.68) for $\Delta\bar{v}_{o_n}$ provides a formula for updating the initial velocity:

$$\bar{v}_{o_{n+1}} = \bar{v}_{o_n} + P^{-1}\,\bar{e}_n \tag{3.78}$$

The iteration is halted when the error vector $\bar{e}_n$ is sufficiently close to zero.

Once the solution to the modified Lambert problem has been found, the initial impulse is defined as the difference between the initial velocity from the modified Lambert solution and the given intitial velocity of the boundary conditions. The final impulse is a tangential impulse in the direction of the final velocity to adjust the magnitude of the final velocity so that a circular orbit at the given altitude is established.

The solution to the initial value problem described in Section 3.1 was coded into a Fortran program and subsequently included in a program to solve the two kinds of Lambert problems described in this Section.

CHAPTER 4
THE TRAJECTORY OPTIMIZATION METHOD

4.1 Preliminary Remarks

The previous Chapter examined the multi-conic methods of trajectory propagation and the procedures necessary to solve the three-body Kepler (initial value) problem and Lambert (boundary value) problem. This Chapter explains the application of primer vector theory, the multi-conic trajectory methods, and an accelerated gradient functional minimization algorithm to the determination of minimum impulse (fuel-optimal) trajectories and describes the structure of the computer program which finds these minimum impulse trajectories. The four necessary conditions for optimality introduced in Chapter 2 are repeated here for reference:

1. the primer vector and its first derivative are everywhere continuous:
2. whenever an impulse occurs, the primer vector is aligned with the impulse and has unit magnitude:
3. the primer vector magnitude may not exceed unity on a coasting arc:
4. the time derivative of the primer vector magnitude is zero at all interior junction points separating coasting arcs.

As noted in Chapter 2, these four necessary conditions were derived by Lawden[19]. It should be pointed out that necessary condition (4) is not an independent condition, but is implied by the other three. For if at an interior impulse point, (1) the primer derivative is continuous, (2) the primer magnitude is unity, and (3) the primer magnitude does not exceed unity immediately before or after the impulse, then it must be true that the derivative of the primer magnitude is zero at the impulse point.

4.2 Forming a Three-Impulse Trajectory

For a two-impulse reference solution, by constructing the primer history according to the rules of Section 2.2, necessary conditions (1) and (2) will automatically be satisfied. Condition (4) does not apply to a two-impulse solution and therefore, from condition (3), if the primer

magnitude exceeds unity on the coasting arc between the two impulses, then there is a neighboring three-impulse solution which has less cost. This can be shown by deriving an expression for the differential cost between a two-impulse trajectory and a neighboring three-impulse solution. Jezewski and Rozendaal have shown[3] that this expression may be written as

$$\delta J = (1 - \bar{\lambda}_m{}^T \bar{\eta}) \, \delta c \qquad (4.1)$$

where δc is the magnitude of the additional impulse, $\bar{\lambda}_m$ is the primer vector at t_m (the time at which the third impulse is to be added), and $\bar{\eta}$ is a unit vector in the direction of the additional impulse. Equation (4.1) expresses the first order difference only. Therefore, it can be seen that if $|\bar{\lambda}_m|$ exceeds unity, the two-impulse reference trajectory can be improved by adding a third impulse in the direction of $\bar{\lambda}_m$ at t_m. To first order, the greatest improvement is made if the additional impulse occurs at the point where $|\bar{\lambda}_m|$ is maximum.

The three-impulse trajectory is formed by perturbing the position on the two-impulse trajectory at t_m. This position perturbation is found to be

$$\delta \bar{r}_m = A^{-1} \frac{\bar{\lambda}_m}{|\bar{\lambda}_m|} \, \delta c \qquad (4.2)$$

where

$$A = \varphi_{22}(t_m, t_f) \, \varphi_{12}{}^{-1}(t_m, t_f) - \varphi_{22}(t_m, t_o) \, \varphi_{12}{}^{-1}(t_m, t_o) \qquad (4.3)$$

The procedure of forming the three-impulse trajectory is as follows: given t_m and $\bar{\lambda}_m$, $\delta \bar{r}_m$ is calculated as above and two boundary value problems are solved, the first between $\bar{r}_o$ and $\bar{r}_m + \delta \bar{r}_m$ with time of flight $t_m - t_o$, and the second between $\bar{r}_m + \delta \bar{r}_m$ and $\bar{r}_f$ with time of flight $t_f - t_m$. The interior impulse is then just the difference in the velocities of the two trajectory segments at t_m. The resulting three-impulse trajectory will have less cost than the reference two-impulse trajectory as long as δc is not too large. Values of δc equal to one percent of the cost of the two-

impulse trajectory are not unreasonable.

4.3 Converging to a Local Minimum

The new three-impulse trajectory will in general not be optimal. By construction, the primer vector at each impulse time (t_o, t_{in}, t_f) is a unit vector in the direction of the impulse. From these boundary conditions the initial value of the primer derivative for each two impulse segment of the three-impulse trajectory may be calculated as in Equation (2.15) and the primer magnitude is thus continuous. The first part of necessary condition (1) and necessary condition (2) will be satisfied. However, the primer derivative will in general not be continuous at the interior impulse (second part of condition (1)), nor will the derivative of the primer magnitude be zero at that time (condition (4)). The primer history for this first three-impulse trajectory will look something like Figure 1(d). On the optimal three-impulse trajectory both these conditions will be satisfied (as in Figure 1(e)). Therefore, the position and time of the interior impulse must be adjusted iteratively until the optimal three-impulse trajectory is found.

The cost of the three-impulse trajectory is the sum of the three ΔV's. The problem here is to minimize a scalar function of four variables: three components of position and the time at the interior impulse. The gradient of the cost on the three-impulse trajectory with respect to the position and time of the interior impulse is found[3] to be

$$\frac{\partial J}{\partial \bar{r}_m} = (\dot{\bar{\lambda}}_m^+ - \dot{\bar{\lambda}}_m^-)^T \tag{4.4}$$

$$\frac{\partial J}{\partial t_m} = -(\dot{\bar{\lambda}}_m^{+T} \bar{v}_m^+ - \dot{\bar{\lambda}}_m^{-T} \bar{v}_m^-) \tag{4.5}$$

where the - and + superscripts refer to times just before and after the mid-course impulse, respectively. The quantities in Equations (4.4) and (4.5) are easily obtained once the two boundary value problems for the two trajectory segments have been solved.

Any efficient function minimization algorithm can be used to find the minimum of J by iterating on $\bar{r}_m$ and t_m. Since analytic partials for J exist, an accelerated gradient procedure is suggested. In this study a new function minimization algorithm of Jacobson and Oksman[20] is used. This algorithm approximates the actual function by a homogeneous function in order to update the independent variables of each iteration. The iteration is halted when the decrease in the cost on successive iterations has become negligible. The trajectory optimization method uses the function minimization algorithm as a "black box" which has as inputs the current set of independent variables (r_m and t_m), the cost, and the cost gradient, and which yields as outputs the new set of independent variables:

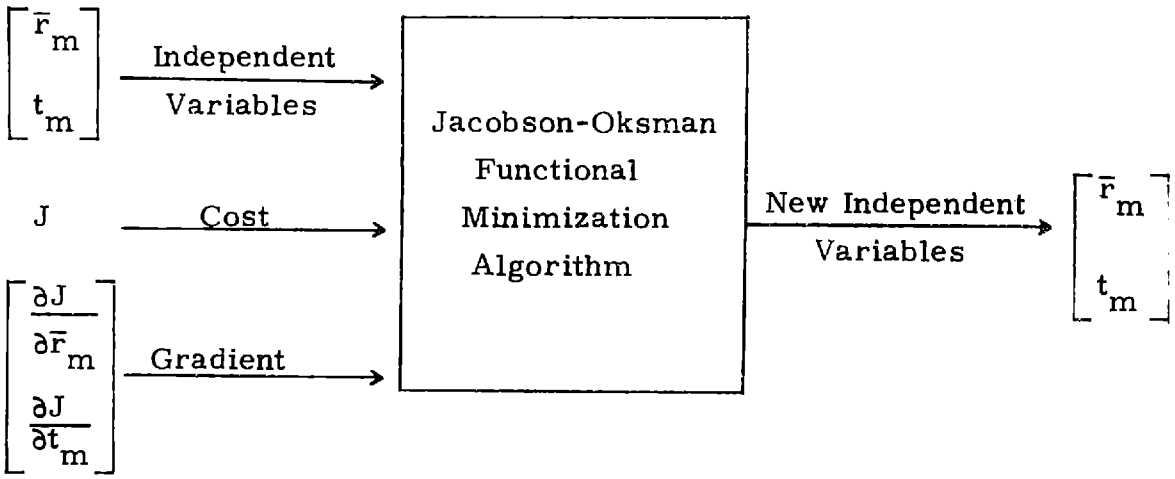

When the cost has been minimized, a converged three-impulse trajectory will be obtained which will satisfy all the necessary conditions except perhaps condition (3), that the primer magnitude must not exceed unity on any coasting arc. To prove the above statement, first recall that by construction the primer vector will be aligned with the impulse and have unit magnitude at all impulse points (condition (2)), and the primer vector will be continuous (first part of condition (1)). When the cost of the three-impulse trajectory has been minimized, the gradient of the cost will be zero. Setting the expressions in Equations (4.4) and (4.5) equal to zero yields

$$\dot{\bar{\lambda}}_m^+ = \dot{\bar{\lambda}}_m^- \tag{4.6}$$

$$\dot{\bar{\lambda}}_m^{+T} \bar{v}_m^+ - \dot{\bar{\lambda}}_m^{-T} \bar{v}_m^- = 0 \tag{4.7}$$

Equation (4.6) insures that now the primer derivative will be continuous at the interior impulse point and hence condition (1) is fully satisfied. Substituting Equation (4.6) into (4.7) results in

$$\dot{\bar{\lambda}}_m^T (\bar{v}_m^+ - \bar{v}_m^-) = 0 \tag{4.8}$$

But since the primer vector is a unit vector in the direction of the impulse at t_m, the following relation may be written:

$$(\bar{v}_m^+ - \bar{v}_m^-) = |\bar{v}_m^+ - \bar{v}_m^-|\bar{\lambda}_m = |\Delta\bar{v}_m|\bar{\lambda}_m \tag{4.9}$$

Substituting Equation (4.9) into (4.8) yields

$$\dot{\bar{\lambda}}_m^T \bar{\lambda}_m = 0 = \dot{\lambda}_m \tag{4.10}$$

since $|\bar{\lambda}_m| = 1$. Thus the derivative of the primer magnitude at the interior impulse point is zero and also condition (4) is satisfied. If the magnitude of the primer vector exceeds unity on either coasting arc of the converged three-impulse trajectory, another impulse could be added and a converged four-impulse solution found, etc.

4.4 Summary of the Trajectory Optimization Method

The overall step-by-step procedure for finding fuel-optimal impulsive trajectories is summaried below with pertinent formulas included (this outline also gives the structure of the Fortran program used to obtain the results of the next Chapter):

1. Given the initial and final state vectors and the transfer time, solve the boundary value problem to find a two-impulse reference solution.

2. Compute $\bar{\lambda}_o$, $\bar{\lambda}_f$, $\dot{\bar{\lambda}}_o$ from

$$\bar{\lambda}_o = \frac{\Delta\bar{v}_o}{|\Delta\bar{v}_o|} \qquad \bar{\lambda}_f = \frac{\Delta\bar{v}_f}{|\Delta\bar{v}_f|} \tag{4.11a, b}$$

$$\dot{\bar{\lambda}}_o = \varphi_{12}^{-1}(t_f, t_o)\,[\bar{\lambda}_f - \varphi_{11}(t_f, t_o)\,\bar{\lambda}_o] \tag{4.12}$$

and generate a primer history according to

$$\bar{\lambda}(t) = \varphi_{11}(t, t_o)\,\bar{\lambda}_o + \varphi_{12}(t, t_o)\,\dot{\bar{\lambda}}_o \tag{4.13}$$

3. Examine the primer history and if $|\bar{\lambda}(t)|$ exceeds unity anywhere between the initial and final times, the two-impulse solution is not optimal and a small third impulse is added at t_m, the time at which $|\bar{\lambda}(t)|$ is maximum, by perturbing the position at t_m:

$$\delta\bar{r}_m = A^{-1}\frac{\bar{\lambda}_m}{|\bar{\lambda}_m|}\,\delta c \tag{4.14}$$

$$A = \varphi_{22}(t_m, t_f)\,\varphi_{12}^{-1}(t_m, t_f) - \varphi_{22}(t_m, t_o)\,\varphi_{12}^{-1}(t_m, t_o) \tag{4.15}$$

Solve two boundary value problems:
(1) from $\bar{r}_o$ to $\bar{r}_m + \delta\bar{r}_m$ with transfer time $t_m - t_o$
(2) from $\bar{r}_m + \delta\bar{r}_m$ to $\bar{r}_f$ with transfer time $t_f - t_m$
This yields a non-optimal three-impulse solution.

4. Use the Jacobson-Oksman algorithm to iterate on $\bar{r}_m$ and t_m and minimize the cost of the three-impulse trajectory. The cost and cost gradient are found at each iteration by first solving the two boundary value problems and then using the following relations:

$$J = |\Delta\bar{v}_o| + |\Delta\bar{v}_m| + |\Delta\bar{v}_f| \tag{4.16}$$

$$\frac{\partial J}{\partial\bar{r}_m} = (\dot{\bar{\lambda}}_m^+ - \dot{\bar{\lambda}}_m^-)^T \tag{4.17}$$

$$\frac{\partial J}{\partial t_m} = -\left(\dot{\bar{\lambda}}_m^{+T}\,\bar{v}_m^{+} - \dot{\bar{\lambda}}_m^{-T}\,\bar{v}_m^{-}\right) \tag{4.18}$$

where

$$\bar{\lambda}_o = \frac{\Delta\bar{v}_o}{|\Delta\bar{v}_o|} \qquad \bar{\lambda}_m = \frac{\Delta\bar{v}_m}{|\Delta\bar{v}_m|} \qquad \bar{\lambda}_f = \frac{\Delta\bar{v}_f}{|\Delta\bar{v}_f|} \tag{4.19a, b, c}$$

$$\dot{\bar{\lambda}}_o = \varphi_{12}^{-1}(t_m, t_o)\left[\bar{\lambda}_m - \varphi_{11}(t_m, t_o)\,\bar{\lambda}_o\right] \tag{4.20}$$

$$\dot{\bar{\lambda}}_m^{-} = \varphi_{21}(t_m, t_o)\,\bar{\lambda}_o + \varphi_{22}(t_m, t_o)\,\dot{\bar{\lambda}}_o \tag{4.21}$$

$$\dot{\bar{\lambda}}_m^{+} = \varphi_{12}^{-1}(t_f, t_m)\left[\bar{\lambda}_f - \varphi_{11}(t_f, t_m)\,\bar{\lambda}_m\right] \tag{4.22}$$

5. Examine the primer history of the converged three-impulse trajectory by computing $\bar{\lambda}(t)$ from

$$\bar{\lambda}(t) = \varphi_{11}(t, t_o)\,\bar{\lambda}_o + \varphi_{12}(t, t_o)\,\dot{\bar{\lambda}}_o \qquad t_o \le t \le t_m \tag{4.23}$$

$$\bar{\lambda}(t) = \varphi_{11}(t, t_m)\,\bar{\lambda}_m + \varphi_{12}(t, t_m)\,\bar{\lambda}_m \qquad t_m \le t \le t_f \tag{4.24}$$

With $\bar{\lambda}_o$, $\bar{\lambda}_m$, $\dot{\bar{\lambda}}_o$, and $\dot{\bar{\lambda}}_m$ calculated as in Equations (4.19) to (4.21) in order to determine if necessary condition (3) is satisfied or if a fourth impulse should be added.

It should be noted that the above theory and procedure will calculate minimum impulse trajectories only between fixed initial and final states. In particular, the position at the final time is fixed throughout the convergence procedure. Therefore, at this point, in order to find the optimal transfer to a circular orbit at a given inclination about a body, for instance, one would have to vary the final position on a circle of desired magnitude and re-solve the problem until a minimum was found. Of course, the corresponding velocity at each new position to establish a circular orbit at that altitude must be supplied to complete the specification of the final state. Such a procedure is a cumbersome and time-consuming

method of attacking the problem. A much better way of handling variable end-point constraints will be discussed in Chapter 7.

Another version of the program was written which accepts a starting non-optimal three-impulse solution and begins convergence to the three-impulse optimal trajectory immediately. This procedure is useful if a previous problem has not fully converged. Also, some existing three-impulse solutions, the optimality of which may be of interest, do not readily derive from two-impulse solutions. An example of such a trajectory, which is investigated in Chapter 5, is a three-impulse trajectory from L_2 to the Earth with a powered lunar swingby.

The trajectory optimization method outlined above utilizes primer vector theory, an accelerated gradient functional minimization algorithm, and multi-conic trajectory propagation methods. The multi-conic methods are used to solve the numerous three-body initial and boundary value trajectory problems involved in the iteration so that an optimal trajectory can be found. For the purposes of generating the numerical optimization results of the next Chapter, the trajectory propagation routine used either the Earth-Moon or Moon-Earth multi-conic method from Section 3.1 (with a step size of 6 hours) and switched from one method to the other according to whether the spacecraft was moving toward or away from the Moon. The radial velocity of the spacecraft relative to the Moon was calculated prior to each step in the propagation; if the spacecraft was moving toward the Moon, the Earth-Moon method was used for the next step, and if the spacecraft was moving away from the Moon, the Earth-Moon method was used.

CHAPTER 5
NUMERICAL RESULTS

5.1 Coordinate System, Image Trajectories, and Dimensionless Units

The basic coordinate system in which most of the results will be displayed is a rotating barycentric coordinate system. The origin of this coordinate system is at the Earth-Moon barycenter point. The x-axis points along the Earth-Moon line towards the Moon; the z-axis is perpendicular to the Earth-Moon plane and points in the direction of the Moon's angular momentum vector; and the y-axis is in the Earth-Moon plane so as to form a right-handed system. This coordinate system and the L_2 libration point are shown in Figure 4.

Miele has shown[21] that for every trajectory which exists in this coordinate system there are three image trajectories, one with respect to the xy plane, one with respect to the xz plane, and one with respect to the x-axis. Let the position and velocity on the original trajectory be given by

$$\bar{r}(t) = \begin{bmatrix} x(t) \\ y(t) \\ z(t) \end{bmatrix} \tag{5.1}$$

$$\bar{v}(t) = \begin{bmatrix} \dot{x}(t) \\ \dot{y}(t) \\ \dot{z}(t) \end{bmatrix} \tag{5.2}$$

where $t_o \leq t \leq t_f$. Then the position and velocity for the image with respect to the xy plane may be defined as

$$\bar{r}(t) = \begin{bmatrix} x(t) \\ y(t) \\ -z(t) \end{bmatrix} \tag{5.3}$$

Fig. 4 ROTATING BARYCENTRIC COORDINATE SYSTEM

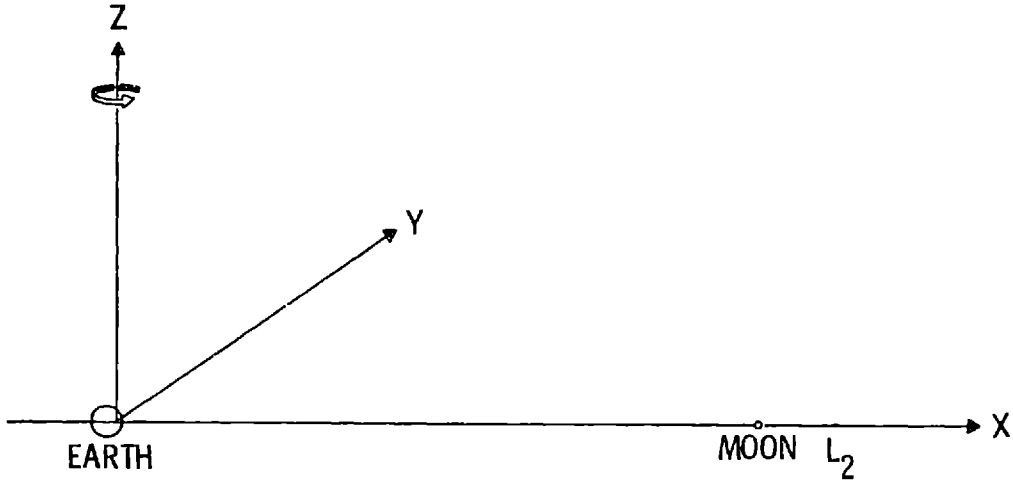

$$\bar{v}(t) = \begin{bmatrix} \dot{x}(t) \\ \dot{y}(t) \\ -\dot{z}(t) \end{bmatrix} \tag{5.4}$$

For the image with respect to the xz plane, the position and velocity are

$$\bar{r}(t) = \begin{bmatrix} x(t') \\ -y(t') \\ z(t') \end{bmatrix} \tag{5.5}$$

$$\bar{v}(t) = \begin{bmatrix} -\dot{x}(t') \\ \dot{y}(t) \\ -\dot{z}(t') \end{bmatrix} \tag{5.6}$$

where

$$t' = t_o + t_f - t \tag{5.7}$$

Finally, for the image with respect to the x-axis, the position and velocity are given by

$$\bar{r}(t) = \begin{bmatrix} x(t') \\ -y(t') \\ -z(t') \end{bmatrix} \tag{5.8}$$

$$\bar{v}(t) = \begin{bmatrix} -\dot{x}(t') \\ \dot{y}(t') \\ z(t') \end{bmatrix} \tag{5.9}$$

with t' defined as in Equation (5.7). In the case of a trajectory which remains totally in the xy plane, the images with respect to the xz plane and the x-axis are identical, as are the original trajectory and the image with respect to the xy plane. The image with respect to the xy plane is flown in the same sense as the original trajectory and the images with respect to the xz plane and the x-axis are flown in the opposite sense

(the initial and final points are interchanged).

This knowledge of image trajectories is useful for two reasons. First of all, whenever the solution to a boundary value problem is found, three other trajectories are established as well, one or more of which may be of interest. For instance, in order to find the particular point on a circular orbit about the Moon from which to leave via a tangential impulse to arrive at L_2 in a given transfer time, the boundary value problem from L_2 to a given position magnitude with no radial velocity is solved as explained in Section 3.3 with the desired position magnitude set according to the altitude of the circular orbit. Since this trajectory is an image of the desired trajectory, the problem can be solved in this manner although it could not be solved in its original form, since both options of the boundary value routine assume a fixed initial position.

The second reason image trajectories are useful is that even though it may be possible to solve a boundary value problem as stated, it may be more advantageous in terms of minimizing convergence difficulties to solve for an image trajectory instead.

The system of units in the computer programs is dimensionless and is defined as follows: the unit of mass is the sum of the masses of the Earth and the Moon; the unit of distance is the Earth-Moon distance; and the unit of time is the period of the Moon's orbit divided by 2π so that the angular velocity of the Earth-Moon line is unity. Conversion factors are given below:

1 UNIT OF DISTANCE	=	384410 km
1 UNIT OF TIME	=	104.362 hrs
1 UNIT OF VELOCITY	=	1023.17 m/sec

In this system of units, the gravitational parameter of the Moon is μ ($\cong$ .01215), and the gravitational parameter of the Earth is $1 - \mu$. In the rotating barycentric coordinate system (Figure 4), the Earth is situated in the xy plane at $(-\mu, 0)$ and the Moon is at $(1-\mu, 0)$. The L_2 libration

point is approximately at the point (1.156, 0).

All trajectories in this Chapter start at the L_2 libration point and end at either the Moon or the Earth; all trajectories are in the Earth-Moon plane. Trajectories from a body to L_2 are found by forming the image which is a reflection about the x-axis.

5.2 Two-Impulse Trajectories Between the Moon and L_2

The modified three-body Lambert routine for solving boundary value problems was used to find a family of relatively fast trajectories between the L_2 libration point and a 185.2 km (100 nautical mile) circular orbit about the Moon. The first impulse at L_2 is the difference between the velocity the spacecraft has at L_2 and the velocity required to transfer to the Moon. The required velocity at L_2 comes from the solution to the boundary value problem. The second impulse occurs at the Moon and establishes the spacecraft in a circular orbit. The routine was used in the mode which converges to a desired position magnitude with no radial velocity and zero inclination. Therefore the impulse at the Moon is tangential.

Trajectories were found for transfer times from 48 to 100 hours. Three of these trajectories are shown in Figure 5, and the transfer time, the magnitudes of the impulses at L_2, and the departure and arrival angles are indicated for each.

Only the magnitude of the impulse at L_2 will be plotted versus transfer time because minimizing this impulse minimizes the total cost, which includes the impulse at the Moon. Jacobi's integral for the three-body problem may be written as

$$2V^2 - U(R, r) = C \qquad (5.10)$$

where V is the velocity of the spacecraft in the rotating barycentric coordinate system; U(R, r) is the potential function; and C is a constant.

Fig. 5
FAST TWO-IMPULSE TRAJECTORIES BETWEEN THE MOON AND L_2

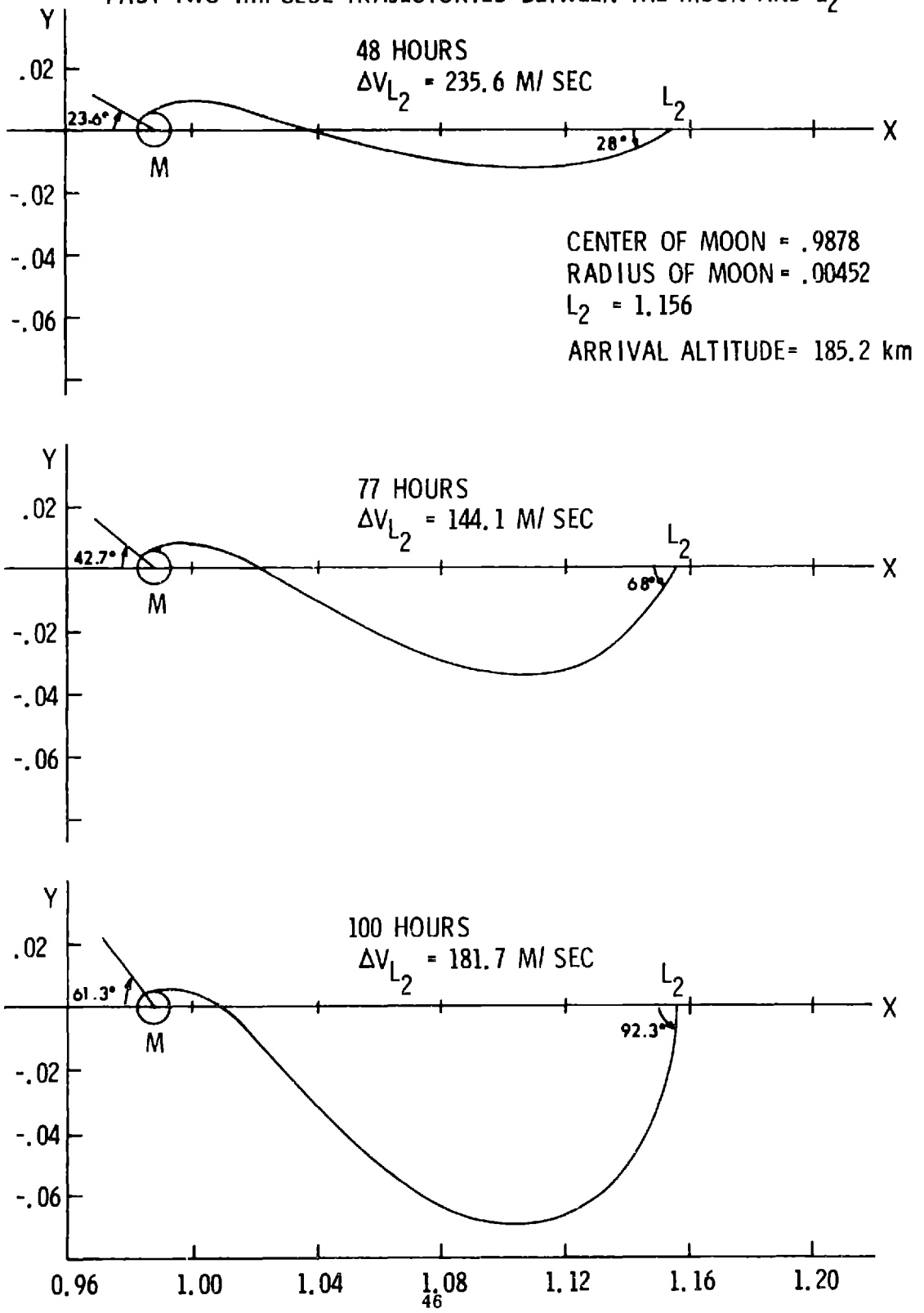

In the rotating coordinate system, the velocity of the spacecraft before the impulse at L_2 is zero, and therefore the velocity after the impulse has the same magnitude as the impulse itself. Writing Equation (5.10) at the initial and final times, we have

$$2V_o^2 - U_o = C \tag{5.11}$$

$$2V_f^2 - U_f = C \tag{5.12}$$

Substituting for C in Equation (5.12) from Equation (5.11) results in

$$2V_f^2 = 2V_o^2 + U_f - U_o \tag{5.13}$$

Now the potential U is a function only of the magnitudes of the position vectors relative to the Earth and Moon[12]. Since all these trajectories are required to be exactly the same distance from the Moon at the final time and since, to a good approximation, they are the same distance from the Earth, the quantity U_f has the same value for all trajectories. Certainly the quantity U_o is the same for all trajectories because they all have the same initial point. Therefore, from Equation (5.13), if V_o is minimized (remember that V_o has the same magnitude as the impulse at L_2) then V_f is minimized. Minimizing the magnitude of the impulse at L_2 minimizes the magnitude of the arrivel velocity at the Moon. Since the impulse at the Moon for all these trajectories is a tangential one which merely slows the spacecraft, then minimizing the magnitude of the arrival velocity minimizes the magnitude of the final impulse. Through a logical chain of reasoning it has been shown that minimizing the impulse at L_2 minimizes the impulse at the Moon and therefore also the total cost. The same argument applies to trajectories from L_2 to the Earth.

In Figure 6, the magnitude of the impulse at L_2 and the departure and arrival angles are plotted versus transfer time. With the information presented on the two plots of Figure 6, anyone could reproduce any of these trajectories as solutions to boundary value problems. The minimum two-impulse transfer for this family occurs at about 77 hours. The impulse

Fig. 6
ΔVs AND DEPARTURE AND ARRIVAL ANGLES FOR FAST TWO - IMPULSE TRAJECTORIES BETWEEN THE MOON AND L_2

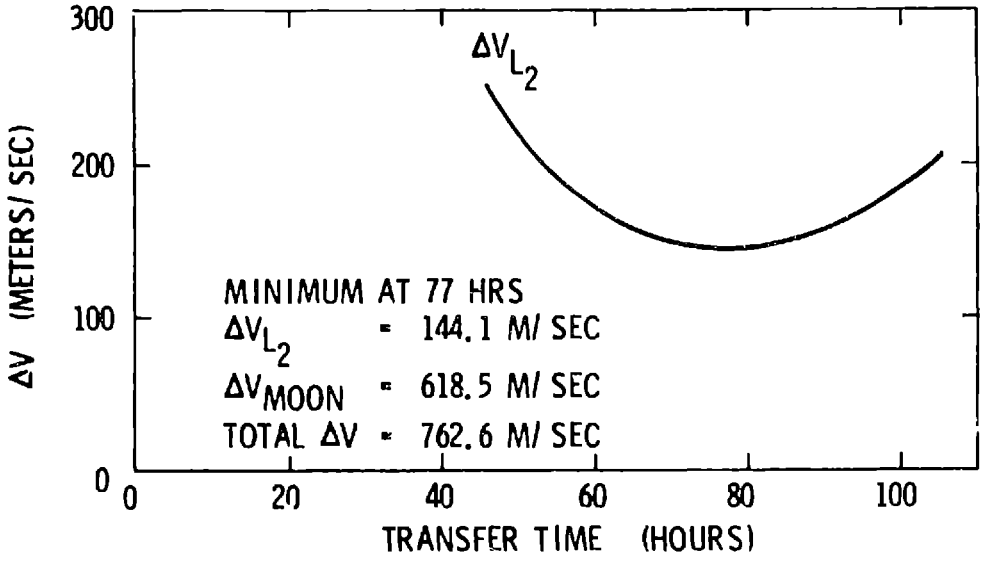

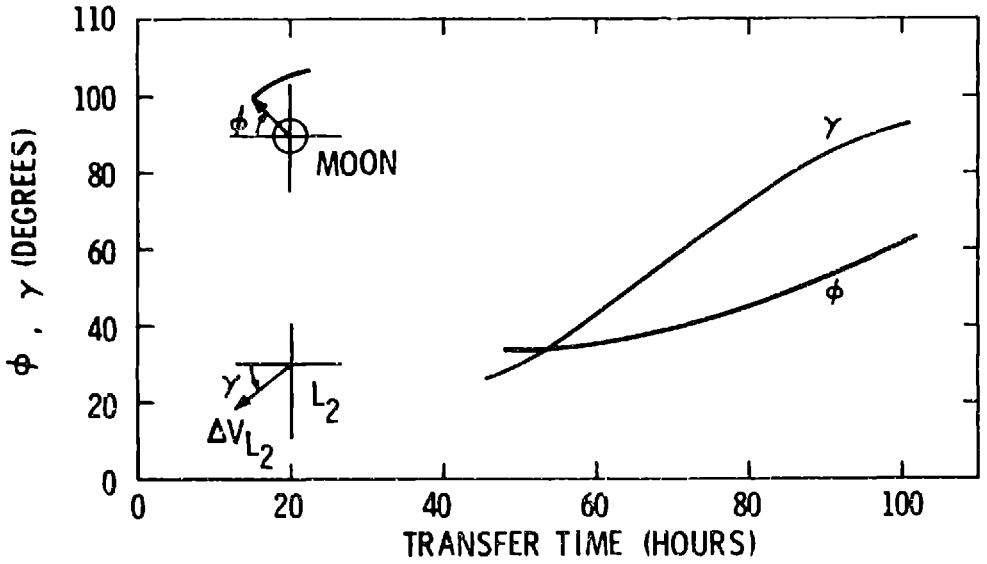

at L_2 is 144.1m/sec, the impulse at the Moon is 618.5m/sec, and the total cost is thus 762.6m/sec.

The three trajectories in Figure 5 correspond to transfer times less than, equal to, and greater than the transfer time for the minimum two-impulse transfer. By computing the primer vector histories for these trajectories, we can determine if an additional impulse will decrease the total cost. If the magnitude of the primer vector rises above unity anywhere between the initial and final times, adding an impulse will decrease the total cost. The primer histories for the three trajectories in Figure 5 are given in Figure 7.

Note, first of all, that the derivative of the primer magnitude at the initial time is zero for the minimum two-impulse 77 hour transfer. Although it can not be seen on the figure, the derivative is zero at the final time also. This situation is true of all minimums with respect to time of flight. The primer history indicates that either increasing or decreasing the transfer time by slightly changing the initial or final times will not affect the cost since the primer magnitude approaches unity asymptotically at both the initial and final times. Since the cost is a minimum at 77 hours, the gradient of the cost with respect to transfer time is indeed zero at this transfer time.

Secondly, it appears that trajectories in this family with transfer times less than or equal to that of the minimum satisfy all the necessary conditions and are locally optimal, while trajectories with transfer times greater than that of the minimum are not. This is true because for two-impulse solutions, the necessary conditions are also sufficient conditions as has been shown by Lion[22]. These non-optimal trajectories can be improved by an additional impulse in the direction of the primer vector at its maximum. However, because the primer vector history for the transfer time which yields the minimum cost does not rise above unity, there exists no three-impulse solution which requires less cost in the neighborhood of this two-impulse solution. The minimum two-impulse solution is locally optimal. From Chapter 2 it is true that for primer

FIG. 7
PRIMER HISTORIES FOR FAST TWO-IMPULSE TRAJECTORIES BETWEEN THE MOON AND L_2

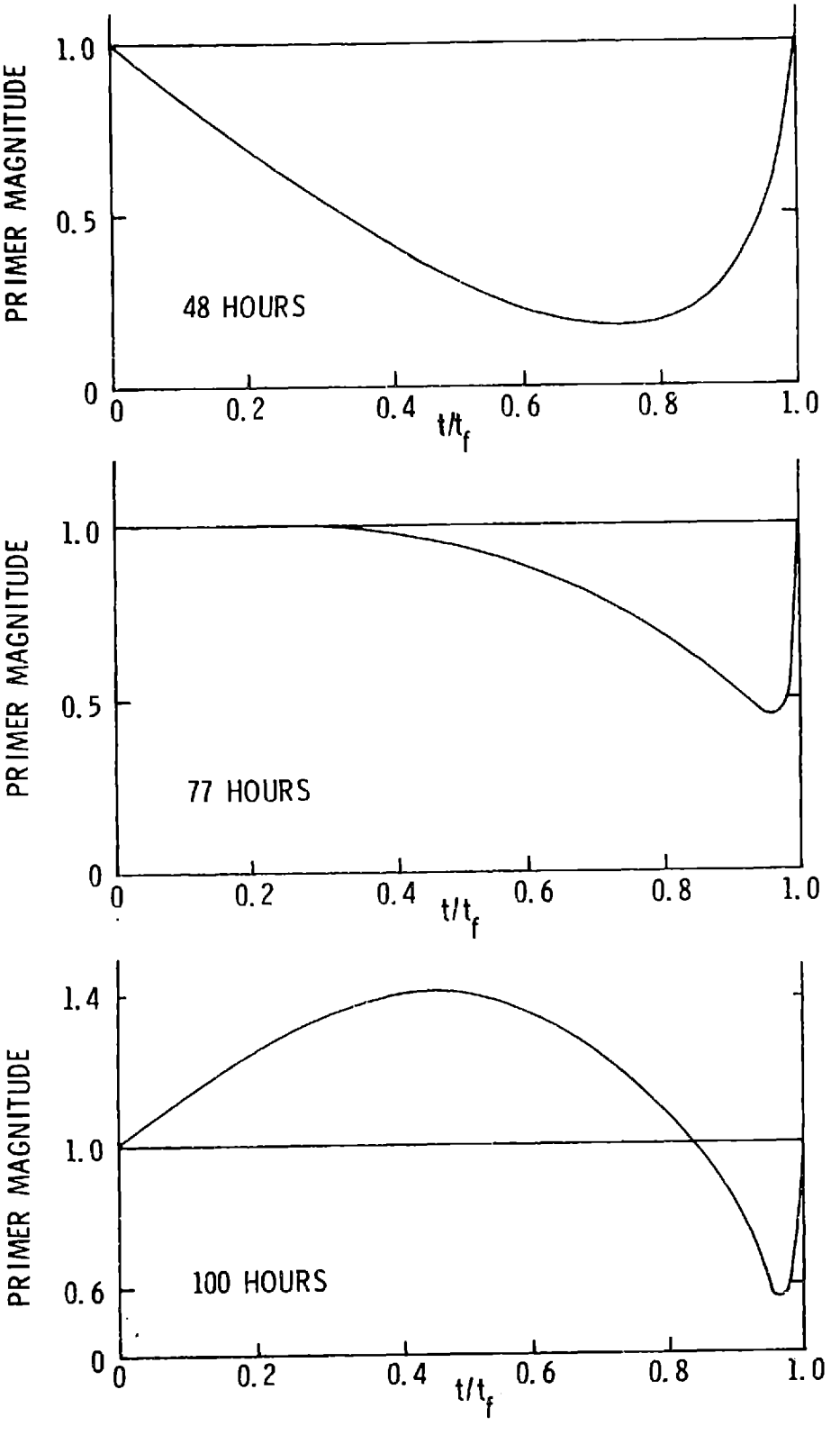

vector histories of the type which occurred for the 100 hour transfer, the cost can be improved by an initial coast. If a third impulse were added for the 100 hour transfer at the maximum of the primer magnitude and an iteration started to converge to an optimal three-impulse solution, what would occur is that the interior impulse would grow in magnitude and the initial impulse would decrease and eventually disappear. The optimal solution for 100 hours is to coast for 23 hours (remain at L_2) and then apply an impulse to transfer to the Moon in 77 hours. For any time of flight greater than that of the minimum two-impulse solution, it appears that the optimal trajectory consists of an initial coast until the time remaining is equal to the transfer time of the minimum two-impulse trajectory and then a minimum two-impulse transfer.

Thus for this fast family of trajectories between the Moon and L_2, a minimum two-impulse trajectory with a total cost of 762.6m/sec is locally optimal. There exists no neighboring three-impulse solution which requires less cost than the minimum two-impulse solution since the primer vector magnitude remains below unity over the entire transfer time.

A family of slower two-impulse trajectories between the Moon and L_2 which have smaller ΔV requirements will be investigated next. There does exist[10] a third family of trajectories which arrive at the trailing side of the Moon (negative φ), but these trajectories have even higher ΔV requirements than the fast trajectories already discussed and for that reason they were not investigated.

Trajectories from the slower family of two-impulse transfers between the Moon and L_2 were generated for transfer times ranging between 209 and 254.4 hours. These transfers are quite slow compared to the family discussed above. Three of the trajectories are plotted on Figure 8: one for a transfer time below the minimum, one for the transfer which yields the minimum cost, and one for a transfer time greater than the minimum. The ΔV requirement at L_2 as a function of transfer time and the departure and arrival angles are given on Figure 9. The minimum

FIG. 8
SLOW TWO-IMPULSE TRAJECTORIES BETWEEN THE MOON AND L_2

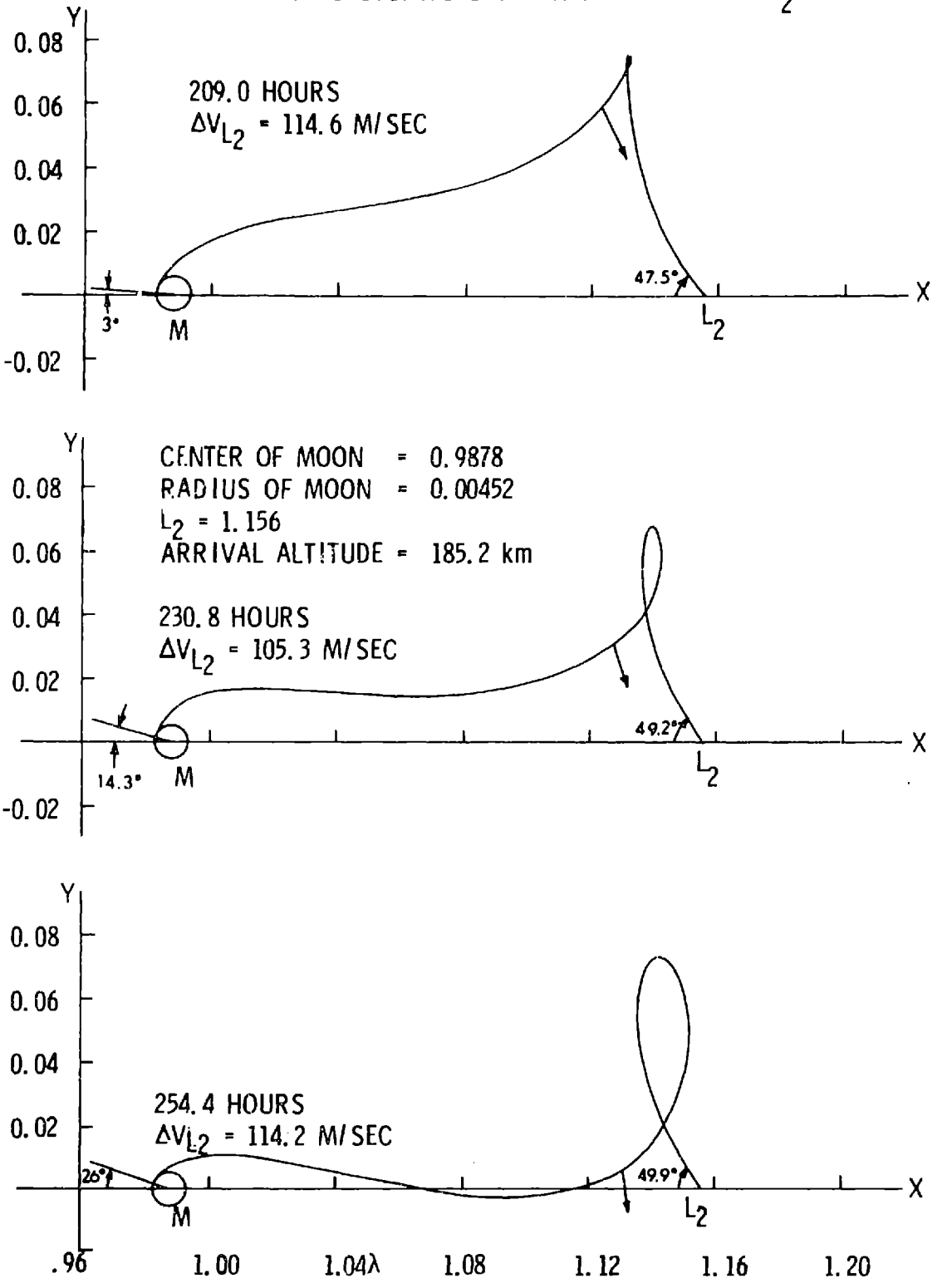

FIG. 9
ΔV'S AND DEPARTURE AND ARRIVAL ANGLES FOR SLOW TWO-IMPULSE TRAJECTORIES BETWEEN THE MOON AND L_2

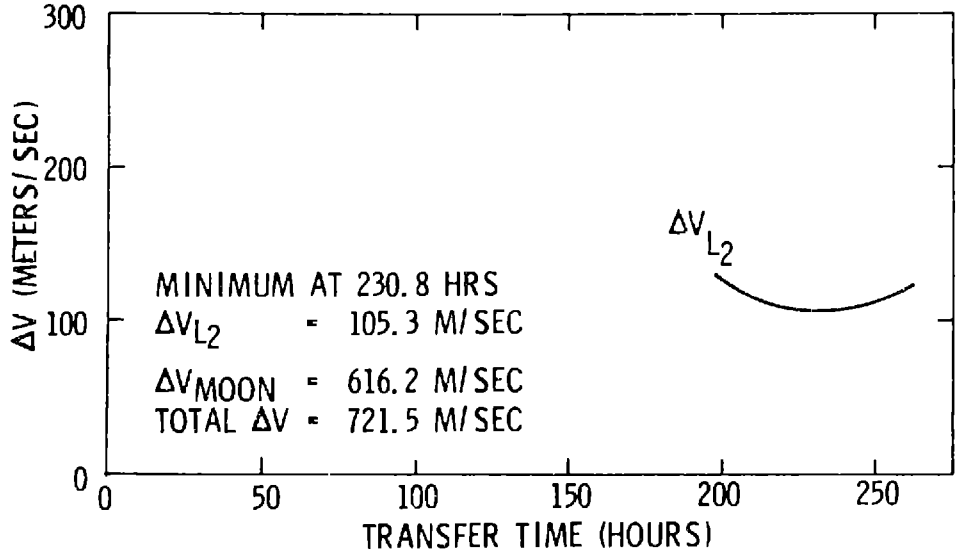

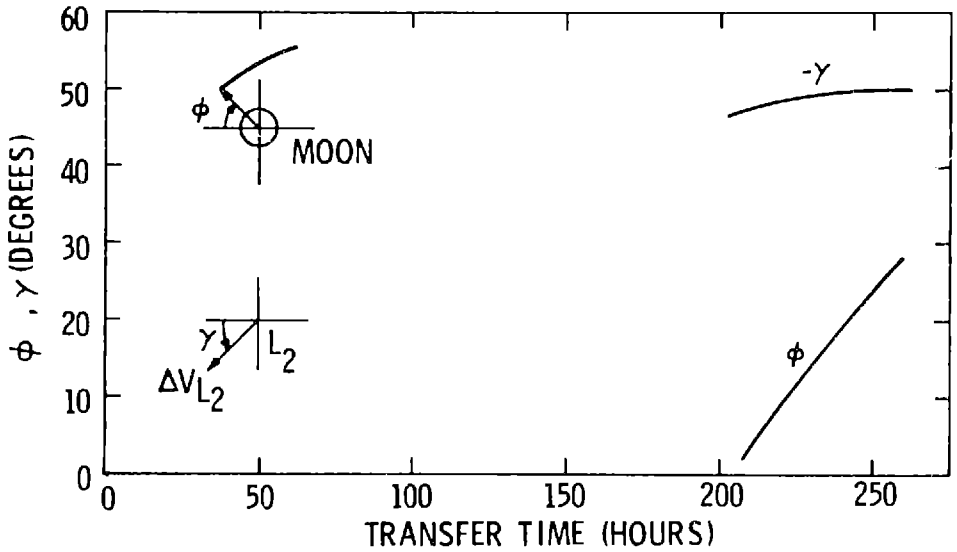

two-impulse trajectory for this family has a transfer time of about 230.8 hours. The required impulse at L_2 is 105.3m/sec; the impulse at the Moon is 616.2m/sec; the total cost is thus 721.5m/sec. These values compare to 144.1m/sec, 618.5m/sec, and 762.6m/sec for the minimum two-impulse solution for the fast family discussed previously. The minimum two-impulse solution for the slow family is 5.4% cheaper in total cost than that for the fast family. The impulse at L_2 is 26.9% smaller. It appears that all the trajectories in this family have a distinctive cusp or loop when plotted in the rotating barycentric coordinate system.

The primer vector histories for the three trajectories shown in Figure 8 are given in Figure 10. When compared to the primer vector histories of the fast family (Figure 7), certain similarities appear. Note once again that the primer history for the minimum two-impulse transfer necessarily has a zero derivative at the initial time (and also, although unapparent, at the final time) since it is a minimum with respect to time of flight. All trajectories with times of flight greater than that of the minimum can be improved by an initial coast since the primer magnitude rises above unity immediately after the initial impulse.

However it can clearly be seen that none of the primer vector histories satisfy the necessary conditions for a local optimum. From the behavior of the three primer histories on Figure 10, it appears that primer histories for trajectories with transfer times less than that of the minimum have one maximum above unity. Also trajectories with transfer times greater than that of the minimum will have two maximums. The first is always above unity and the second will be above unity up to some transfer time, as yet undetermined, but greater than 254.4 hours, at which the second maximum will be exactly equal ato 1. Beyond this undetermined transfer time, the second maximum will be below unity. The arrows on Figure 8 show the location, direction, and magnitude of the primer vector at the second maximum. The third impulse would be added in this direction.

Most importantly, it should be noted that the primer history for the minimum two-impulse solution does not satisfy the necessary conditions

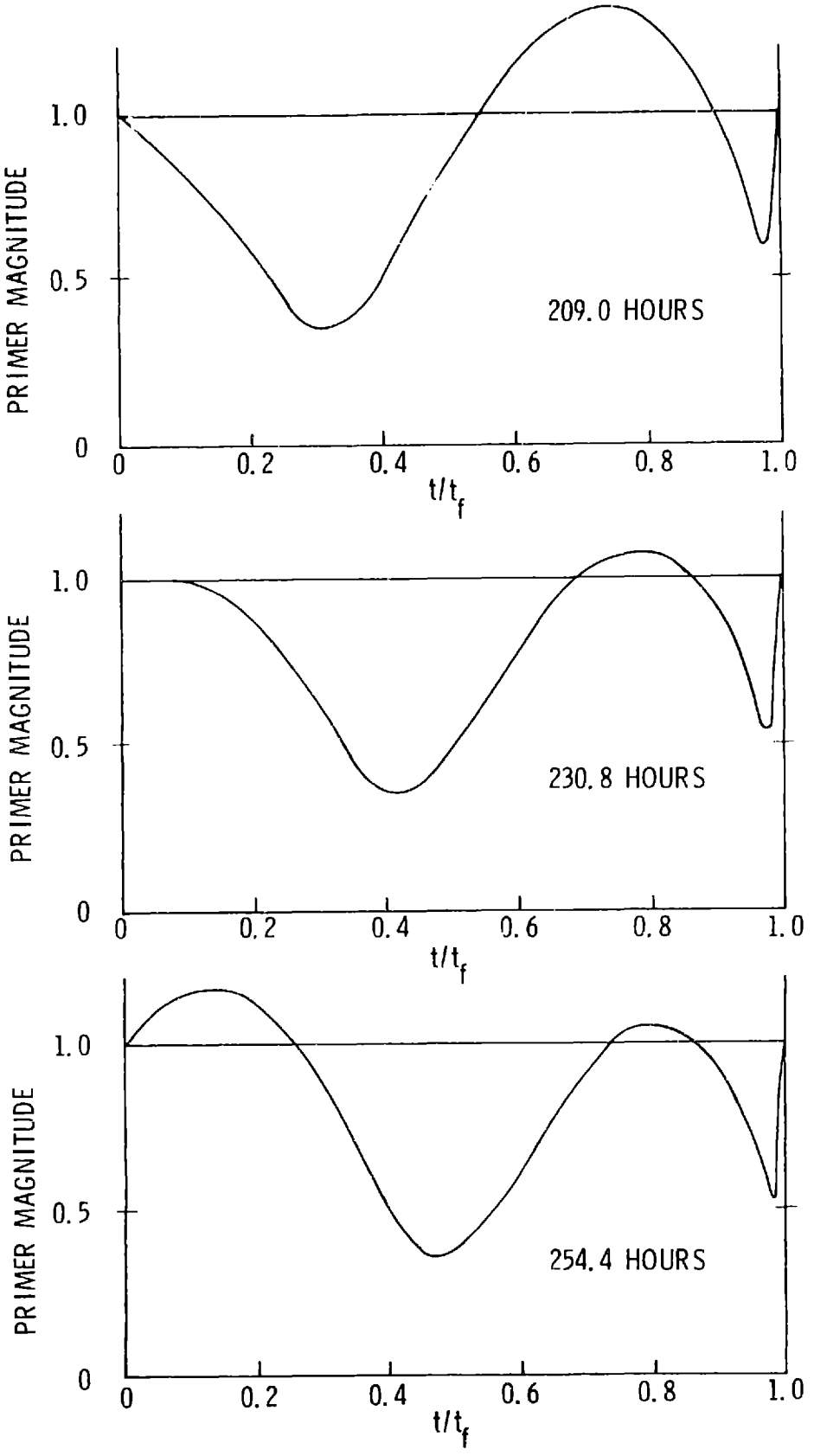

Fig. 10
PRIMER HISTORIES FOR SLOW TWO-IMPULSE TRAJECTORIES BETWEEN THE MOON AND L_2

for a local optimum because the second maximum is still above unity. Thus there does exist a neighboring three-impulse solution which requires less cost than the minimum two-impulse solution for this slow family. Recall that the minimum two-impulse solution for the fast family was locally optimal. It is believed that the three-impulse solutions which can be derived from the non-optimal minimum two-impulse solutions at 230.8 hours have never before been investigated. Some of these trajectories are discussed in the following Section.

5.3 Three-Impulse Trajectories Between the Moon and L_2

The minimum impulse program was used to add a third impulse to the non-optimal minimum two-impulse solution of the previous Section and converge to a minimum three-impulse solution. Pictured in Figure 11 are three trajectories. The top one is the non-optimal minimum two-impulse solution. The middle trajectory is the starting three-impulse solution which results from adding a small impulse of chosen magnitude in the direction of the primer vector at its maximum on the non-optimal minimum two-impulse solution. The bottom trajectory is the solution to which the minimum impulse program converged. Note that the loop has disappeared in the converged three-impulse trajectory.

The arrows in the figure give the location, direction, and magnitude of the primer vector at the interior impulse. For the non-optimal minimum two-impulse trajectory the arrow points in the direction that an impulse would be added. Hence the direction and location are the same for the upper two trajectories. The magnitude of the primer vector at the interior impulse is necessarily equal to 1 for the lower two trajectories. The minimum two impulse trajectory differs very little from the starting three-impulse trajectory since the magnitude of the interior impulse is small.

The minimum two-impulse trajectory had a 105.3m/sec impulse at L_2 and a 616.2m/sec impulse at the Moon for a total cost of 721.5m/sec (see Figure 9). The converged three-impulse trajectory has a 6.7 m/sec impulse at L_2, a 94.1m/sec impulse 185.8 hours after leaving L_2, and a

FIG. 11 TWO AND THREE-IMPULSE TRAJECTORIES BETWEEN THE MOON AND L_2

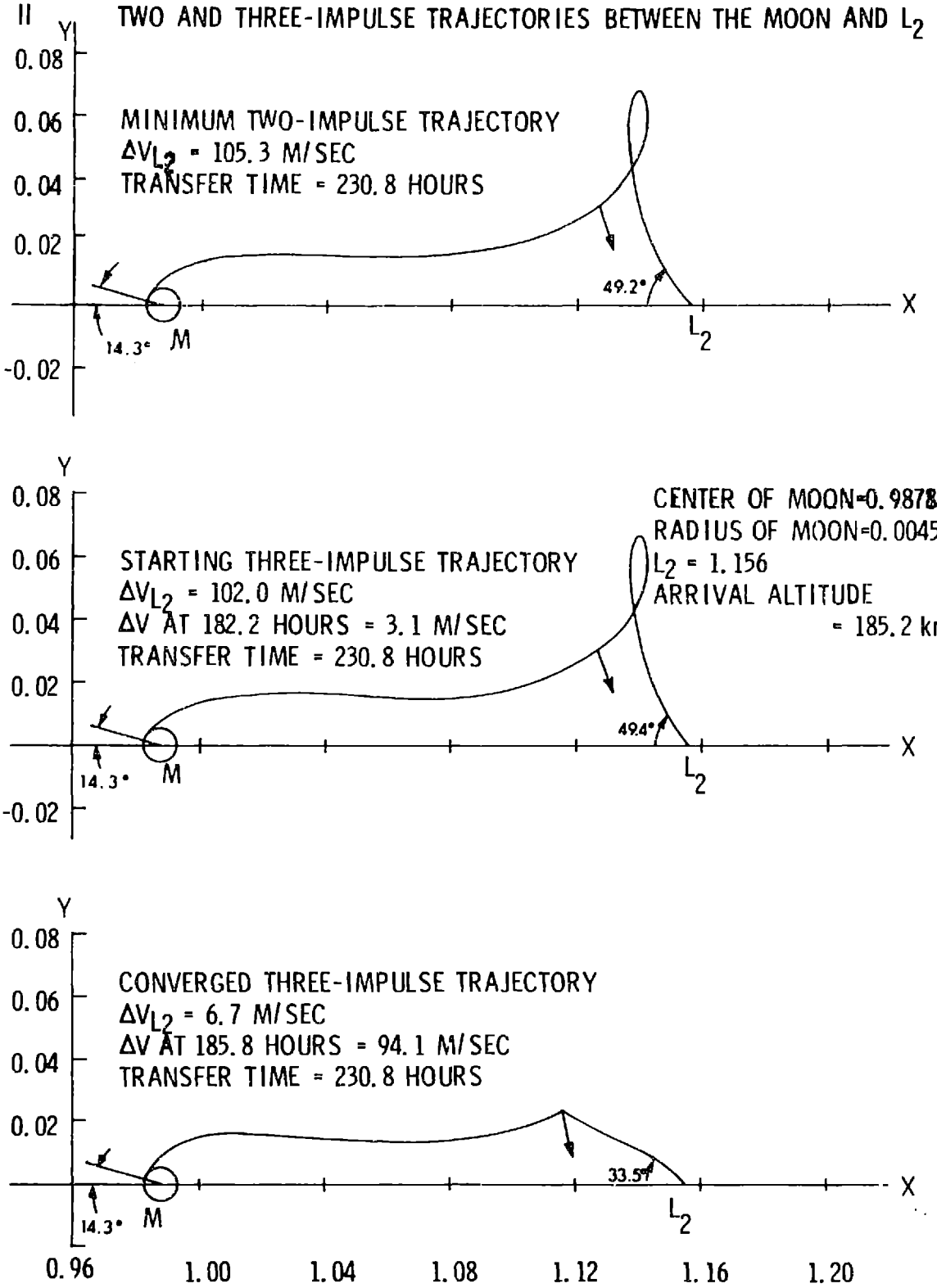

612.9m/sec impulse at the Moon, for a total cost of 713.7m/sec. The total cost is 1.1% cheaper whereas, excluding the impulse at the Moon, the improvement is 4.3%. Comparing the starting three-impulse trajectory to the converged three-impulse trajectory, one can see that the interior impulse has grown to almost the magnitude of the original impulse at L_2. Consequently the impulse at L_2 has become quite small.

The primer histories associated with the three trajectories in Figure 11 are given in Figure 12. Note that the primer histories for the minimum two-impulse solution and the starting three-impulse solution do not satisfy the necessary conditions. However, the primer history for the converged three-impulse solution does. For two-impulse solutions the necessary conditions are also sufficient for a local two-impulse optimum as was noted in the previous Section. For three-impulse solutions the necessary conditions are not sufficient for a local three-impulse optimum[22]. However, satisfaction of these necessary conditions in conjunction with an accelerated gradient search procedure does yield a sufficiency condition for for three impulses except under unusual circumstances. The Jacobson-Oksman algorithm iterates to reduce the cost function at each step such that a minimum is eventually found. If a neighboring three-impulse solution existed which also satisfied the primer necessary conditions but was not a local minimum (such as a saddle-point), the algorithm would almost certainly not converge to it, because an accelerated gradient search procedure reduces the cost at each step and cannot normally converge to anything but a local minimum. It can also be stated that since the primer magnitude for the converged three-impulse solution does not exceed unity, there exists no neighboring four-impulse solution with less cost.

Recall that the minimum impulse program finds the trajectory with minimum total cost with respect to the time and position of the interior impulse by iterating to force the primer derivative to be continuous and to force the derivative of the primer magnitude to be equal to zero at the interior impulse. The theory requires that the initial and final states and the transfer time be fixed during the iteration. Actually, if one desires that at the final time (immediately after the final impulse) the

FIG. 12 PRIMER HISTORIES FOR TWO AND THREE-IMPULSE TRAJECTORIES BETWEEN THE MOON AND L_2

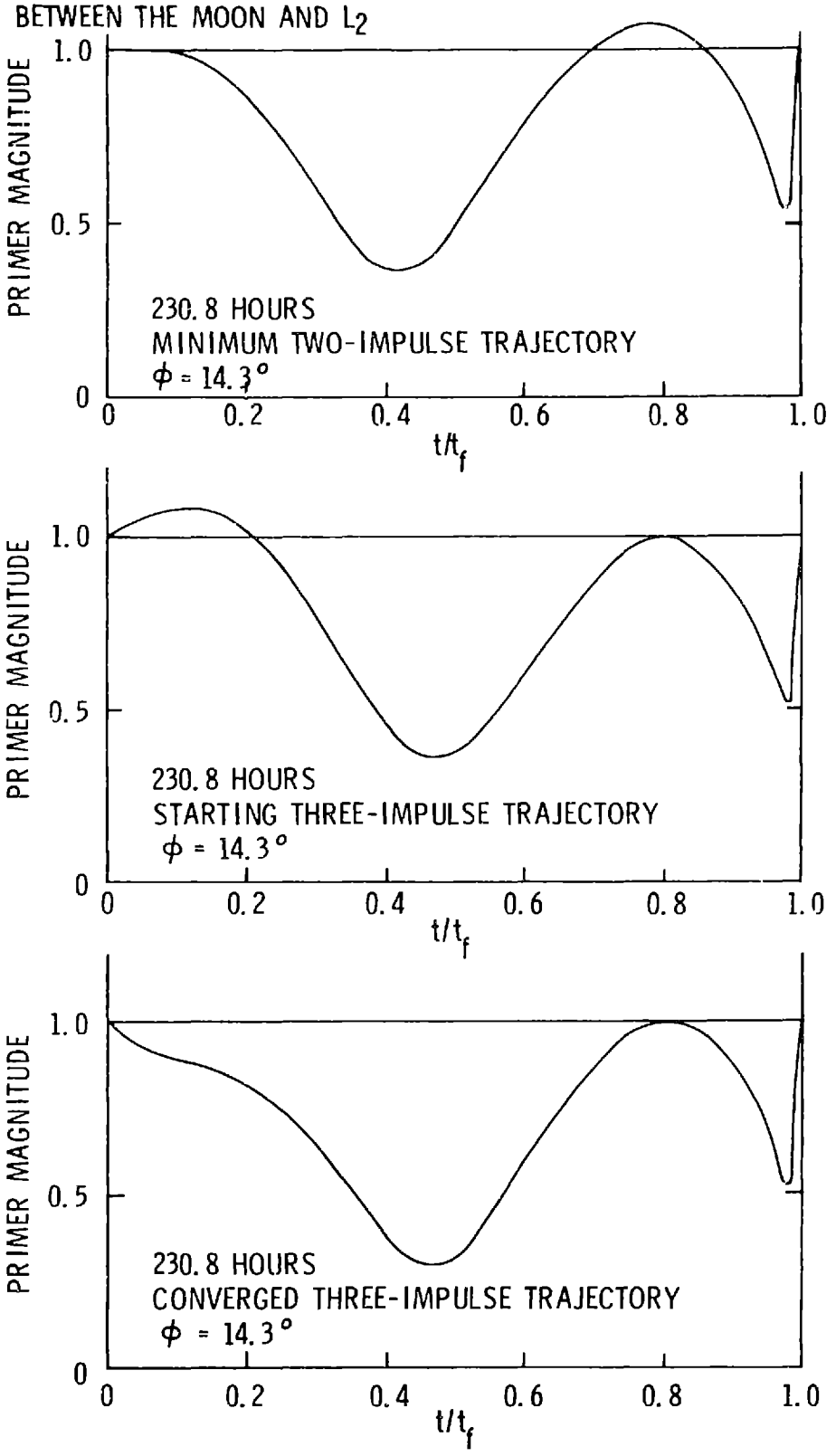

spacecraft be in a circular orbit of desired altitude, then the position vector at the final time may have any arrival angle as long as the circular orbit is attained. In other words, the point on a circle of specified distance from the body at which the circular orbit is entered is not fixed. The problem may be re-solved with different fixed final states determined by varying the arrival angle φ while keeping the altitude fixed at 185.2 km, and a minimum may be found over a set of converged three-impulse solutions. This was done and it was found that the original converged three-impulse solution ($\varphi = 14.3^{\circ}$) was the minimum of total cost with respect to arrival angle. The derivative of the primer magnitude at the initial time for this converged three-impulse trajectory is negative as can be seen in Figure 12. For a minimum with respect to transfer time, it is zero (see Figures 7 and 10). This indicates that lengthening the transfer time will improve the total cost. Ideally for various transfer times the minimum with respect to arrival angle should be found and then the minimum of this set of solutions would give the minimum three-impulse transfer between L_2 and a 185.2 km circular orbit about the Moon. Another method would be to reformulate the iteration to include variable end conditions, as is done in Chapter 7.

Since the final position is fixed during the iteration, the final impulse is not necessarily tangential as it was for the minimum two-impulse solution. The final state may be pre-periseleneum or post-periseleneum. The converged three-impulse trajectory for an arrival angle of 14.3° nevertheless arrives almost exactly at periseleneum.

A short list of several L_2 to Moon trajectories and their costs is given below:

	Trajectory	Total Cost (m/sec)
1.	Minimum Two-Impulse Solution: Fast Family	762.6
2.	Minimum Two-Impulse Solution: Slow Family	721.5
3.	Converged Three-Impulse Solution	713.7

5.4 Two-Impulse Trajectories Between the Earth and L_2

A family of two-impulse trajectories between L_2 and a 185.2 km altitude circular orbit about the Earth was generated. These trajectories have transfer times ranging from 100 to 200 hours. Three trajectories, for transfer times below, at, and above the minimum, are given in Figure 13. Also indicated on the figure are the transfer times, the magnitudes of the impulses at L_2 and the departure and arrival angles. The ΔV requirement at L_2 and the departure and arrival angles as a function of transfer time are given on Figure 14. The minimum two-impulse transfer for this family occurs at about 150 hours. The required impulse at L_2 is 1098.4 m/sec, the impulse at the Earth is 3145.9m/sec, and the total cost is 4244.3m/sec.

The primer vector histories for the three trajectories of Figure 13 are given on Figure 15. The same situation exists for this family of trajectories as existed for the fast family of two-impulse transfers to the Moon. Trajectories with times of flight less than that of the minimum two-impulse solution are locally optimal since the necessary conditions for the primer history are satisfied. Trajectories with times of flight greater than that of the minimum are not locally optimal and their cost can be reduced to that of the minimum by an initial coast. Most importantly, the primer history for the minimum two-impulse solution does satisfy the necessary conditions for a local optimum. Recall that for the two-impulse case, the necessary conditions are also sufficient. Therefore there exists no neighboring three-impulse solution which requires less cost than the minimum two-impulse solution. For this family of trajectories, a two-impulse solution with a transfer time of 150 hours and a total cost of 4244.3m/sec is locally optimal.

No other families of two-impulse transfers between the Earth and L_2 were investigated but a family of three-impulse trajectories is studied in the next Section.

FIG. 13 TWO-IMPULSE TRAJECTORIES BETWEEN THE EARTH AND L_2

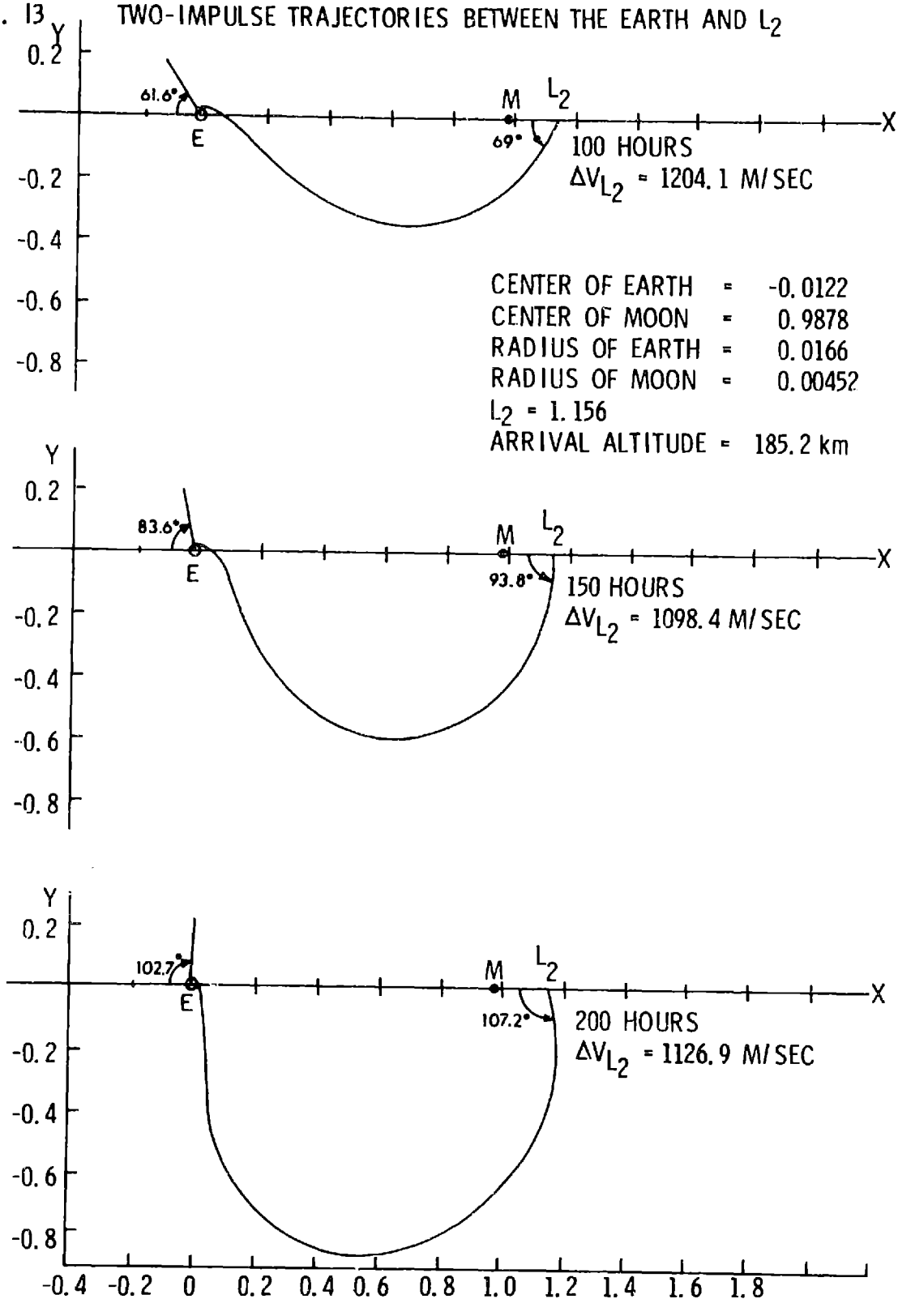

FIG. 14
ΔV'S AND DEPARTURE AND ARRIVAL ANGLES FOR TWO-IMPULSE TRAJECTORIES BETWEEN THE EARTH AND L_2

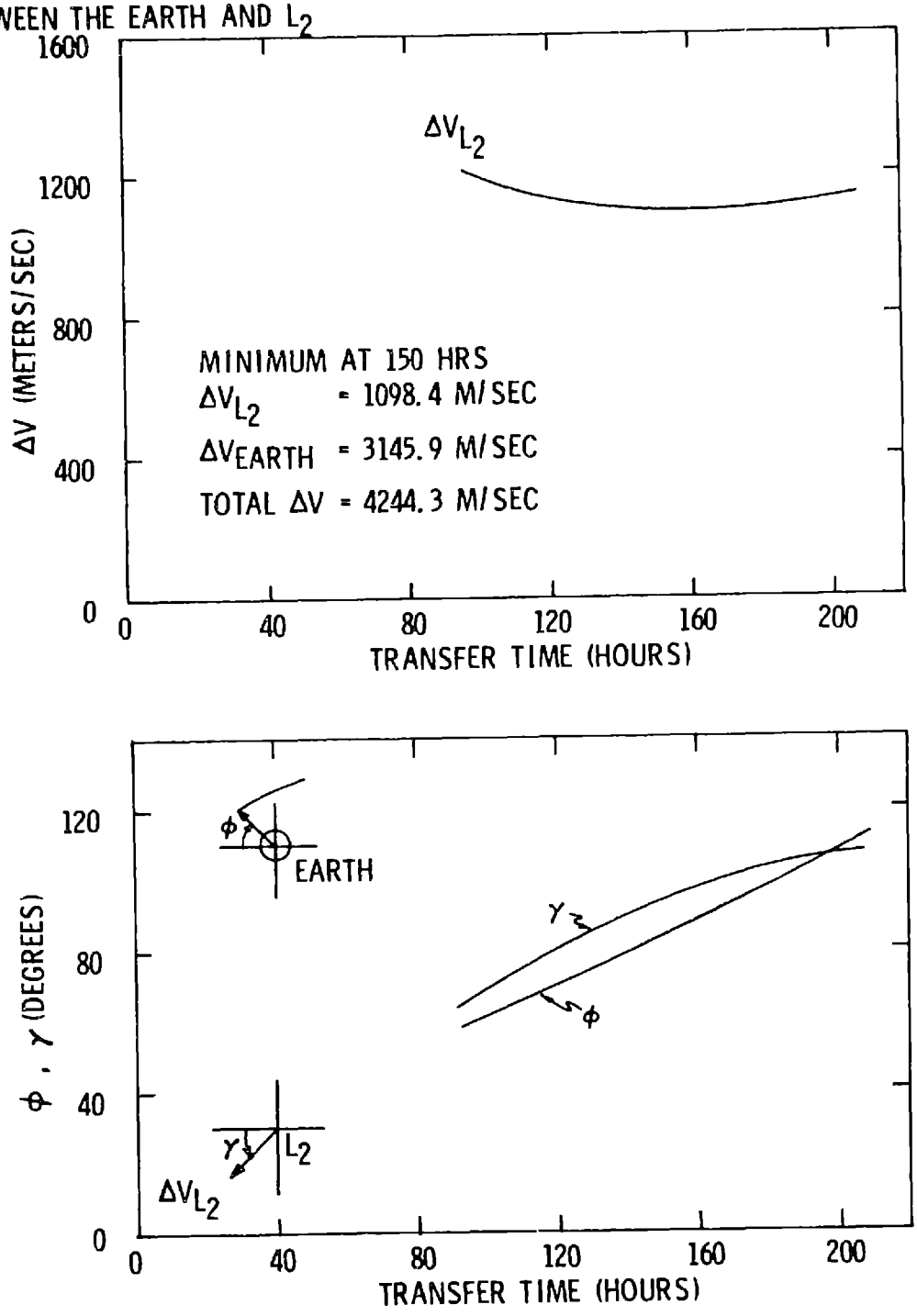

FIG. 15
PRIMER HISTORIES FOR TWO-IMPULSE TRAJECTORIES BETWEEN THE EARTH AND L_2

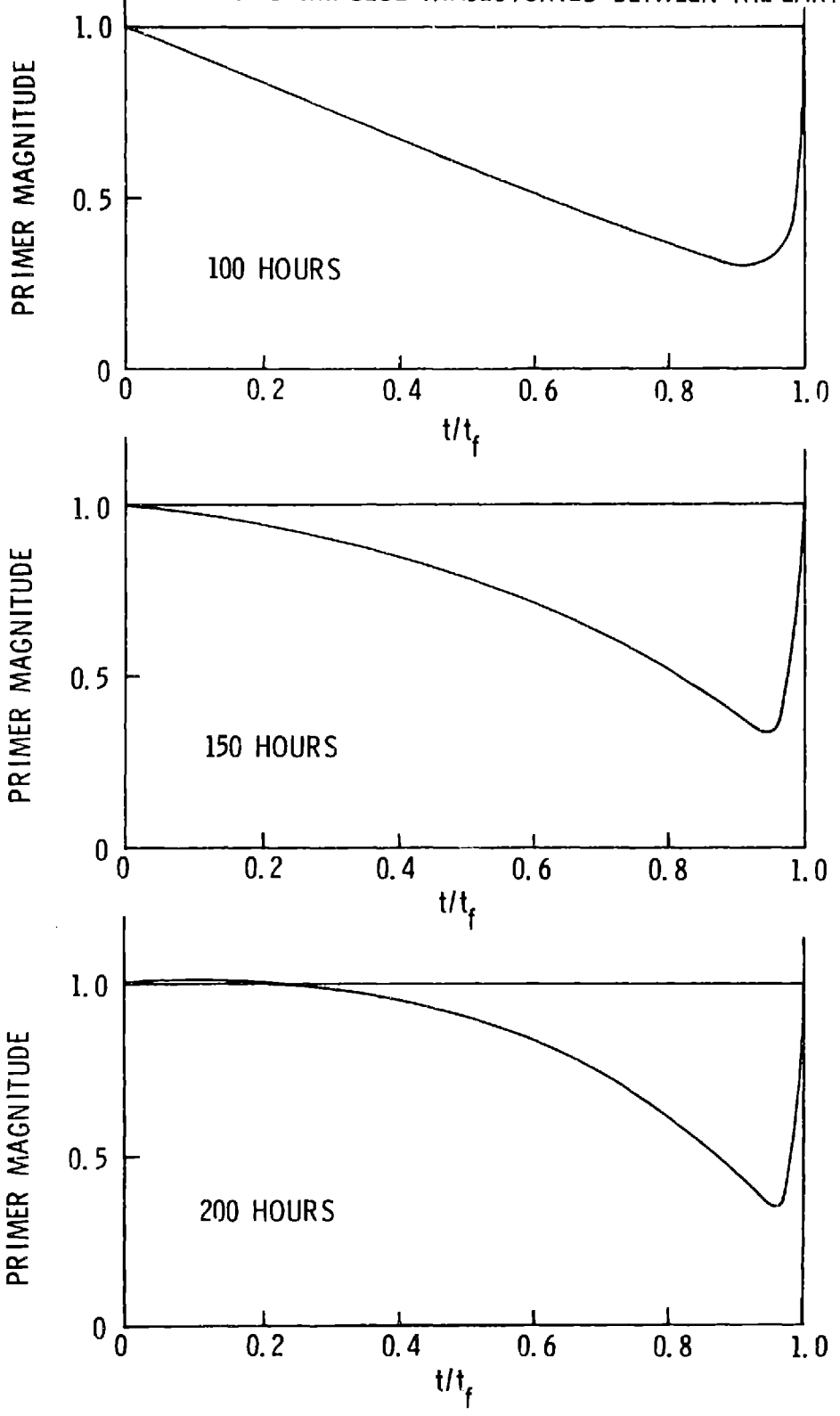

5.5 Three-Impulse Trajectories Between the Earth and L_2

Three-impulse trajectories between the Earth and L_2 which employ a powered lunar swingby are known to exist[9]. Thus the minimum impulse program can be used to converge to a minimum three-impulse solution using any known three-impulse solution as a starting point. The starting three-impulse solution is a 206.2 hour transfer from L_2 to a 185.2 km circular orbit about the Earth. The L_2-Moon leg takes 77.5 hours with a required ΔV at L_2 of 144.1m/sec (this portion of the trajectory is essentially the minimum two-impulse solution of the fast family of transfers between the Moon and L_2). At the point of closest approach to the Moon a tangential impulse of 192.4m/sec is applied to put the spacecraft on a 128.7 hour transfer to the Earth where a tangential 3131.1m/sec impulse establishes the 185.2 km circular orbit. The total cost of this starting three-impulse trajectory is 3467.6m/sec. The minimum two-impulse transfer of the previous section had a total cost of 4244.3m/sec. The close lunar swingby produces an 18.3% saving in total cost.

The minimum impulse program was run using this three-impulse solution as a starting point. The original and converged trajectories are given in Figure 16; the lunar swingby is expanded in Figure 17; and the primer histories of the two trajectories are given in Figure 18. Note from the primer histories that although the primer history for the starting three-impulse solution is non-optimal since the primer magnitude rises above unity just before the interior impulse, it is already quite close to satisfying the necessary conditions so that it would not be expected that the improvement of the converged trajectory would be very significant. The converged trajectory requires a 154.9m/sec impulse at L_2, a 172.1 m/sec impulse at the Moon, and a 3131.2m/sec impulse at the Earth, for a total of 3458.2m/sec. The improvement over the starting three-impulse solution is only a fraction of a percent. The starting solution is indeed quite close to the optimum. The similarity of the trajectories is obvious from Figure 16.

The converged three-impulse trajectory has one serious problem

Fig. 16
THREE-IMPULSE TRAJECTORIES BETWEEN THE EARTH AND L_2

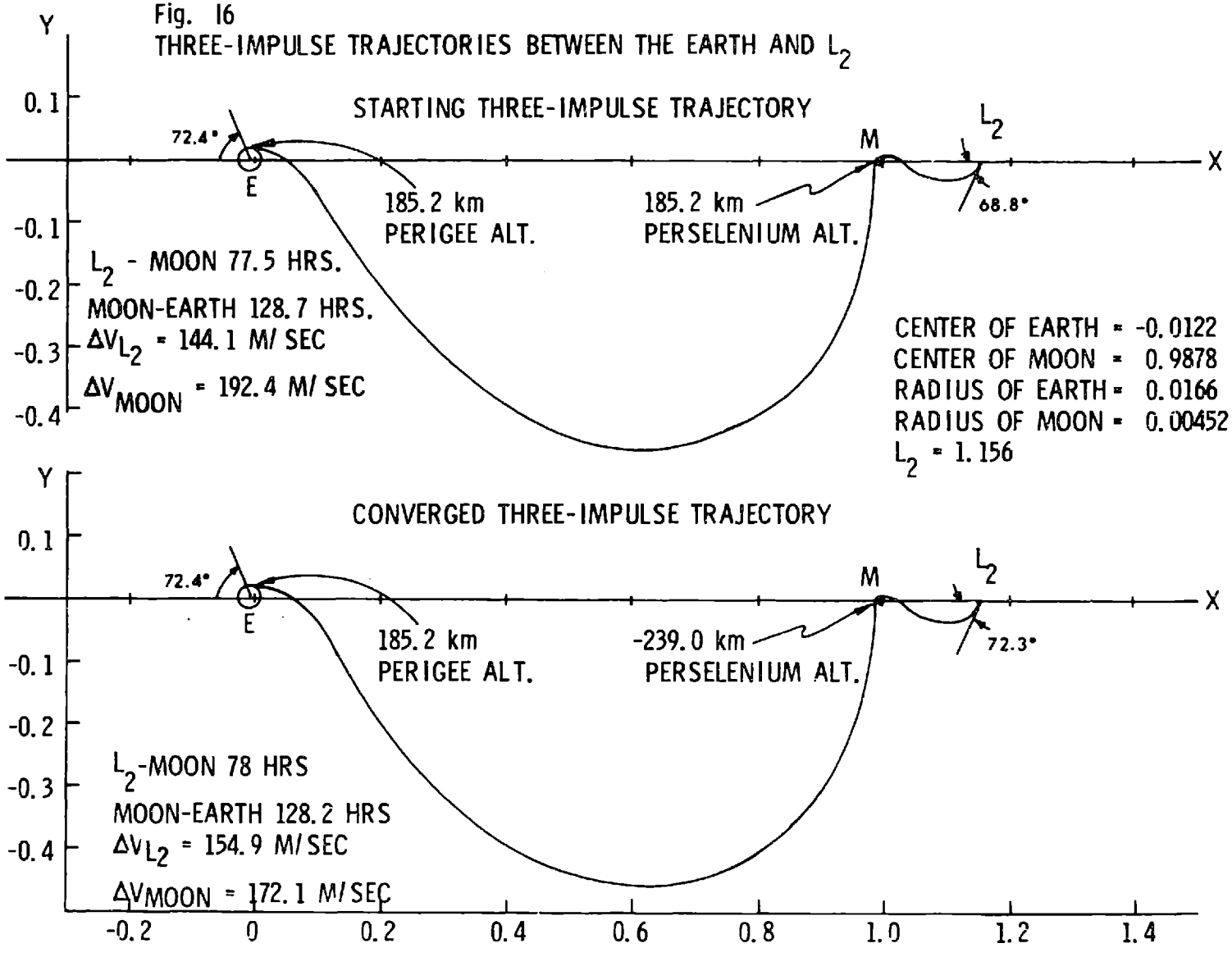

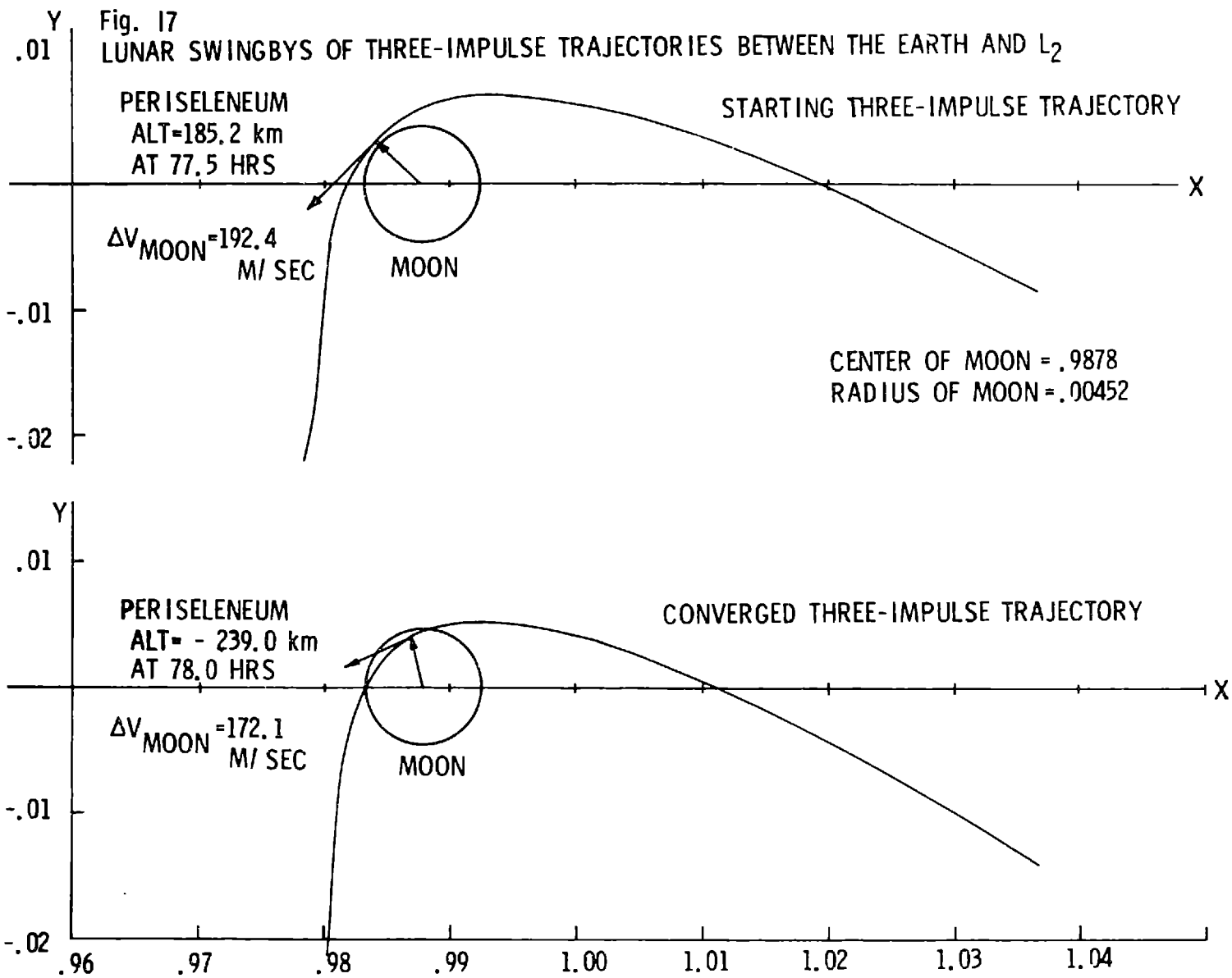

Fig. 17
LUNAR SWINGBYS OF THREE-IMPULSE TRAJECTORIES BETWEEN THE EARTH AND L_2

Fig. 18
PRIMER HISTORIES FOR THREE-IMPULSE TRAJECTORIES BETWEEN THE EARTH AND L_2

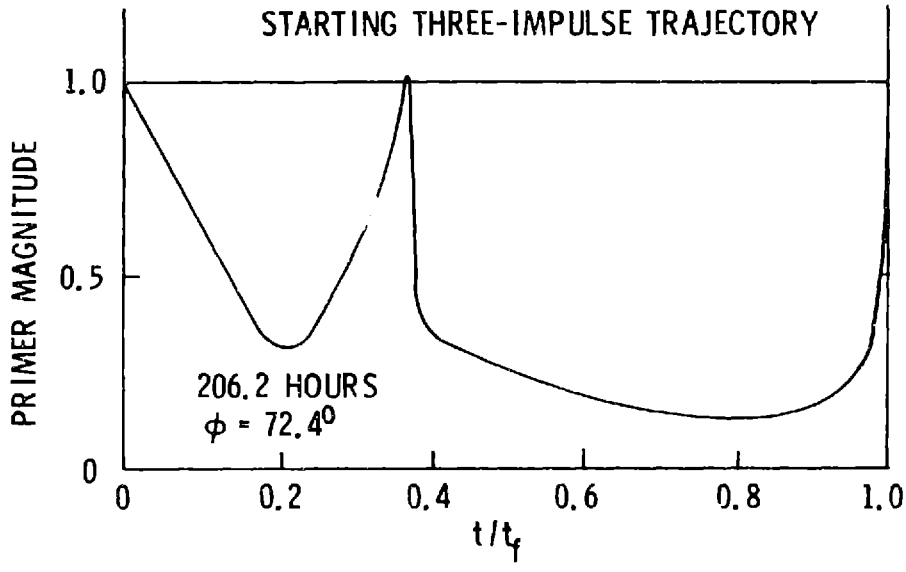

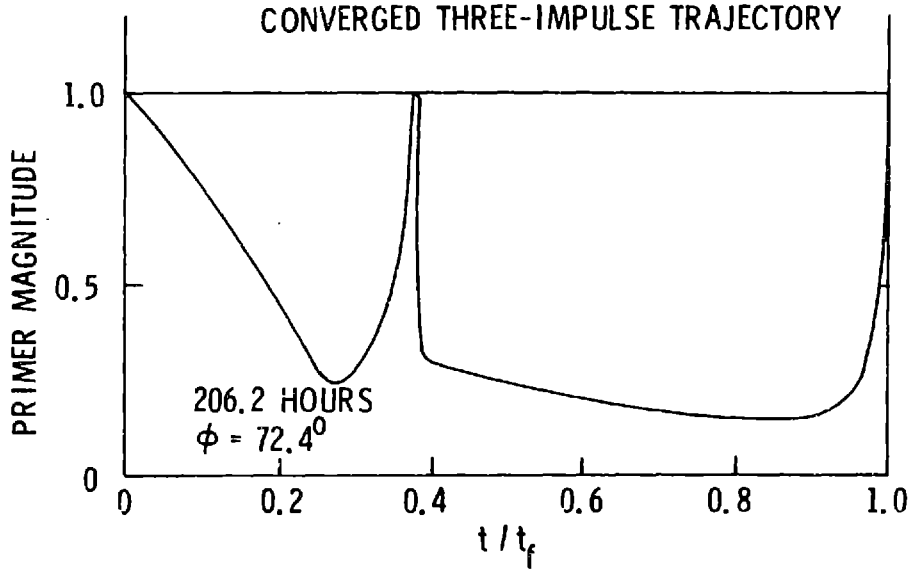

however: it passes below the surface of the Moon. At its point of closest approach it is 239 km below the surface. The impulse at the Moon for the starting three-impulse solution occurred 185.2 km above the surface and at periseleneum. The impulse at the Moon for the converged trajectory has been forced by the iterative procedure of the minimum impulse program to a point below the surface and prior to periseleneum. The position and time of the interior impulse are the iterative variables, and they are unconstrained as the program is presently set up; the theory does not take into account surfaces since it assumes point masses for the Earth and Moon. The fact that the position of the interior impulse moved to a point below the surface was not unexpected. This problem can be eliminated either by adding to the cost a penalty function which adds a large component of cost if the interior impulse descends below a prescribed altitude or by changing the theory to allow for interior point constraints. Thus the altitude at periseleneum could be fixed and only the angle of the position vector allowed to vary. In either case, most of the small saving which the converged trajectory obtained would be lost in bringing the interior impulse out from under the surface of the Moon.

The first converged three-impulse trajectory has an arrival angle at the Earth of 72.4° (see Figure 16). Varying the arrival angle indicated that the minimum total cost occurred at 70.4°. For that transfer, the required impulse at L_2 is 158.1m/sec, the impulse at the Moon is 168.9 m/sec, the impulse at the Earth is 3130.7m/sec, for a total cost of 3457.7m/sec. The primer history of this minimum with respect to arrival angle looks essentially like the ones on Figure 18. What is important is that the derivative of the primer magnitude as the initial time (and also the final time) is not zero. Hence a longer time of flight should reduce the cost. To get the true minimum three-impulse trajectory, the transfer time should be varied and the minimum over arrival angle for each time of flight found. There will be some time of flight for which the total cost will be a minimum.

The impulse at the Earth for the starting three-impulse solution is a tangential impulse at perigee, but for the first converged three-impulse

trajectory ($\varphi = 72.4^{o}$), it occurs before perigee. For the three-impulse trajectory which yielded the minimum cost with respect to arrival angle ($\varphi = 70.4^{o}$), it occurs almost exactly at perigee again.

The primer histories for the converged three-impulse trajectories satisfy the necessary conditions. Therefore, these three-impulse trajectories are locally optimal and there exist no neighboring four-impulse solutions which require less cost.

A short list of several L_2 to Earth trajectories and their costs is given below:

	Trajectory	Total Cost (m/sec)
1.	Minimum Two-Impulse Solution	4244.3
2.	Three-Impulse Solution: Close Lunar Swingby	3467.6
3.	Minimum Three-Impulse Solution	3457.7

The results presented in this Chapter concerning optimized three-impulse trajectories represent the first application known to the author of trajectory optimization for the three-body problem and for trajectories to and from libration points.

CHAPTER 6
ERROR ANALYSIS OF THE MULTI-CONIC METHODS

6.1 Preliminary Remarks

It is the purpose of this Chapter to perform a general error analysis of the three different multi-conic methods of trajectory integration derived in Chapter 3 in order to determine the deviations of the analytic approximations from the actual three-body trajectory for a single time step. These deviations are the errors in position and velocity at the end of a step due only to that step. Two forms of the errors will be developed: a Taylor series representation and an integral representation. The Taylor series are used to find contours of constant error in the Earth-Moon space, to find boundaries on which the errors of any two methods are equal, and to provide a method of internal step-size control for the multi-step integration procedure.

In the process of converging to any of the minimum impulse solutions presented in Chapter 5, many trajectories were propagated with a combination of the Earth-Moon and Moon-Earth multi-conic methods as described at the end of Section 4.4. As noted there, the trajectory propagation scheme utilized a simple constant step-size procedure. Let us consider a trajectory propagated with n steps. The error in position or velocity at the end of the nth step consists of two parts. The first part is the error due to the analytic approximation to the true trajectory used to update the position and velocity from t_{n-1} to t_n, i.e., the single-step error for the last step. The second part of the error is the contribution at t_n from the error which existed at t_{n-1}. This error propagates from t_{n-1} to t_n according to the state transition matrix. This Chapter is concerned with the single-step error of the multi-conic approximation to the true three-body trajectory.

6.2 Comparison of the Error Functions for the Multi-Conic Methods

Because the derivations of the single-step position and velocity error functions for the three multi-conic methods are quite lengthy and

tedious, they are given in Appendices C and D. We proceed in this Section directly to an analytic comparison of the error functions.

The single-step position and velocity error functions are found in Appendices C and D by expanding the errors as Taylor series in powers of the time step. The coefficients of the series are functions of the state at the beginning of the step. The derivations in Appendices C and D were carried out until the first non-zero term in the series for each error was found. For the position errors this term was the fourth-order term, and for the velocity errors it was the third order term.

The single-step position error functions for the three multi-conic methods, given by Equations (C. 44), (D. 55), and (D. 58), are

$$\delta\bar{R}_s(h) = \frac{A\,a}{24\,(Rr\rho)_I^3}\Big[(I-3\bar{u}_R\bar{u}_R^T)\,(\rho^3\bar{r}+r^3\bar{\rho}) + (I-3\bar{u}_r\bar{u}_r^T)\,(\rho^3\bar{R}-R^3\bar{\rho})\Big]_I h^4 + 0(h^5) \qquad (6.1)$$

$$\delta\bar{R}_{em}(h) = \frac{A\,a}{24\,(Rr\rho)_I^3}\Big[(I-3\bar{u}_R\bar{u}_R^T)\,(\rho^3\bar{r}+r^3\bar{\rho}) + 3\,(I-3\bar{u}_r\bar{u}_r^T)\,(\rho^3\bar{R}-R^3\bar{\rho})\Big]_I h^4 + 0(h^5) \qquad (6.2)$$

$$\delta\bar{R}_{me}(h) = \frac{A\,a}{24\,(Rr\rho)_I^3}\Big[3\,(I-3\bar{u}_R\bar{u}_R^T)\,(\rho^3\bar{r}+r^3\bar{\rho}) + (I-3\bar{u}_r\bar{u}_r^T)\,(\rho^3\bar{R}-R^3\bar{\rho})\Big]_I h^4 + 0(h^5) \qquad (6.3)$$

The single step velocity error functions for the three multi-conic methods are identical to third order and are given by Equation (C. 46):

$$\delta\ddot{\bar{R}}(h) = \frac{A\,a}{6\,(Rr\rho)^3_I}\Big[(I-3\bar{u}_R\bar{u}_R{}^T)\,(\rho^3\bar{r} + r^3\bar{\rho}) + (I-3\bar{u}_r\bar{u}_r{}^T)\,(\rho^3\bar{R} - R^3\bar{\rho})\Big]_I h^3 + 0\,(h^4) \qquad (6.4)$$

To fourth order the position or velocity error for a single step is a function only of the position at the beginning of the step and the step size. Note also that the errors are infinite at the center of either body. No assumptions other than that the mass of the spacecraft is negligible were made in order to derive the above equations. These error expressions are equally valid everywhere in the Earth-Moon space, and the Moon's orbit about the Earth is not required to be circular. In order to neglect the higher order terms of the Taylor series expansions so that the fourth-order truncation can be used as an estimate of the single-step position error, one would have to assume that the step size is small enough to make the Taylor series convergent. That is, the magnitude of the step size must be smaller than or equal to the radius of convergence for the series. The radius of convergence depends on the coefficients of the series, and the coefficients become infinite at the center of either body.

Note that the position error of any multi-conic approximation behaves as a fourth-order function of the time step for sufficiently small step sizes, and the coefficients of this fourth-order term becomes infinite at the center of either body. It can be shown that the position error of a two-body approximation behaves as a second-order function of the time-step, but the coefficient of the second order term becomes zero at the center of one of the bodies. Therefore, as the initial state from which a step is propagated is moved closer to either the Earth or the Moon, a point is reached at which a two-body approximation has a smaller position error than a multi-conic approximation for the same step size.

In the limit as the step size approaches zero, the position error for any method behaves as a fourth-order function of the time step and the velocity error as a third order function. In the limit the single-step position and velocity errors are functions only of the position relative to

the Earth and the Moon at the beginning of the step and the step size. The errors are not functions of the velocity at the beginning of the step.

The quantities in the above expressions for the error functions may be written in a more convenient form. First, the geocentric and selenocentric two-body accelerations at any time t_J are defined as

$$\bar{g}_{A_J} = - A \frac{\bar{R}_J}{R_J^3} \tag{6.5}$$

$$\bar{g}_{a_J} = - a \frac{\bar{r}_J}{r_J^3} \tag{6.6}$$

The corresponding gravity gradient matrices are

$$G_{A_J} = \frac{\partial \bar{g}_{A_J}}{\partial \bar{R}_J} = - \frac{A}{R_J^3} (I - 3\bar{u}_R \bar{u}_R^T)_J \tag{6.7}$$

$$G_{a_J} = \frac{\partial \bar{g}_{a_J}}{\partial \bar{r}_J} = - \frac{a}{r_J^3} (I - 3\bar{u}_r \bar{u}_r^T)_J \tag{6.8}$$

Finally, the geocentric and selenocentric disturbing accelerations are defined as

$$\delta \bar{g}_{A_J} = \ddot{\bar{R}}_J - \bar{g}_{A_J} = - a \frac{\bar{r}_J}{r_J^3} - a \frac{\bar{\rho}_J}{\rho_J^3} \tag{6.9}$$

$$\delta \bar{g}_{a_J} = \ddot{\bar{r}}_J - \bar{g}_{a_J} = - A \frac{\bar{R}_J}{R_J^3} + A \frac{\bar{\rho}_J}{\rho_J^3} \tag{6.10}$$

Combining Equations (6.7) to (6.10) with Equations (6.1) to (6.3) allows one to write the fourth-order position errors as

$$\delta \bar{R}_s(h) = (G_A \, \delta \bar{g}_A + G_a \, \delta \bar{g}_a)_I \frac{h^4}{24} \tag{6.11}$$

$$\delta\bar{R}_{em}(h) = (G_A\ \delta\bar{g}_A + 3G_a\ \delta\bar{g}_a)_I \frac{h^4}{24} \tag{6.12}$$

$$\delta\bar{R}_{me}(h) = (3G_A\ \delta\bar{g}_A + G_a\ \delta\bar{g}_a)_I \frac{h^4}{24} \tag{6.13}$$

The third-order velocity error (Equation (6.4)), which is the same for all the methods becomes

$$\delta\dot{\bar{R}}(h) = (G_A\ \delta\bar{g}_A + G_a\ \delta\bar{g}_a) \frac{h^3}{6} \tag{6.14}$$

The new expressions for the error functions are weighted sums of the same two terms. The three-body geocentric acceleration is the sum of a two-body acceleration and a disturbing acceleration:

$$\ddot{\bar{R}}_J = \bar{g}_{A_J} + \delta\bar{g}_{A_J} \tag{6.15}$$

where

$$\bar{g}_{A_J} = -A \frac{\bar{R}_J}{R_J^3} \tag{6.16}$$

$$\delta\bar{g}_{A_J} = -a \frac{\bar{r}_J}{r_J^3} - a \frac{\bar{\rho}_J}{\rho_J^3} \tag{6.17}$$

The first term in any of the errors ($G_A\ \delta\bar{g}_A$) is the produce of the geocentric two-body gravity gradient matrix, Equation (6.7), and the geocentric disturbing acceleration, Equation (6.17). At the Earth the disturbing acceleration, $\delta\bar{g}_A$, is zero, but the gravity gradient matrix, G_A, has a third order singularity. The net effect of the product is still that of a singularity. At the Moon, the disturbing acceleration is infinite and the product has another singularity. The same arguments can be applied to the other term, $G_a\ \delta\bar{g}_a$, so that both terms have singularities at both the Earth and the Moon.

That the first non-zero terms in the Taylor series expansions of the

errors can be expressed by means of gravity gradient matrices and disturbing accelerations, leads to a new integral formulations of the error functions in Section 6.4.

Because the fourth-order position error expressions are functions only of position relative to the Earth and Moon, these expressions can be evaluated at various points in the Earth-Moon space to determine what the magnitude of the position would be for a given step size starting at that point. All the results which will be discussed in the remaining part of this Section are valid only in the limit as the step size approaches zero. Otherwise, we could not truncate the Taylor series for the error function and use the fourth order term as a valid representation of the error function. The coordinate system in which the results will be displayed is illustrated in Figure 19. Its origin is at the point on the Earth-Moon line midway between the two bodies. The xy plane is the plane of the Moon's orbit about the Earth and the z-axis points in the direction of the Moon's angular momentum vector. The same dimensionless units are used here as were described in Section 5.1, so that the Earth and Moon, which are both on the x-axis, are at the points (-.5, 0, 0) and (.5, 0, 0) respectively. Also included on Figure 19 are examples of the position vectors $\overline{R}$, $\overline{r}$, and $\overline{\rho}$.

The fourth-order position error for the Stumpff-Weiss method from Equation (6.1) is

$$\delta\overline{R} = \frac{A\,a}{24\,(Rr\rho)^3}\left[(I - 3\bar{u}_R\bar{u}_R{}^T)\,(\rho^3\overline{r} + r^3\overline{\rho})\right.$$
$$\left. + (I - 3\bar{u}_r\bar{u}_r{}^T)\,(\rho^3\overline{R} - R^3\overline{\rho})\right] h^4 \qquad (6.18)$$

where for convenience all subscript notation has been dropped. In the dimensionless units noted above, $A = 1-\mu$, $a = \mu$ and $\rho = 1$, so that the error may be written as

Fig. 19 COORDINATE SYSTEM FOR THE ERROR CURVES

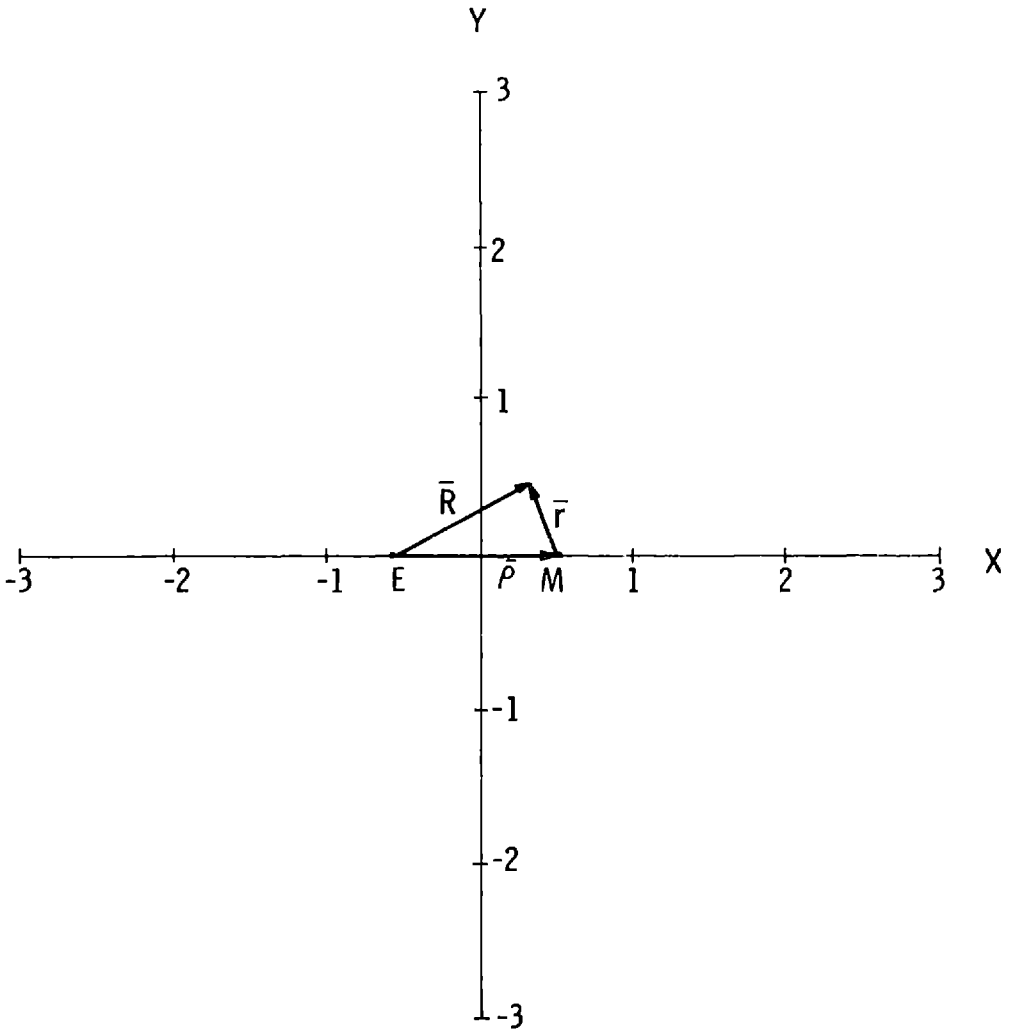

$$\delta\bar{R} = \frac{\mu\,(1-\mu)}{24\,R^3 r^3}\left[(I-3\bar{u}_R\bar{u}_R{}^T)\,(\bar{r}+r^3\bar{\rho})\right.$$

$$\left.+\,(I-3\bar{u}_r\bar{u}_r{}^T)\,(\bar{R}-R^3\bar{\rho})\right]h^4 \qquad (6.19)$$

Furthermore, $\bar{\rho} = \bar{R} - \bar{r}$, so that the above expression further simplifies to

$$\delta\bar{R} = \frac{\mu\,(1-\mu)}{24\,R^3 r^3}\left[(I-3\bar{u}_R\bar{u}_R{}^T)\,(\bar{r}+r^3\bar{R}-r^3\bar{r})\right.$$

$$\left.+\,(I-3\bar{u}_r\bar{u}_r{}^T)\,(\bar{R}+R^3\bar{r}-R^3\bar{R})\right]h^4 \qquad (6.20)$$

From the definition of the coordinate system of Figure 19, $\bar{R}$ and $\bar{r}$ are given by

$$\bar{R} = \begin{bmatrix} x+.5 \\ y \\ z \end{bmatrix} \qquad (6.21)$$

$$\bar{r} = \begin{bmatrix} x-.5 \\ y \\ z \end{bmatrix} \qquad (6.22)$$

In order to calculate the position error for the Stumpff-Weiss method at any point in the Earth-Moon space, one chooses x, y, and z, thus specifying $\bar{R}$ and $\bar{r}$, and then Equation (6.20) yields the error for a given step size or the error per unit of step if the step size is unspecified. Expressions similar to Equation (6.20) may be written for the Earth-Moon and Moon-Earth methods. The only difference would be the weights of the two quantities within the brackets, which would not be unity as for the Stumpff-Weiss method.

First the magnitudes of the position errors along the x and y axes are investigated. Along the x-axis, y=z=0, and only x need be chosen to specify $\bar{R}$ and $\bar{r}$. Along the y-axis, x=z=0, and only y need be chosen

to specify $\overline{R}$ and $\overline{r}$.

On Figure 20, the logarithm (base 10) of the magnitude of the position error (for a one hour time step) divided by a reference error (taken to be one kilometer) is plotted versus position along the x-axis, which is the Earth-Moon line. The positions of the Earth and Moon on the x-axis are denoted by "E" and "M" respectively. Note that between the Earth and the Moon, the Stumpff-Weiss method has the smallest error; on the far side of the Moon, the Moon-Earth method has the smallest error; and on the far side of the Earth, the Earth-Moon method has the smallest error. For the Stumpff-Weiss method there is one point (x=0) on the Earth-Moon line where the magnitude of the Stumpff-Weiss error is zero. The magnitude of the error for the Earth-Moon method is zero at the points $x = -1.0$ and $x = -1.5$, and the magnitude of the error for the Moon-Earth method is zero at the points $x = 1.0$ and $x = 1.5$. Also the magnitude of the error for all three methods is infinite at the center of either body. Finally, note that the curve for the Earth-Moon method is a reflection of the curve for the Moon-Earth method about the point x=0.

On Figure 21, the logarithm (base 10) of the magnitude of the position error (for a one hour time step) divided by a one kilometer reference error is plotted versus position along the y-axis. Everywhere along the y-axis, the Stumpff-Weiss method has the smallest error, and the errors of the other two methods are equal. There are three points at which the Stumpff-Weiss method has zero error. They are at 0 and $\pm .492$, approximately.

The velocity error divided by the cube of the step size is almost exactly the same function as the Stumpff-Weiss position error divided by the fourth power of the step size. This can be seen by comparing Equations (6.1) and (6.4). The only difference is that the velocity error has a factor of 6 in the denominator and the position error has a factor of 24 in its denominator. Thus, it may be concluded that the plot of the magnitude of the velocity error divided by the cube of the step size along

Fig. 20 ERROR MAGNITUDES ALONG THE EARTH - MOON LINE

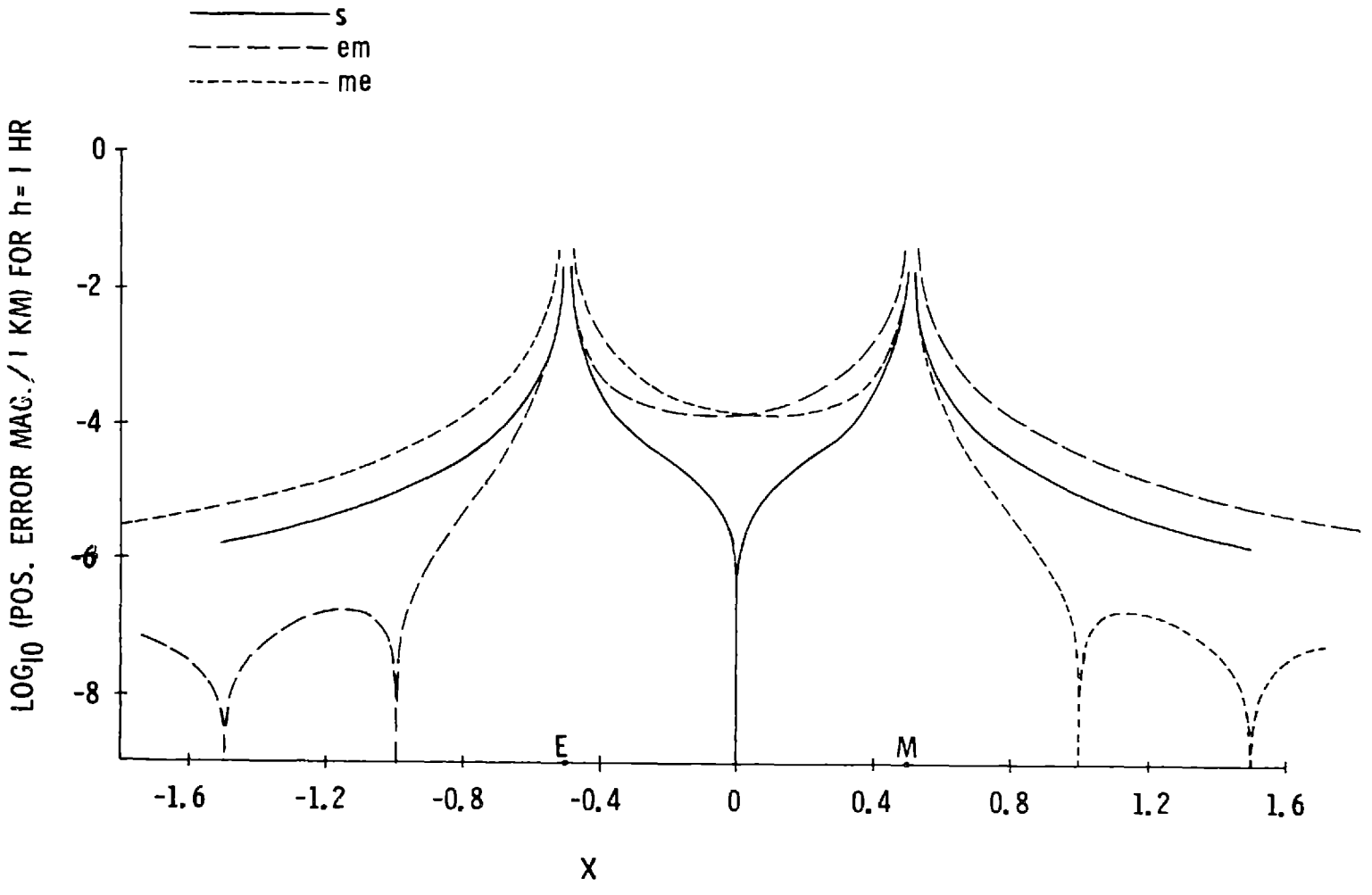

Fig. 21 ERROR MAGNITUDES ALONG THE Y-AXIS

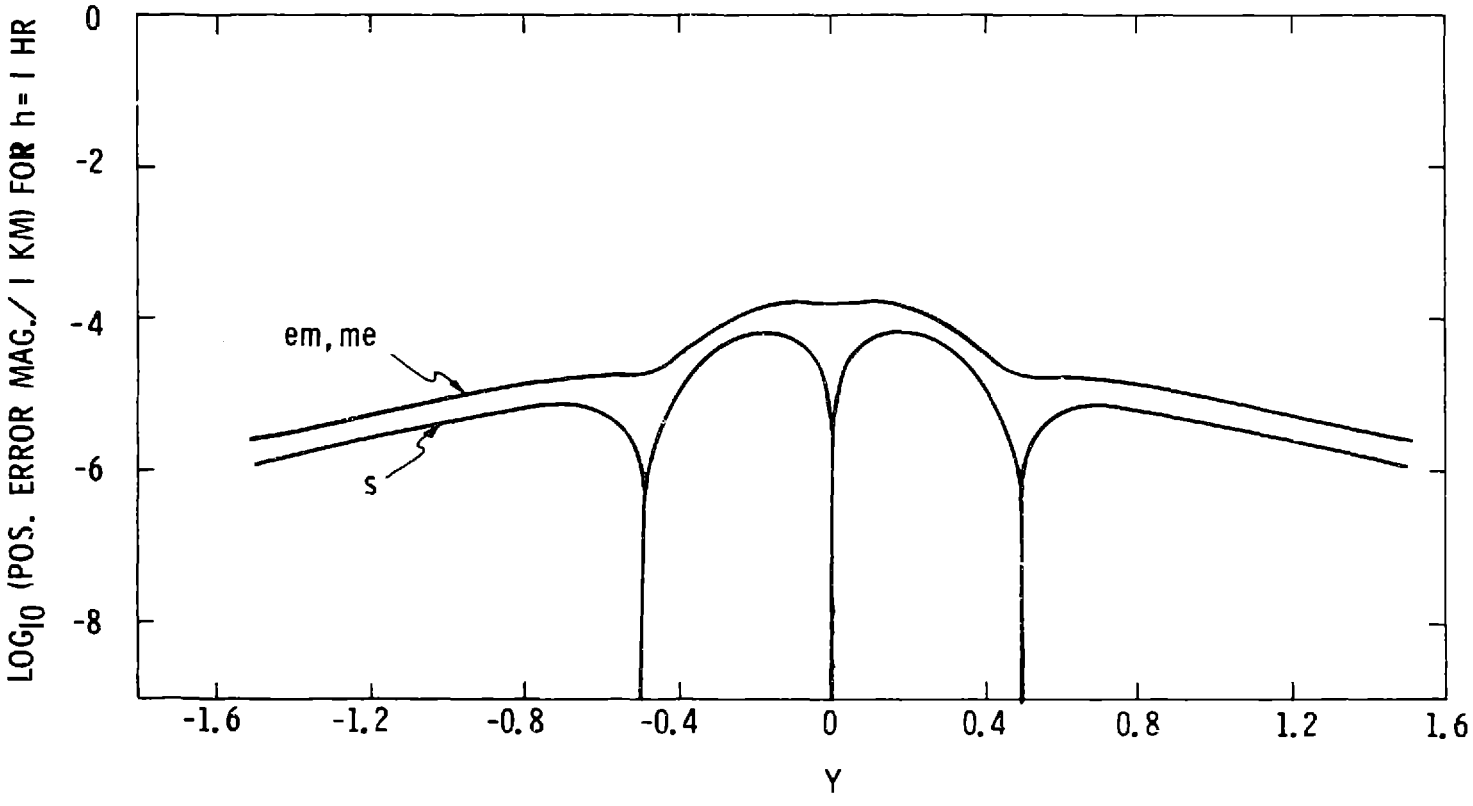

the x or y axis has the same shape as plots of the Stumpff-Weiss position error on Figures 20 and 21. The actual values of the velocity error would be measured in km./sec. for a one hour time step, and the reference velocity error would be one kilometer per second. The level of the curve would be displaced upward by an amount equal to $\log_{10}(4)$.

Next, contours of constant error magnitude for each method are found in the xy plane. All the points on any one such curve, if used as the initial point for a step, have the same position error associated with them for a given step size. Equation (6.20), which gives the position error for the Stumpff-Weiss method, may be written as

$$\delta\bar{R} = \frac{\mu\,(1-\mu)}{24\,R^3 r^3}\,(\bar{\alpha} + \bar{\beta})\,h^4 \tag{6.23}$$

where $\mu \cong 1/82.3$ and

$$\bar{\alpha} = (I - 3\bar{u}_R \bar{u}_R{}^T)\,(\bar{r} + r^3\bar{R} - r^3\bar{r}) \tag{6.24}$$

$$\bar{\beta} = (I - 3\bar{u}_r \bar{u}_r{}^T)\,(\bar{R} + R^3\bar{r} - R^3\bar{R}) \tag{6.25}$$

Note that interchanging $\bar{R}$ and $\bar{r}$ in the above expression for $\bar{\alpha}$ yeidls the expression for $\bar{\beta}$. If one forms the dot product of Equation (6.23) with itself, one obtains

$$|\delta\bar{R}|^2 = \frac{\mu^2\,(1-\mu)^2}{576\,R^6 r^6}\,(\alpha^2 + 2\bar{\alpha}^T\bar{\beta} + \beta^2)\,h^8 \tag{6.26}$$

In order to find contours of constant error magnitude in the xy plane for the Stumpff-Weiss method, the x and y which satisfy Equation (6.26), given $|\delta\bar{R}|$ and h, must be found (z=0 in the xy plane). Let the parameter k be defined as

$$k = \frac{576\,|\delta\bar{R}|^2}{\mu^2\,(1-\mu)^2\,h^8} \tag{6.27}$$

Then Equation (6.26) may be written as

$$\frac{1}{R^6 r^6}(\alpha^2 + 2\bar{\alpha}^T\bar{\beta} + \beta^2) = k \qquad (6.28)$$

The parameter k is a parabolic function of the magnitude of the position error, and for a one hour time step a value for k of 10^{11} corresponds to a position error of about .5 km.

Curves of constant error for the Stumpff-Weiss method were found as follows: choose a value for k and then, with x specified, iteratively determine the y which will satisfy Equation (6.28). Expressions similar to Equation (6.28) for the Earth-Moon and Moon-Earth methods are found in a similar fashion. The only differences will be the weights of the three terms within the parentheses. The expression for the Earth-Moon method is

$$\frac{1}{R^6 r^6}(\alpha^2 + 6\bar{\alpha}^T\bar{\beta} + 9\beta^2) = k \qquad (6.29)$$

and the expression for the Moon-Earth method is

$$\frac{1}{R^6 r^6}(9\alpha^2 + 6\bar{\alpha}^T\bar{\beta} + \beta^2) = k \qquad (6.30)$$

It can be shown that if the point (x, y) satisfies Equation (6.28), then the points (-x, y), (x, -y), (-x, -y) also satisfy the equation. The contours of constant error for the Stumpff-Weiss method are therefore symetric with respect to the x-axis and the y-axis. For Equations (6.29) and (6.30) only symmetry with respect to the x-axis exists. But it is also true that if (x, y) satisfies Equation (6.29), then (-x, y) satisfies Equation (6.30). Therefore, the contours of constant error for the Earth-Moon method may be found by simply reflecting the contours for the Moon-Earth method about the y-axis. Some of this symmetry may be explained by the fact that the vectors $\bar{\alpha}$ and $\bar{\beta}$ are transformed into one another by interchanging $\bar{R}$ and $\bar{r}$.

The contours of constant error for the Stumpff-Weiss method and the Moon-Earth method are shown in Figures 22 and 23 respectively.

Each curve is labeled with its value of k. Increasing values of k for a constant step size correspond to increasing values of the error magnitude. The figures take on a three-dimensional appearance if one imagines the magnitude of the error as the third dimension, increasing in the direction out of the xy plane toward the observer. Hence, the error contours for the Stumpff-Weiss method in Figure 22 appear to describe a wide plateau far from the bodies, three valley-like depressions on the y-axis, and two infinite mountains centered at the Earth and Moon. The error magnitude approaches zero at the bottoms of the derpresions and at infinity and approaches infinity at the centers of the Earth and the Moon.

For the contours of the Moon-Earth method on Figure 23, the plateau far from the bodies is again evident but there is a deep valley on the x-axis on the far side of the Moon. There are three depressions close to the y-axis but they are quite shallow. The two mountains centered at the Earth and the Moon have differently shaped cross-sections. The contours for the Earth-Moon method are found by reflecting Figure 23 about the y-axis. In the lower right hand portion of Figure 23 is shown an expanded view of that part of the k=1 curve which crosses the x-axis. The curvature of the contour is continuous at this crossing, a fact which is not obvious from the other curves. Not appearing in Figure 23 are two more very slight depressions beyond the Moon on the x-axis.

The shapes of the curves on Figures 22 and 23 and the fact that there are locations where the error magnitude approaches zero lead to the conclusion that the errors of the methods are strongly dependent on the position relative to the Earth and Moon. An expanded view of the contours of constant error magnitude very close to the Earth for all three methods is shown on Figure 24. The strong dependence of the error on the position relative to the Earth is quite evident. The contours of constant error are not circular very close to the body as one might expect.

The shape of the contours of constant velocity error magnitude for all three methods will be the same and identical to the contours of

Fig. 22
CONTOURS OF CONSTANT ERROR FOR THE STUMPFF-WEISS METHOD

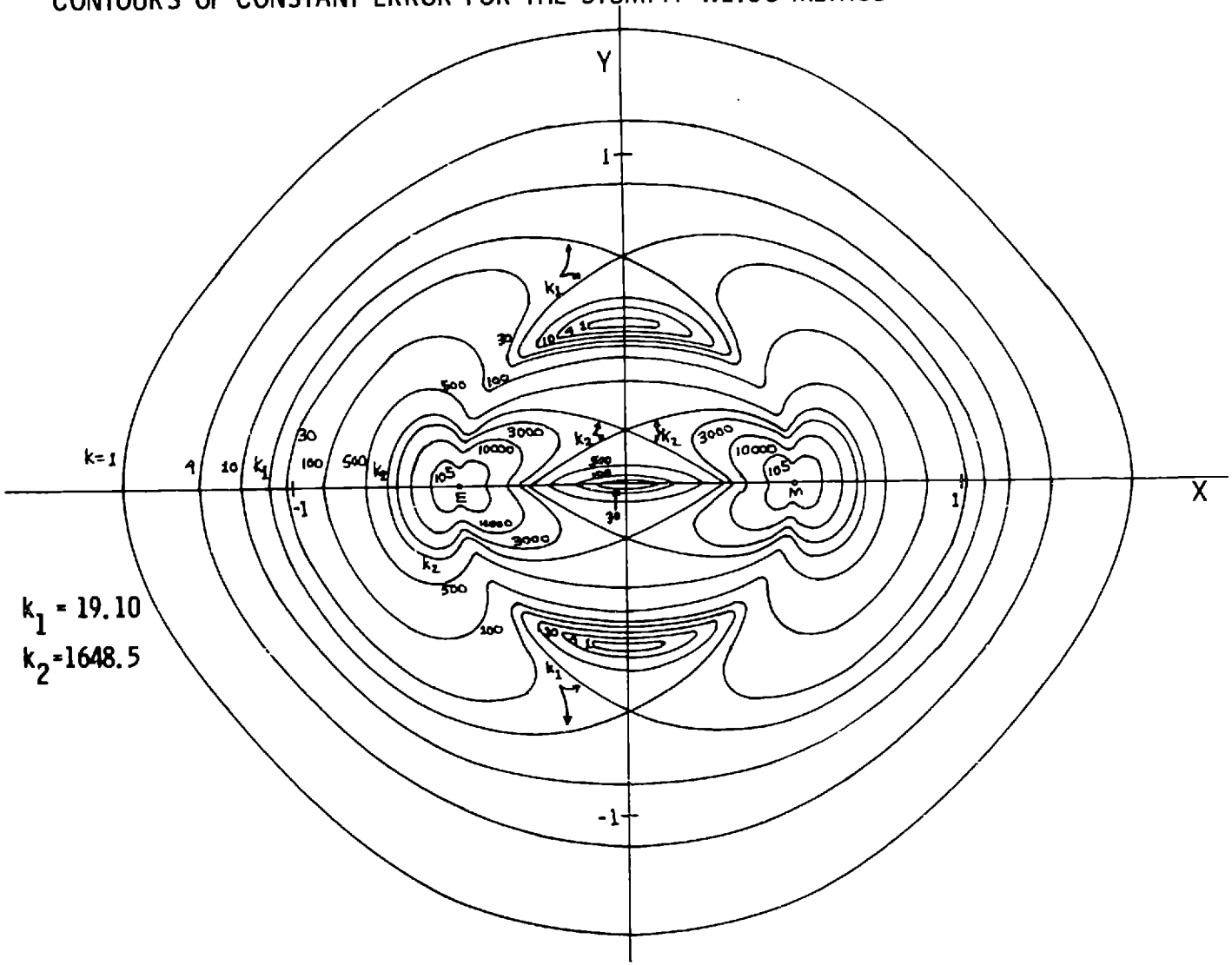

$k_1 = 19.10$

$k_2 = 1648.5$

Fig. 23
CONTOURS OF CONSTANT ERROR FOR THE MOON-EARTH METHOD

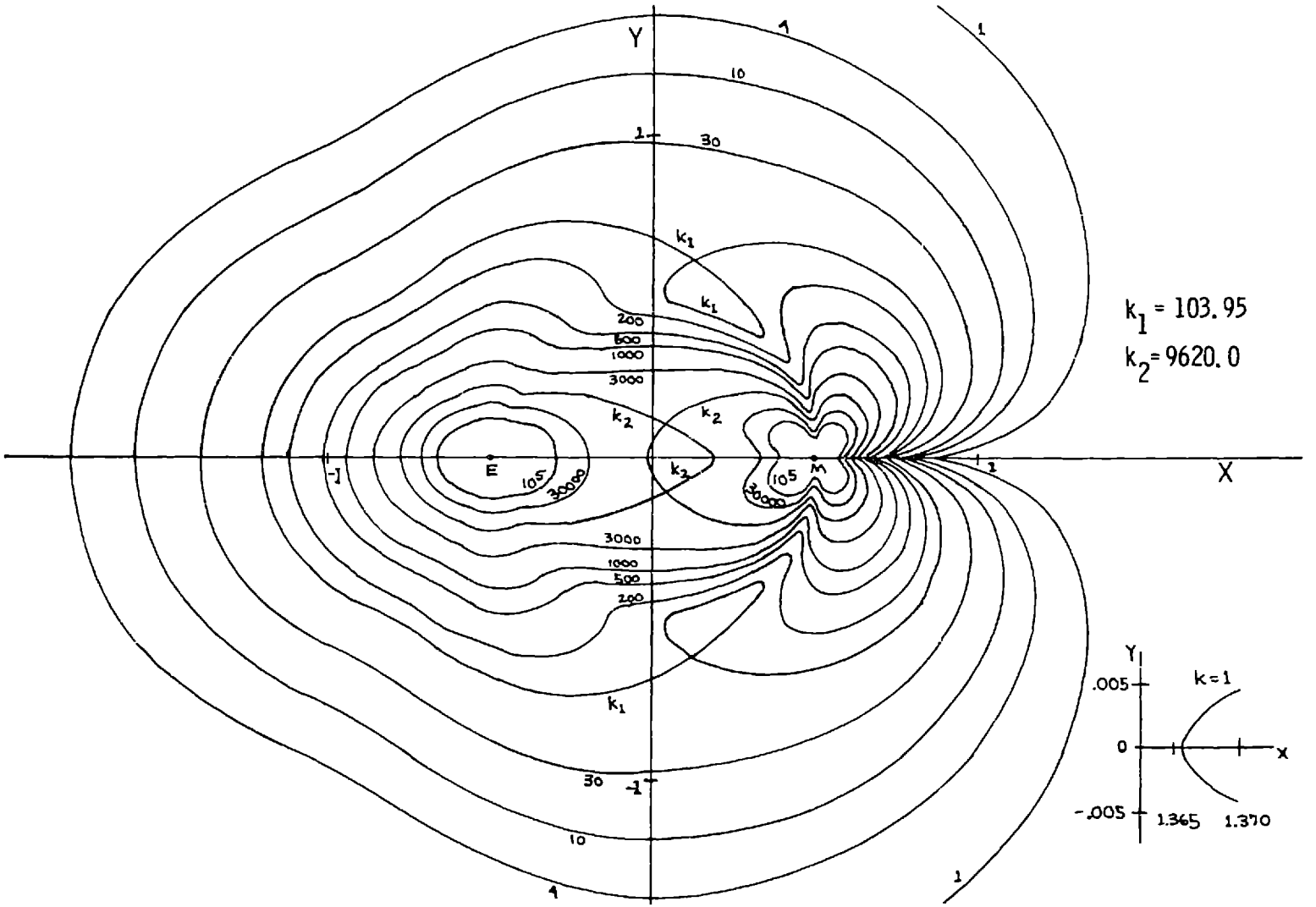

Fig. 24
CONTOURS OF CONSTANT ERROR VERY CLOSE TO THE EARTH

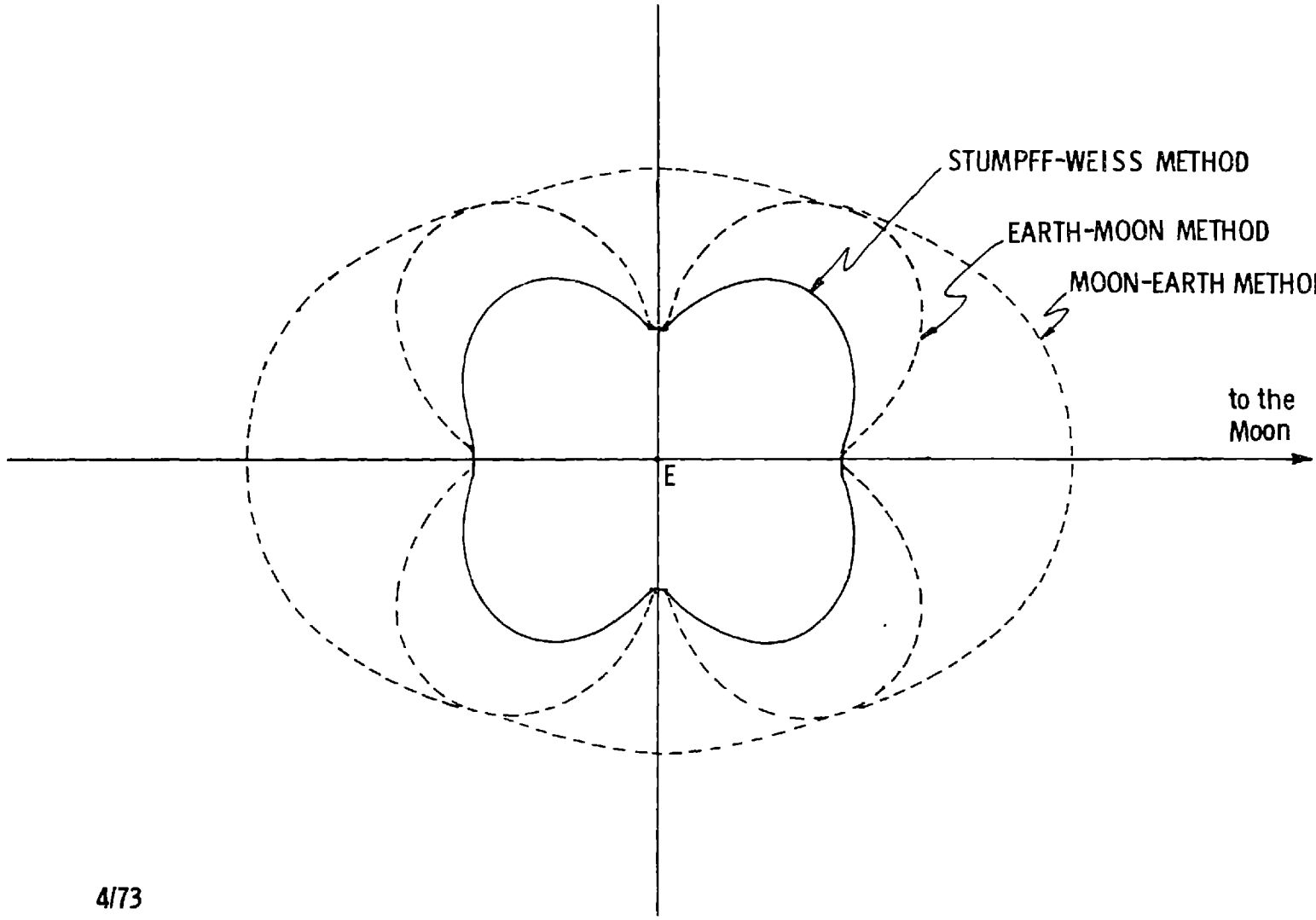

4/73

constant position error magnitude for the Stumpff-Weiss method shown in Figure 22 since the velocity error function, Equation (6.4), is the same function of position relative to the Earth and Moon as the Stumpff-Weiss position error function, Equation (6.1). If one wishes to interpret the curves on Figure 22 as constant velocity error curves, then the parameter k must be defined as

$$k = \frac{36\ |\delta\dot{\bar{R}}|^2}{\mu^2\ (1-\mu)^2\ h^6} \tag{6.31}$$

where $|\delta\dot{\bar{R}}|$ is a velocity error magnitude.

Finally, a few comments can be made about the error functions and their dependence on the relative masses of the Earth and the Moon. It is obvious from an inspection of the error functions for the three multi-conic methods, Equations (6.1) to (6.3), that the masses of the Earth and the Moon enter into the error functions through the gravitational parameters A and a which appear in a coefficient. Therefore, the shape of the contours of constant error is indpendent of the masses of the Earth and the Moon and these contours are equally valid for all three-body systems in which the mass of the third body is negligible. Furthermore, if the error functions are divided by the product of the masses of the two massive bodies, then the direction and magnitude of the errors are independent of the masses and the mass ratio of the two massive bodies.

One more geometric application of the error functions is to find curves in the Earth-Moon space on which the magnitudes of the errors for any two methods are equal. These curves would divide the Earth-Moon space into regions in which the error of one method is less than the error of another. Equating the error magnitudes for the Earth-Moon and Moon-Earth methods from Equations (6.2) and (6.3) and using the definitions of $\bar{\alpha}$ and $\bar{\beta}$ given in Equations (6.24) and (6.25) the following expression is obtained:

$$|\bar{\alpha} + 3\bar{\beta}| = |3\bar{\alpha} + \bar{\beta}| \tag{6.32}$$

which leads to

$$\alpha^2 - \beta^2 = 0 \tag{6.33}$$

Restricting the search to the xy plane, in order to find curves on which the magnitude of the errors of the Earth-Moon and Moon-Earth methods are equal, one specifies x and then iteratively determines the value of y which satisfies Equation (6.33). The vectors $\bar{R}$ and $\bar{r}$ are given by Equations (6.21) and (6.22) with z=0. Equating the error magnitudes for the Stumpff-Weiss method and the Earth-Moon method results in the following expression

$$2\beta^2 + \bar{\alpha}^T\bar{\beta} = 0 \tag{6.34}$$

and equating the error magnitudes for the Stumpff-Weiss method and the Moon-Earth method yields

$$2\alpha^2 + \bar{\alpha}^T\bar{\beta} = 0 \tag{6.35}$$

The curves which satisfy Equations (6.33), (6.34), and (6.35) are shown on Figures 25 and 26. Figure 25 shows all the curves on which the error magnitudes for the Earth-Moon and Moon-Earth methods are equal. In the crosshatched area, the Earth-Moon method has a smaller error magnitude and this fact is denoted by the inequality em < me. This region includes most of the area on the side of the y-axis toward the Earth except for two large segments. In the non-crosshatched area, the error magnitude for the Moon-Earth method is the smaller. These curves have symmetry with respect to both the x and y axis.

Figure 26 shows the curves on which the error magnitude of the Stumpff-Weiss method is equal to that of either the Earth-Moon or Moon Earth method. In the region within the curve to the left of the y-axis the Earth-Moon method has a smaller error magnitude than the Stumpff-Weiss method. In that same region, the Earth-Moon method has a smaller error magnitude than the Moon-Earth method as can be seen from

Fig. 25 CURVES ON WHICH THE ERRORS FOR THE EARTH-MOON AND MOON-EARTH METHODS ARE EQUAL

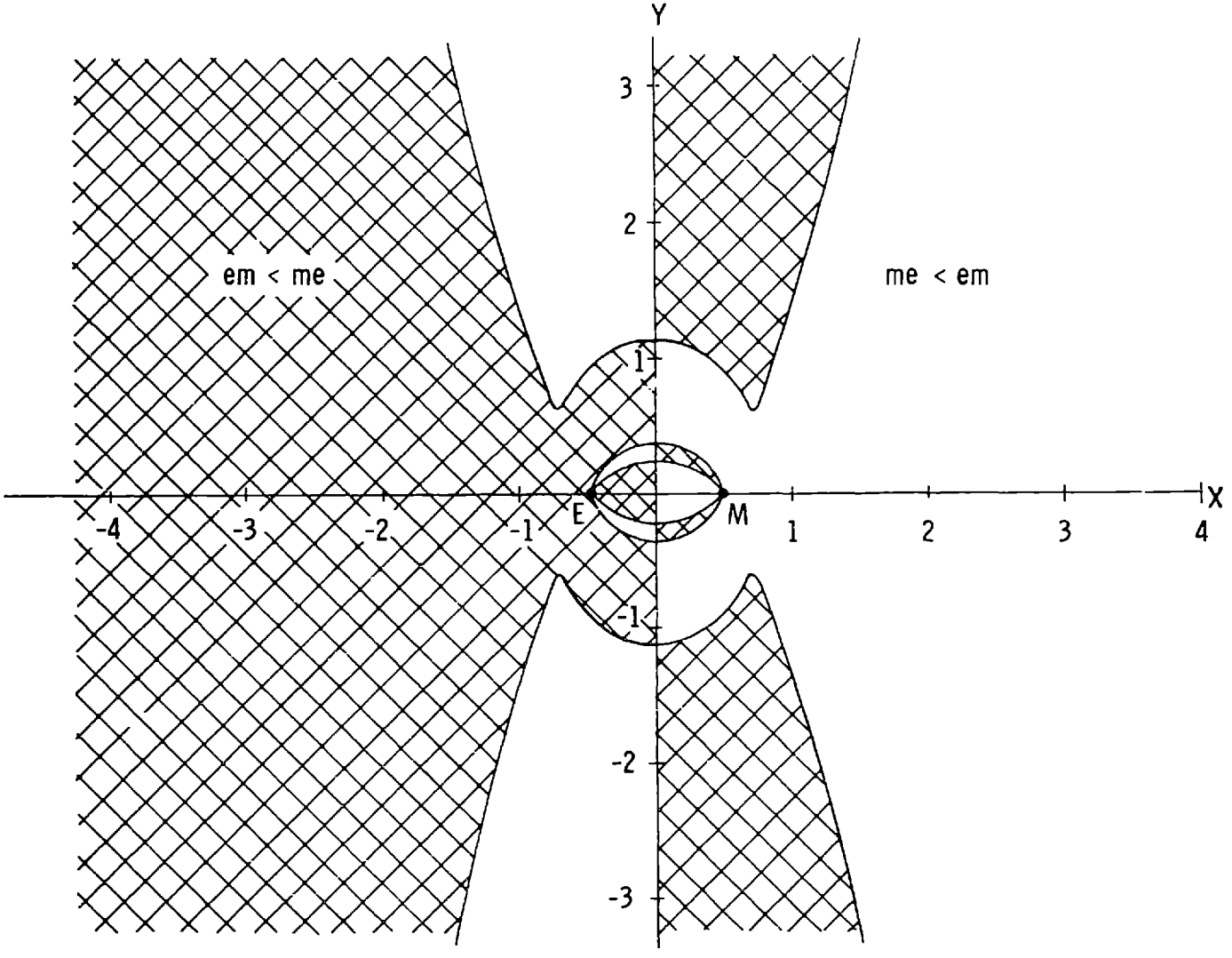

Fig. 26 CURVES ON WHICH THE ERRORS FOR THE STUMPFF WEISS METHOD AND EITHER THE EARTH MOON OR MOON EARTH METHOD ARE EQUAL

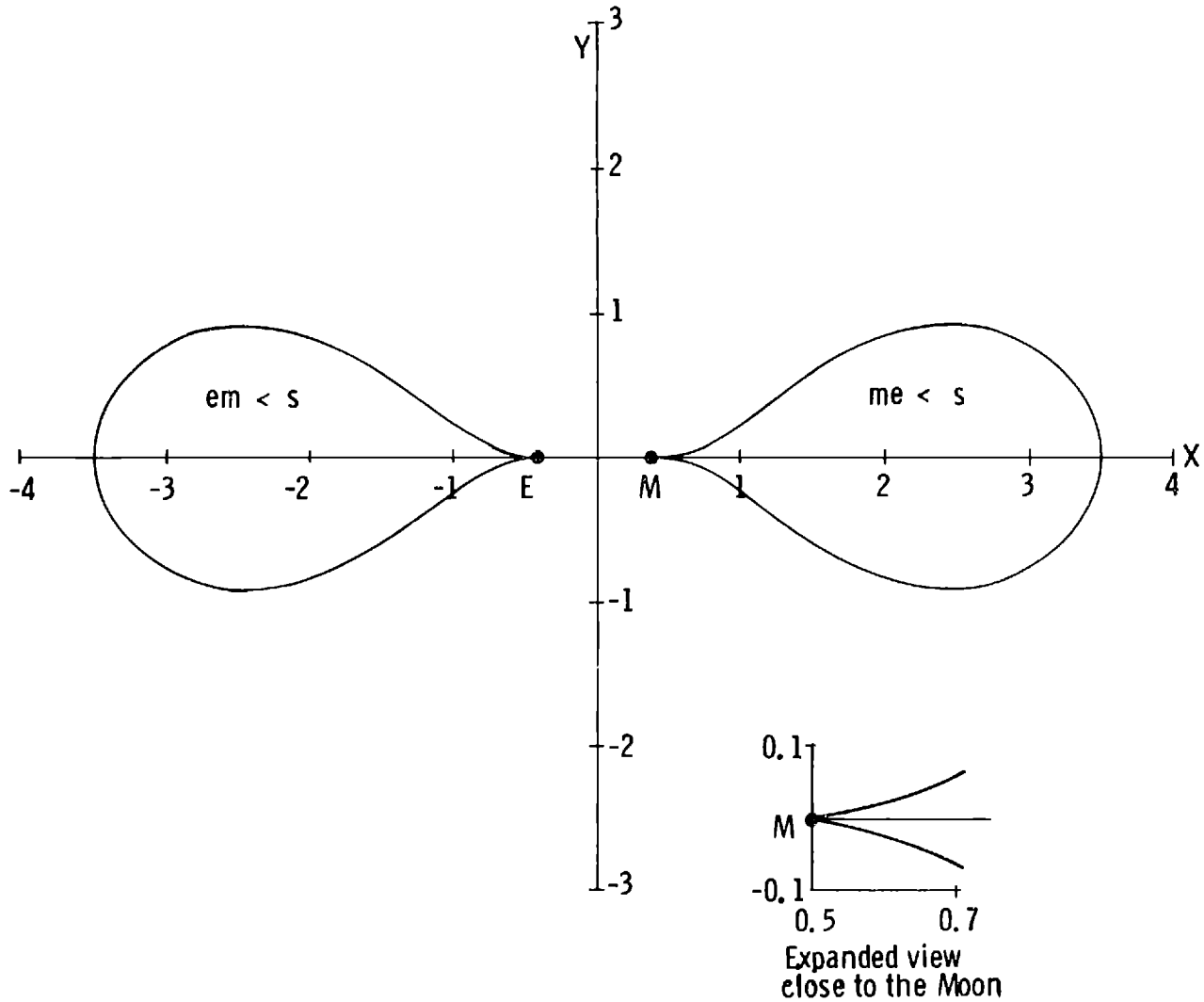

Figure 25. Therefore, within that region, the Earth-Moon method has the smallest error of all three methods. Similarly within the region enclosed by the curve on the right side of the y-axis in Figure 26, the Moon-Earth method has the smallest error. Everywhere other than within those two enclosed regions, the error for the Stumpff-Weiss method is the smallest. It can be shown that the curves in Figures 25 and 26 have rotational symmetry with respect to the x-axis so that to generate the three-dimensional representation of these curves, one need only rotate the curves in the xy plane about the x-axis. From an inspection of Figure 26 and the above arguments, it may therefore be stated that the Stumpff-Weiss method has the smallest error everywhere in the Earth-Moon space except for two teardrop-shaped areas, one on the far side of the Earth and the other on the far side of the Moon, within which the errors of the Earth-Moon and Moon-Earth methods respectively are smallest.

The curves on Figure 26 have a cusp at the Earth and Moon as can be seen by the enlarged segment of the curve near the Moon on Figure 26.

The above results were derived using fourth-order position errors. Since the velocity errors are the same for all methods to third order, all methods are equally good everywhere in the Earth-Moon space in terms of velocity errors.

In this Section, some geometrical and analytical results have been found from the single-step position and velocity error functions for the three multi-conic methods. In the next Section, some multi-step numerical results for final position and velocity errors are discussed.

6.3 Numerical Results Comparing Constant and Variable Step-Size Procedures

The results of the previous Section were derived from single-step position and velocity error functions and were valid in the limit as the step-size became very small. A trajectory is calculated by dividing the total time of flight into several smaller steps and applying the multi-

conic methods as a stepwise numerical integration scheme. The error in the position or velocity at the final time arises from a multi-step procedure. As was noted at the end of Chapter 4, all the trajectory calculations involved in generating the results of Chapter 5 were performed by a routine which used a constant step size of 6 hours. The choice of 6 hours did not result from any analysis but from the experience the author had in using the multi-conic methods to propagate trajectories. A constant step-size procedure is simple but a more efficient procedure might be obtained by varying the step size at each step.

However, the single-step position error functions derived in Appendices C and D can be used to define a variable step-size procedure. The error functions yield the position error as a function of the initial conditions and the step size. If a maximum allowable position error magnitude per step is specified, one could solve for the step size to use on each step. In other words, using the error function as a predictor of the error, we solve for the largest step size possible without exceeding some specified error bound. For instance, the fourth-order position error for the Stumpff-Weiss method is given by

$$\delta\bar{R} = \frac{\mu\,(1-\mu)}{24\,R^3 r^3}\,(\bar{\alpha} + \bar{\beta})\,h^4 \tag{6.36}$$

where $\bar{\alpha}$ and $\bar{\beta}$ are defined by Equations (6.24) and (6.25). Taking the absolute value of both sides and solving for the step size yields

$$h = \left[\frac{24\,R^3 r^3\,|\delta\bar{R}|}{\mu(1-\mu)\,|\bar{\alpha}+\bar{\beta}|}\right]^{1/4} \tag{6.37}$$

Equation (6.37), which is valid only in the dimensionless units (Section 5.1), is a formula for the step size in terms of an error bound $|\delta\bar{R}|$ and may be used to define a variable step-size procedure. Formulas for the step size for the Earth-Moon and Moon-Earth methods are also easily found.

In addition to defining a variable step-size procedure, these formulas

for the step size also may be used to determine which of the multi-conic methods to use at any step. The logic is to use the method which allows the largest step size to be taken for a given error. The error function may therefore be used as a switching function. A switch from one method to another would occur whenever the trajectory crossed one of the curves on Figures 25 and 26 depending on whether all three or only a given pair of the multi-conic methods are available.

It was decided to test the performance of the multi-conic trajectory propagation methods in order to determine the effects of step size on the position and velocity errors at the final time and to find out whether it would be advantageous to use the error functions for determining step size and switching. The five different methods of propagating trajectories which were tested, with a symbol in parenthesis for each which will be used on figures to denote results associated with that method, are listed below:

1. Stumpff-Weiss method with constant step size (s).
2. Earth-Moon method with constant step size (em).
3. Moon-Earth method with constant step size (me).
4. Stumpff-Weiss method with variable step size determined from error function (s - variable step).
5. Combination of Earth-Moon and Moon-Earth methods with variable step size and switching determined from error function (em + me - variable step).

The above five methods were tested on three different trajectories, all of which have times of flight equal to 48 hours. The first of these trajectories is a 48 hour segment of an Earth-to-Moon transfer. This trajectory is shown on Figure 27. The coordinate system used on Figure 27 is a rotating geocentric coordinate system. The x-axis is the Earth-Moon line. This coordinate system is the same as the rotating barycentric coordinate system of Chapter 5 in all respects except that the origin is at the Earth and not the barycenter. Also shown on Figure 27 are those equal error curves from Figures 25 and 26 which this trajectory crosses. A crossing of any of the dotted curves on Figure 27 will cause a switch from one multi-conic mode to another for method (5) above. The second test trajectory is a 48 hour segment of the Moon-to-

Fig. 27 TEST TRAJECTORY I FOR EVALUATING THE ACCURACY OF THE MULTI-CONIC METHODS

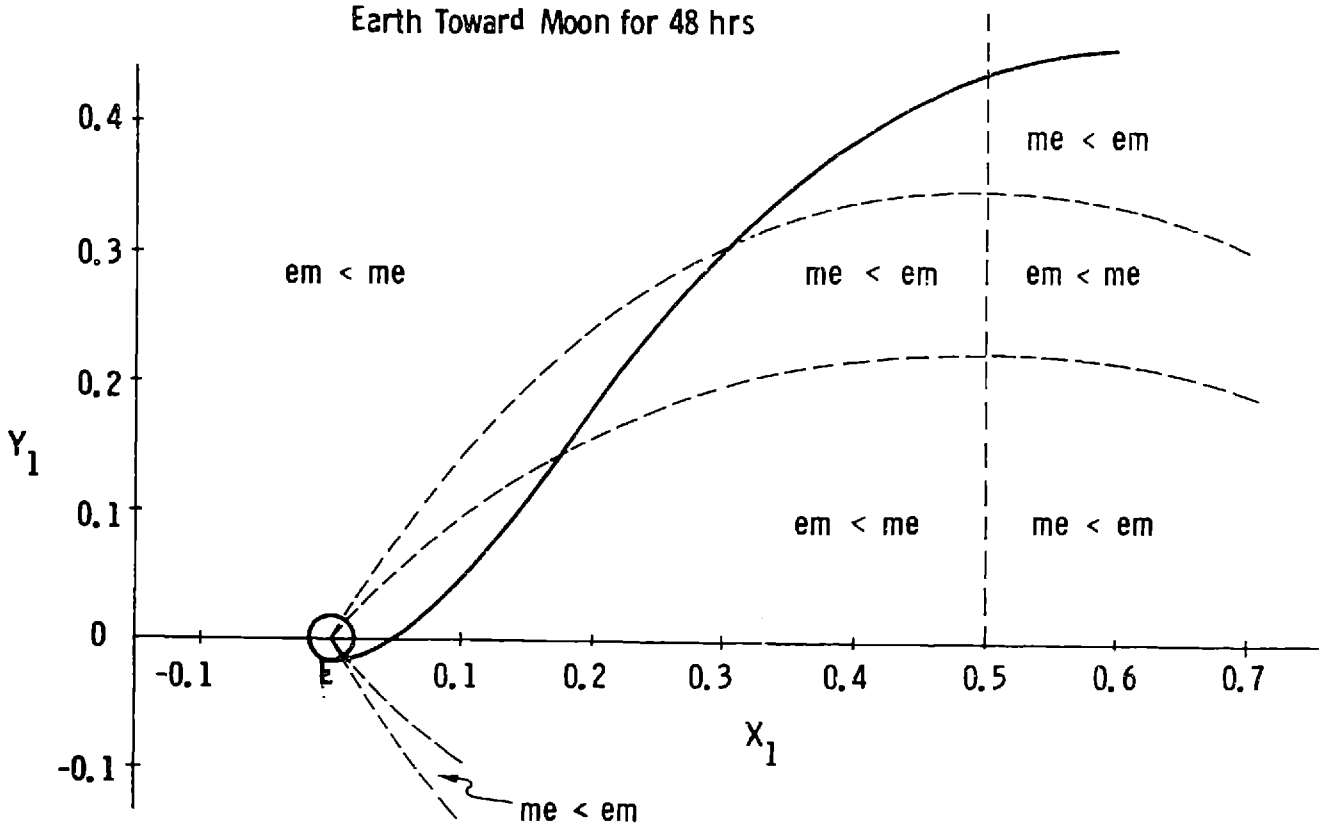

Earth transfer. This trajectory is shown on Figure 28 also in the rotating geocentric coordinate system. The trajectories on Figures 27 and 28 were chosen as test trajectories because they represent motion predominately toward and away from the Moon, respectively. The third test trajectory is shown in Figure 29 again in the rotating geocentric coordinate system. This trajectory was chosen because it is typical of the trajectories investigated in Chapter 5 in that it starts at the L_2 libration point and ends at the Moon.

Each of the five methods of propagating a trajectory was applied to each of the three test trajectories to calculate the final position and velocity for various numbers of steps. For the first three methods which are constant-step methods, the number of steps in the propagation can be specified beforehand, but for the last two methods, which are variable-step methods, a maximum allowable position error per step is specified and then the number of steps the method used is noted. The magnitude of the error in the final position vector is used as a meausre of accuracy, and the number of steps used in the propagation is taken as a measure of how much time was spent in propagating the trajectory, because each step in the integration procedure involves the solution of two Kepler problems and these Kepler solutions are the most time comsuming calculations of the multi-conic procedure. As the number of steps gets very large, the final position vector for any method approaches the exact final position vector. The exact final position vector was taken to be that final position vector such that a further increase in the number of steps would not significantly change the results.

For the 48 hour segment of the Earth-to-Moon transfer, the logarithm (base 10) of the magnitude of the final position error (divided by one kilometer) for the three constant-step methods is polotted on Figure 30 as a function of the logarithm (base 10) of the number of steps used in the propagation. It can be seen that for few steps, i.e., large step sizes, the Earth-Moon method has the smallest error, the Moon-Earth method has the largest error, and the Stumpff-Weiss method has an intermediate performance. However, as the step size gets very small,

Fig. 28 TEST TRAJECTORY 2 FOR EVALUATING THE ACCURACY OF THE MULTI-CONIC METHODS

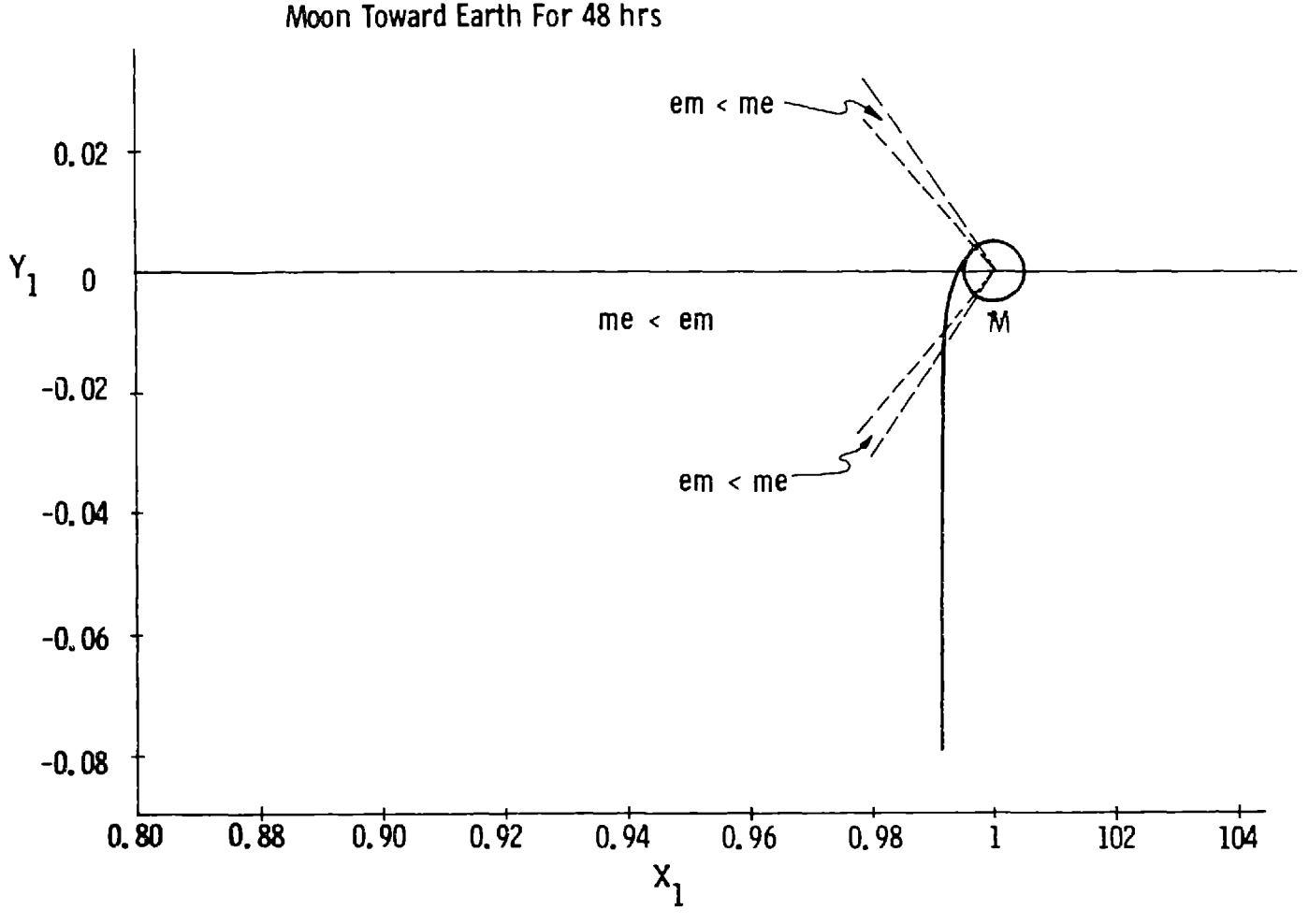

Fig. 29 TEST TRAJECTORY 3 FOR EVALUATING THE ACCURACY OF THE MULTI-CONIC METHODS

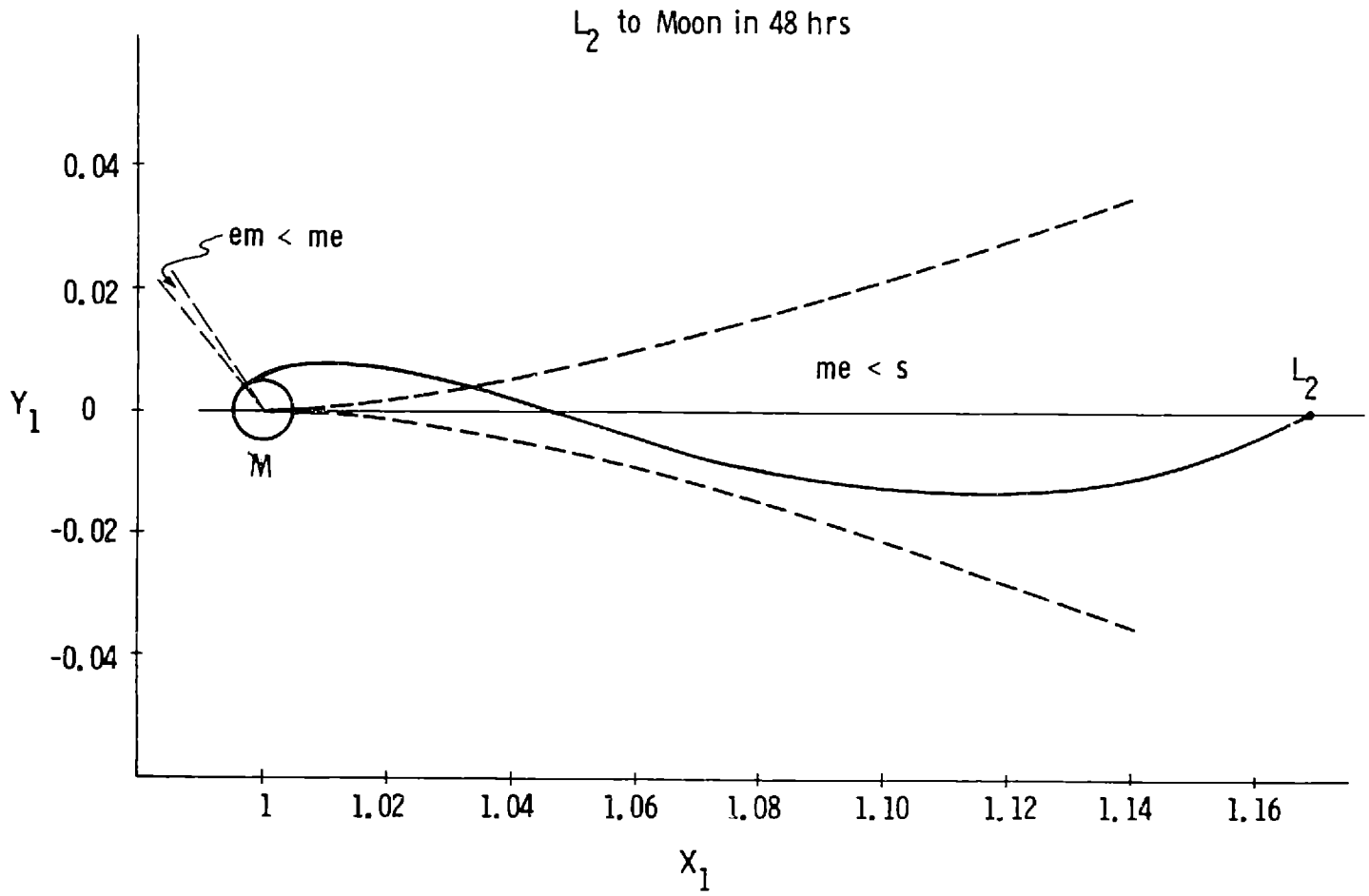

Fig 30

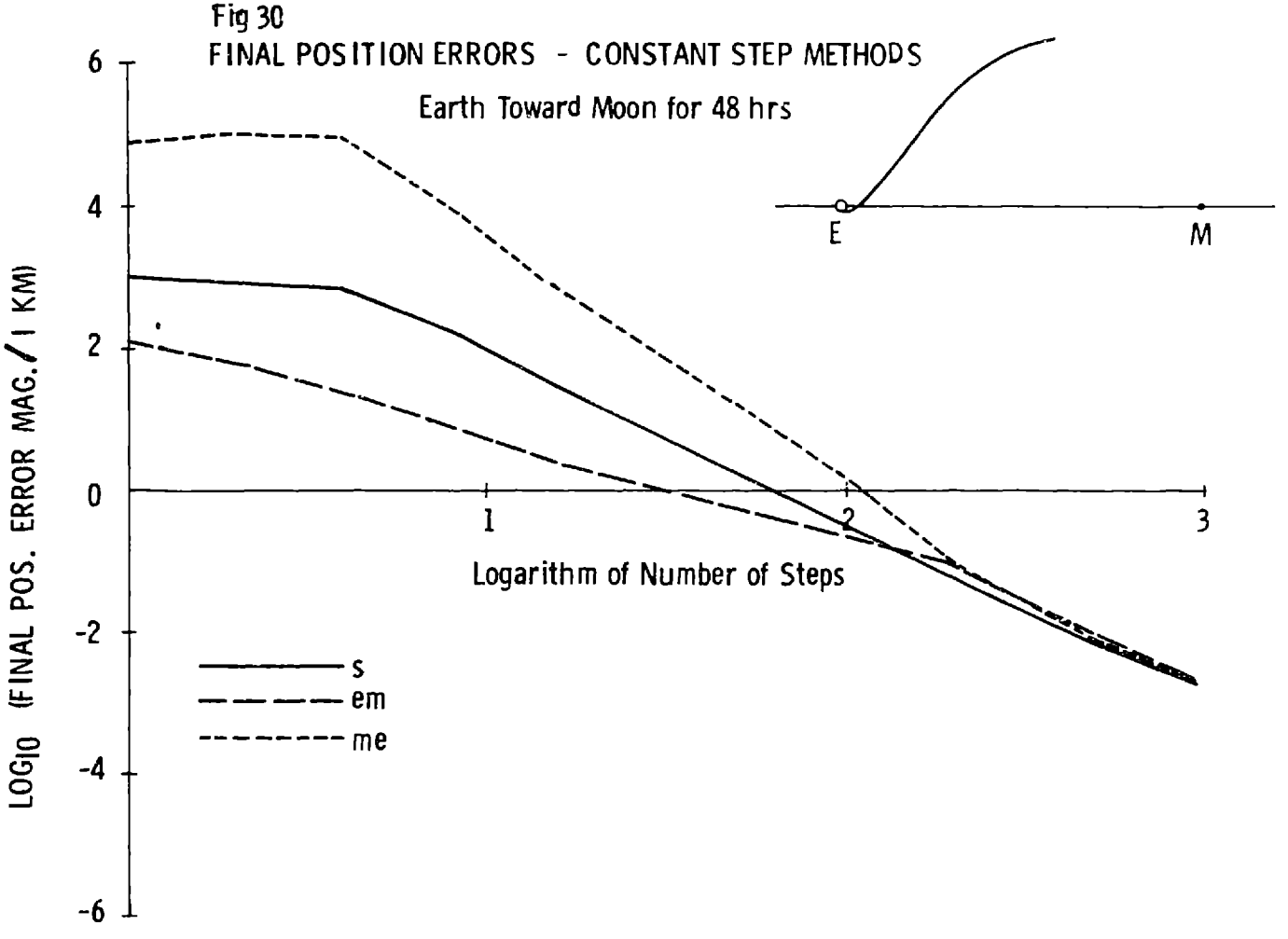
FINAL POSITION ERRORS - CONSTANT STEP METHODS
Earth Toward Moon for 48 hrs
E
M
6
4
2
0
-2
-4
-6
1
2
3
Logarithm of Number of Steps
LOG10 (FINAL POS. ERROR MAG. / 1 KM)
s
em
me

the position errors of all three constant step-size methods become nearly identical. On Figure 31, the same plot is made for the Stumpff-Weiss method with variable step size, the combination variable-step method (method 5), and the Earth-Moon constant-step method. The Earth-Moon constant-step method is included because it was the constant-step method with the best overall performance. It can be seen that except for very large step sizes, the position errors of the two variable step-size methods are about the same and offer an improvement over the constant-step method with the smallest errors.

On Figures 32 and 33 the same plots are displayed for the 48 hour segment of the Moon-to-Earth transfer. A similar behavior is evident on these figures. For the constant-step methods, the best performance for large step sizes is associated with the Moon-Earth method, the worst performance with the Earth-Moon method, and an intermediate performance with the Stumpff-Weiss method. The method whose derivation used the assumption about the nature of the trajectory which were satisfied by the test trajectory has the best performance. The Stumpff-Weiss method which has no such assumptions about the nature of the trajectory has an intermediate performance. The method with the wrong assumptions has the worst performance. However, for small step sizes, all three constant-step methods have approximately equal position errors. Again the variable-step methods show an improvement for a large range of step sizes (Figure 33).

On Figures 34 and 35 the same results are illustrated for the 48 hour L_2-to-Moon transfer. Here the results are slightly different. This trajectory is not a trajectory which really satisfies either set of assumptions used to generate the Earth-Moon and Moon-Earth methods. The motion along the trajectory is neither away from the Earth and toward the Moon nor vice versa. The position errors of all three constant step methods are essentially the same. Also the variable step methods offer no great improvement.

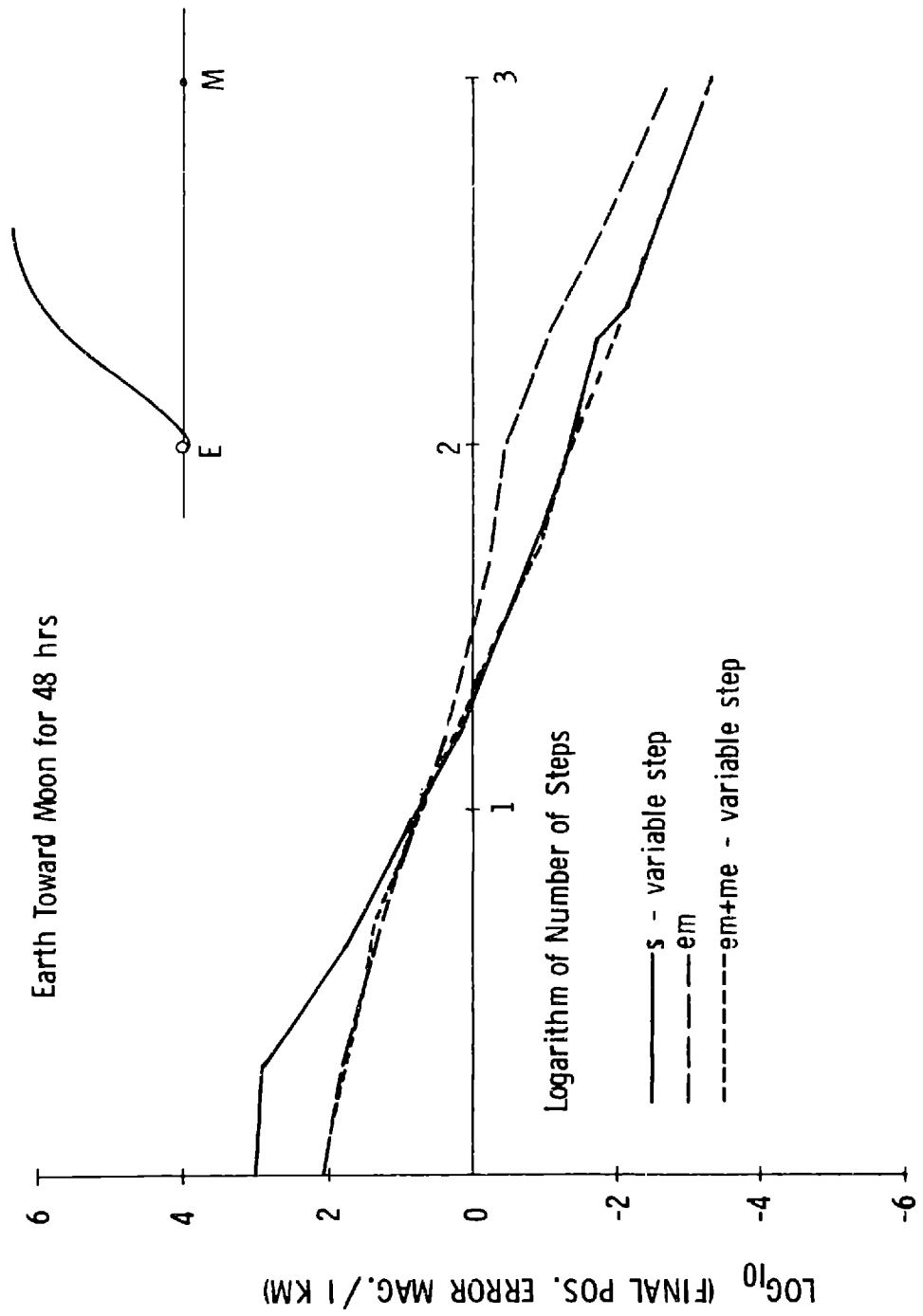

Fig. 31 FINAL POSITION ERRORS - VARIABLE STEP METHODS

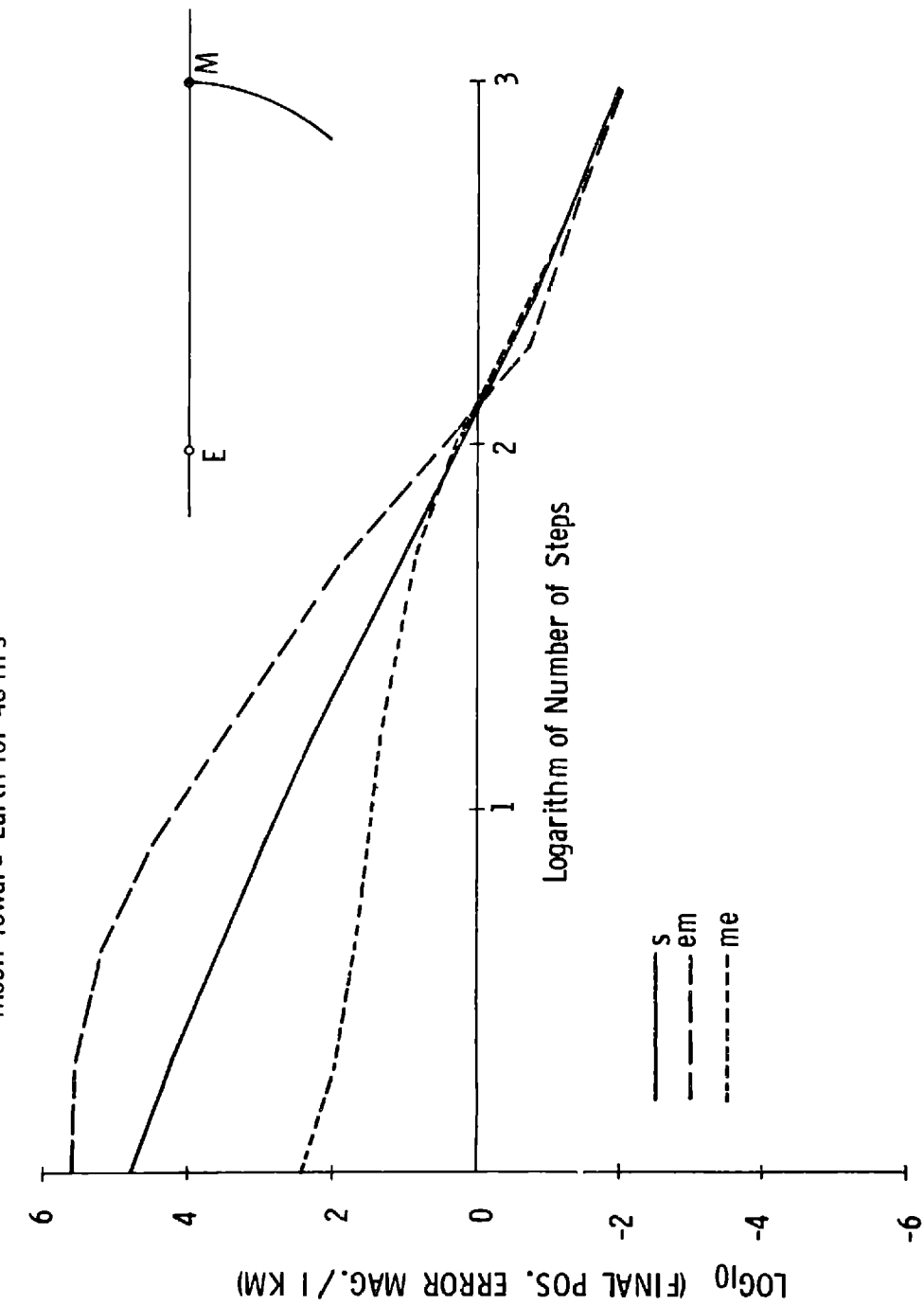

Fig. 32 FINAL POSITION ERRORS - CONSTANT STEP METHODS

Moon Toward Earth for 48 hrs

Fig. 33 FINAL POSITION ERRORS - VARIABLE STEP METHODS

Moon Toward Earth For 48 Hrs

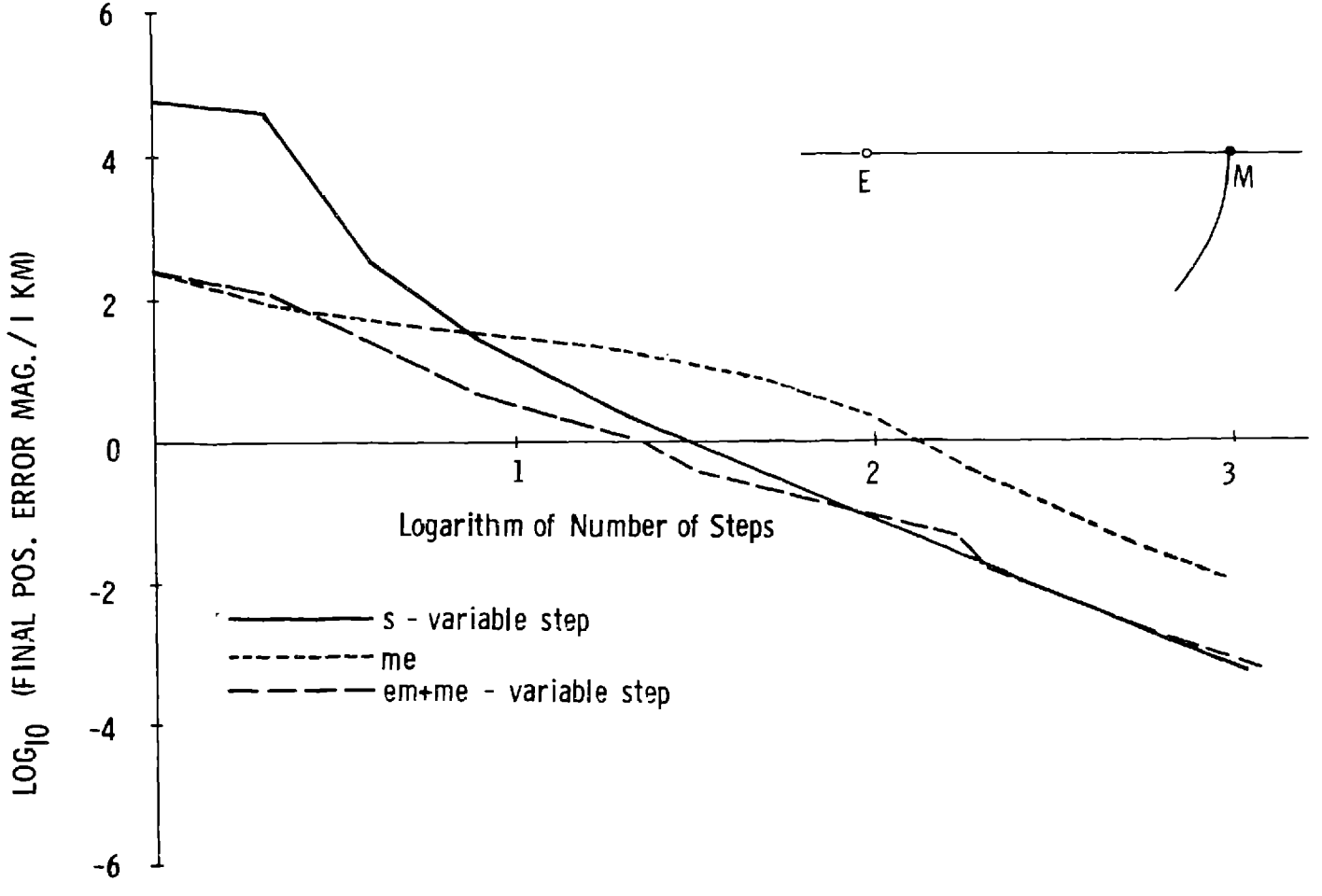

Fig. 34 FINAL POSITION ERRORS - CONSTANT STEP METHODS

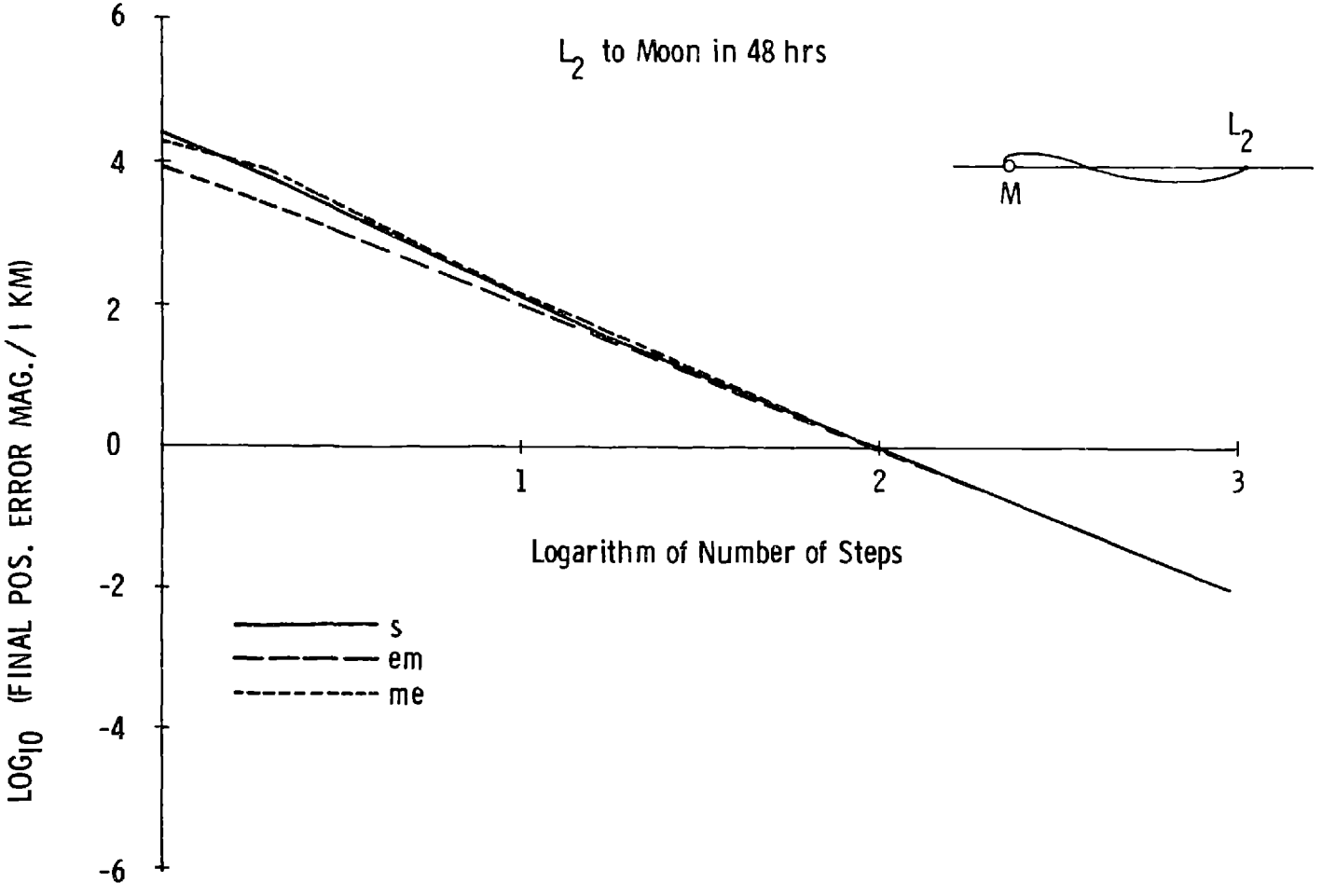

Fig. 35 FINAL POSITION ERRORS - VARIABLE STEP METHODS

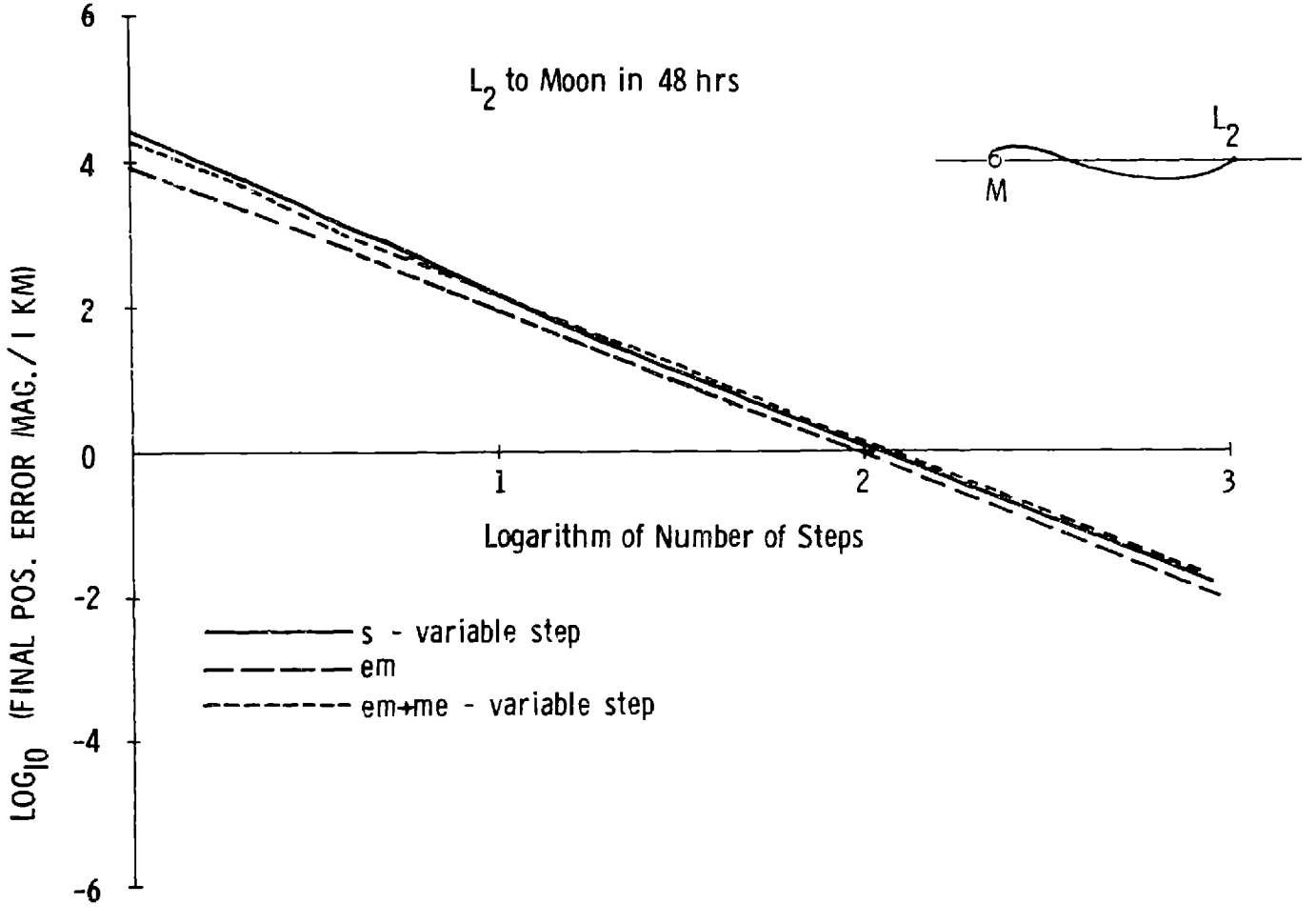

The results which have been presented in this Section can be explained with the help of the single-step position and velocity error functions and by remembering the assumptions used to derive the multi-conic methods. For large step sizes (few steps), the truncated series for the error functions do not apply because they are only valid in the limit as the step size becomes very small. With reference to the constant-step methods, the results showed that the method whose assumptions concerning the direction of motion relative to the Earth and Moon were satisfied by the particular trajectory under investigation, has the smallest position error for large step sizes. Thus the results are consistent with the theory. For instance, if a spacecraft is moving along an Earth-to-Moon trajectory toward the Moon, the multi-conic method which propagates geocentric conics from the initial state and selenocentric conics from the final state, i.e., the Earth-Moon method, will have the smallest error. Furthermore, the method which makes the wrong assumptions would be expected to have worse performance than a method which makes no such assumptions, the Stumpff-Weiss method, which always propagates both conics from the initial state. Hence, if prior information as to the nature of the trajectory is available, then, when large steps are used in propagating the trajectory, the use of either the Earth-Moon or Moon-Earth method yields a definite improvement over the Stumpff-Weiss method in terms of final position errors. This results agrees with that of Wilson[15]. The L_2-to-Moon trajectory is neither an Earth-to-Moon type nor a Moon-to-Earth type, so that no method is substantially superior.

The results also show that for the constant-step methods, all three methods had essentially the same position error for small step sizes regardless of the nature of the trajectory. This does not seem to agree with theory since the single-step position error functions are different for each of the methods. From Figure 27 one can see that the trajectory does not remain in an area of space where either the Earth-Moon or Moon-Earth method has the smaller per-step position error relative to the other but is continually entering and leaving such regions. This would lead one to believe that the Earth-Moon and Moon-Earth methods would have about the same performance. But the trajectory of Figure 27

never leaves that region of space where the Stumpff-Weiss method has the smallest per step position error of all three methods (see Figure 26), yet the final position error for the Stumpff-Weiss method is no better than that of the other two methods for small step sizes (Figure 30). Similar arguments can be made about the other two test trajectories. For instance from Figure 29, it can be seen that the L_2-to-Moon trajectory spends a good deal of its time in a region of space where the Moon-Earth method has the smallest per-step position error, yet again all three methods have about the same final position error for small step sizes (Figure 34).

The single-step position error functions cannot explain these results. The reason is that the final position error after many small steps is caused not only by the per-step position error, but also by the per-step velocity error. In fact, the major portion of the final position error is caused by the per-step velocity error. If a trajectory propagation took n steps, then the final position error at the end of the nth step would consist of the position error due to the nth step and the contributions from the position and velocity errors of the previous n-1 steps, errors which propagate according to the state transition matrix. The velocity derivatives in the state transition matrix typically are larger in magnitude than the position derivatives. The orders of magnitude of the elements in the partitions of the state transition matrix are typically as shown below:

$$\begin{bmatrix} 1 & >1 \\ <1 & 1 \end{bmatrix}$$

The per-step velocity errors have a greater effect at a later time than do the per-step position errors and also the per-step position error is a higher order function of the time step than the per-step velocity error. Hence, in a multi-step propagation, the final position error is caused mainly by the contributions of the per-step velocity errors. The results can now be explained. Since the per-step velocity errors are the same for all three multi-conic methods for small step sizes, then the final

position (and velocity) errors will be of approximately the same magnitude for all three methods because the per-step velocity errors tend to dominate as causes of final position and velocity errors through the state transition matrix.

It was noted from the results that the variable-step methods showed an improvement over the constant-step methods for small step sizes. The reason for this is that although the variable step-size procedure theoretically should work since it adjusts the size of the step according to an error prediction, thus dividing the total time of flight into steps more efficiently, its performance depends on the accuracy of the error function, and the accuracy of the error function becomes better as more steps are used, i.e., as smaller steps are taken.

With the results from this and previous Sections, a statement may be made concerning the relative advantages of the multi-conic methods. For the calculation of accurate trajectories, it appears that the Stumpff-Weiss method is the one to use for several reasons. First, the Stumpff-Weiss method is the simplest to use. The other two methods should always be used together, thus necessitating switching logic. Secondly, the velocity errors, which dominate, are the same for all three methods, so that there would be no advantage to using one of the other methods. Finally, the calculation of the state transition matrix for the Stumpff-Weiss method is an additive process, while for the other two methods it is a multiplicative process, and hence for computer operations, the Stumpff-Weiss calculation is less susceptible to truncation errors.

It was concluded above that the final position and velocity errors after many steps were caused mainly by the per-step velocity error, which is for small steps a third order function of the time step. The final position and velocity errors after many small steps would therefore be expected to be second-order functions of the time step if equal time steps are used, because for a constant step-size numerical integration procedure, the error after many small steps is usually a one order lower function of the step size than the per-step error. The terminal slopes of any of the

final position error curves for the constant step methods on Figures 30, 32, and 34 confirm this second-order behavior since a one order of magnitude decrease in the step size produces a two order of magnitude decrease in the final position error.

6.4 Integral Formulation of the Error Functions

The results at the beginning of Section 6.2 motivated a new approach to the derivation of the error functions. In this new approach, expansions of the geocentric and selenocentric three-body accelerations about the corresponding two-body accelerations are introduced into the derivation of the multi-conic methods in order to develop an integral formulation of the error functions.

First the integral error functions for the Stumpff-Weiss method will be derived. We start as before with the first two integrals of Equation (3.1) which are given by Equations (3.6) and (3.8):

$$\dot{\bar{R}}_F - \dot{\bar{R}}_I = -A\int_I^F \frac{\bar{R}_J}{R_J^3}\,dt_J - a\int_I^F \frac{\bar{r}_J}{r_J^3}\,dt_J - a\int_I^F \frac{\bar{\rho}_J}{\rho_J^3}\,dt_J \tag{6.38}$$

$$\bar{R}_F - \bar{R}_I = h\dot{\bar{R}}_I - A\int_I^F\int_I^K \frac{\bar{R}_J}{R_J^3}\,dt_J dt_K - a\int_I^F\int_I^K \frac{\bar{r}_J}{r_J^3}\,dt_J dt_K - a\int_I^F\int_I^K \frac{\bar{\rho}_J}{\rho_J^3}\,dt_J dt_K \tag{6.39}$$

The integrals involving $\bar{\rho}_J$ in the above expressions are known exactly and are given by Equations (3.16) and (3.17). On the other hand, the integrals involving $\bar{R}_J$ and $\bar{r}_J$ are integrals of functions of the three-body geocentric or selenocentric position and cannot be evaluated exactly. In Chapter 3, the geocentric and selenocentric position vectors were approximated by two-body position vectors propagated forward from the initial time, i.e., $\bar{R}_{IAJ}$ and $\bar{r}_{IaJ}$ in order to derive the Stumpff-Weiss method. Here we go one step further and use as an approximation for $\bar{R}_J$ and $\bar{r}_J$ an expansion of $\bar{R}_J$ and $\bar{r}_J$ about the quantities $\bar{R}_{IAJ}$ and $\bar{r}_{IaJ}$.

The expansions of $\overline{R}_J/R_J^3$ and $\overline{r}_J/r_J^3$ may be written as

$$\frac{\overline{R}_J}{R_J^3} = \frac{\overline{R}_{IAJ}}{R_{IAJ}^3} + \frac{\partial}{\partial \overline{R}_J}\left(\frac{\overline{R}_J}{R_J^3}\right)\Bigg|_{\overline{R}_J=\overline{R}_{IAJ}} \left(\overline{R}_J-\overline{R}_{IAJ}\right) + \ldots \tag{6.40}$$

$$\frac{\overline{r}_J}{r_J^3} = \frac{\overline{r}_{IaJ}}{r_{IaJ}^3} + \frac{\partial}{\partial \overline{r}_J}\left(\frac{\overline{r}_J}{r_J^3}\right)\Bigg|_{\overline{r}_J=\overline{r}_{IaJ}} \left(\overline{r}_J-\overline{r}_{IaJ}\right) + \ldots \tag{6.41}$$

With the definitions of G_{A_J} and G_{a_J} given in Equations (6.7) and (6.8) the above two equations become

$$\frac{\overline{R}_J}{R_J^3} = \frac{\overline{R}_{IAJ}}{R_{IAJ}^3} - \frac{1}{A} G_{A_{IAJ}} \left(\overline{R}_J-\overline{R}_{IAJ}\right) + \ldots \tag{6.42}$$

$$\frac{\overline{r}_J}{r_J^3} = \frac{\overline{r}_{IaJ}}{r_{IaJ}^3} - \frac{1}{a} G_{a_{IaJ}} \left(\overline{r}_J-\overline{r}_{IaJ}\right) + \ldots \tag{6.43}$$

where the notation $G_{A_{IAJ}}$ signifies replacing $\overline{R}_J$ in G_{A_J} by $\overline{R}_{IAJ}$. The quantity $G_{a_{IaJ}}$ is defined similarly. If one defines $\delta\overline{R}_J$ and $\delta\overline{r}_J$ as

$$\delta\overline{R}_J = \overline{R}_J - \overline{R}_{IAJ} \tag{6.44}$$

$$\delta\overline{r}_J = \overline{r}_J - \overline{r}_{IaJ} \tag{6.45}$$

then

$$\frac{\overline{R}_J}{R_J^3} = \frac{\overline{R}_{IAJ}}{R_{IAJ}^3} - \frac{1}{A} G_{A_{IAJ}} \delta\overline{R}_J + \ldots \tag{6.46}$$

$$\frac{\overline{r}_J}{r_J^3} = \frac{\overline{r}_{IaJ}}{r_{IaJ}^3} - \frac{1}{a} G_{a_{IaJ}} \delta\overline{r}_J + \ldots \tag{6.47}$$

The integrals involving R_J in Equations (6.38) and (6.39) may be evaluated with the substitution of Equation (6.46) (neglecting the higher order terms):

$$-A\int_I^F \frac{\bar{R}_J}{R_J^3}\,dt_J \cong -A\int_I^F \frac{\bar{R}_{IAJ}}{R_{IAJ}^3} + \int_I^F G_{A_{IAJ}}\,\delta\bar{R}_J\,dt_J$$

$$= \dot{\bar{R}}_{IAF} - \dot{\bar{R}}_I + \int_I^F G_{A_{IAJ}}\,\delta\bar{R}_J\,dt_J \qquad (6.48)$$

$$-A\int_I^F\int_I^K \frac{\bar{R}_J}{R_J^3}\,dt_J dt_K \cong -A\int_I^F\int_I^K \frac{\bar{R}_{IAJ}}{R_{IAJ}^3}\,dt_J dt_K + \int_I^F\int_I^K G_{A_{IAJ}}\,\delta\bar{R}_J\,dt_J dt_K$$

$$= \bar{R}_{IAF} - \bar{R}_I - h\dot{\bar{R}}_I + \int_I^F\int_I^K G_{A_{IAJ}}\,\delta\bar{R}_J\,dt_J dt_K \qquad (6.49)$$

In a similar fashion, the integrals involving $\bar{r}_J$ in Equations (6.38) and (6.39) become, with the substitution of Equation (6.47):

$$-a\int_I^F \frac{\bar{r}_J}{r_J^3}\,dt_J \cong \dot{\bar{r}}_{IaF} - \dot{\bar{r}}_I + \int_I^F G_{a_{IaJ}}\,\delta\bar{r}_J\,dt_J \qquad (6.50)$$

$$-a\int_I^F\int_I^K \frac{\bar{r}_J}{r_J^3}\,dt_J dt_K \cong \bar{r}_{IaF} - \bar{r}_I - h\dot{\bar{r}}_I + \int_I^F\int_I^K G_{a_{IaJ}}\,\delta\bar{r}_J\,dt_J dt_K \qquad (6.51)$$

Now substituting Equations (6.48), (6.50) and (3.16) into E uation (6.38),

$$\dot{\bar{R}}_F \cong \dot{\bar{R}}_{IAF} + \dot{\bar{r}}_{IaF} - \dot{\bar{r}}_I + \mu\,(\dot{\bar{\rho}}_F - \dot{\bar{\rho}}_I) + \int_I^F \left(G_{A_{IAJ}}\,\delta\bar{R}_J + G_{a_{IaJ}}\,\delta\bar{r}_J\right) dt_J \tag{6.52}$$

and substituting Equations (6.49), (6.51) and (3.17) into Equation (6.39),

$$\bar{R}_F \cong \bar{R}_{IAF} + \bar{r}_{IaF} - \bar{r}_I - h\dot{\bar{r}}_I + \mu\,(\bar{\rho}_F - \bar{\rho}_I - h\dot{\bar{\rho}}_I)$$

$$+ \int_I^F \int_I^K \left(G_{A_{IAJ}}\,\delta\bar{R}_J + G_{a_{IaJ}}\,\delta\bar{r}_J\right) dt_J dt_K \tag{6.53}$$

Therefore the position and velocity error functions for the Stumpff-Weiss method may be written as

$$\delta\bar{R}_s(t_F) = \int_I^F \int_I^K \left(G_{A_{IAJ}}\,\delta\bar{R}_J + G_{a_{IaJ}}\,\delta\bar{r}_J\right) dt_J dt_K \tag{6.54}$$

$$\delta\dot{\bar{R}}_s(t_F) = \int_I^F \left(G_{A_{IAJ}}\,\delta\bar{R}_J + G_{a_{IaJ}}\,\delta\bar{r}_J\right) dt_J \tag{6.55}$$

For the Moon-Earth method, in order to evaluate the integrals of $\bar{R}_J$ and $\bar{r}_J$ in Equations (6.38) and (6.39), the approximations used were $\bar{R}_J \cong \bar{R}_{FAJ}$ and $\bar{r}_J \cong \bar{r}_{IaJ}$. Therefore, in this case, the expansion for $\bar{R}_J/R_J^3$ is

$$\frac{\bar{R}_J}{R_J^3} = \frac{\bar{R}_{FAJ}}{R_{FAJ}^3} - \frac{1}{A}\,G_{A_{FAJ}}\,\delta\bar{R}_J^* + \ldots \tag{6.56}$$

where

$$\delta\bar{R}_J^* = \bar{R}_J - \bar{R}_{FAJ} \tag{6.57}$$

and the expansion for $\bar{r}_J/r_J^3$ is the same as Equation (6.47). The integrals involving $\bar{R}_J$ become

$$-A\int_I^F \frac{\bar{R}_J}{R_J^3}\,dt_J \cong \bar{R}_F - \bar{R}_{FAI} + \int_I^F G_{A_{FAJ}}\,\delta\bar{R}_J^*\,dt_J \tag{6.58}$$

$$-A\int_I^F\int_I^K \frac{\overline{R}_J}{R_J^3}\,dt_K dt_K \cong \overline{R}_F - \overline{R}_{FAI} - h\dot{\overline{R}}_{FAI} + \int_I^F\int_I^K G_{A_{FAJ}}\,\delta\overline{R}_J^{\,*}\,dt_J dt_K \quad (6.59)$$

and the integrals involving $\overline{r}_J$ are the same as Equations (6.50) and (6.51). Substituting Equations (6.50), (6.58) and (3.16) into Equation (6.38), one obtains

$$\dot{\overline{R}}_{FAI} = \dot{\overline{r}}_{IaF} + \dot{\overline{\rho}}_I + \mu\,(\dot{\overline{\rho}}_F - \dot{\overline{\rho}}_I) + \int_I^F \left(G_{A_{FAJ}}\,\delta\overline{R}_J^{\,*} + G_{a_{IaJ}}\,\delta\overline{r}_J\right) dt_J \quad (6.60)$$

Substituting Equations (6.51), (6.59) and (3.17) into Equation (6.39), and simplifying with Equation (6.60),

$$\begin{aligned}\overline{R}_{FAI} &= \overline{r}_{IaF} + \overline{\rho}_I - h\dot{\overline{r}}_{IaF} + \mu\,(\overline{\rho}_F - \overline{\rho}_I - h\dot{\overline{\rho}}_F) \\ &\quad + \int_I^F\int_I^K \left(G_{A_{FAJ}}\,\delta\overline{R}_J^{\,*} + G_{a_{IaJ}}\,\delta\overline{r}_J\right) dt_J dt_K \\ &\quad - h\int_I^F \left(G_{A_{FAJ}}\,\delta\overline{R}_J^{\,*} + G_{a_{IaJ}}\,\delta\overline{r}_J\right) dt_J \qquad (6.61)\end{aligned}$$

The integral expressions in Equations (6.60) and (6.61) yield the errors in the estimates of $\overline{R}_{FAI}$ and $\dot{\overline{R}}_{FAI}$ for the Moon-Earth method. That is, we have found the errors in the position and velocity just prior to the last geocentric conic of the Moon-Earth method. The position and velocity after the last geocentric conic are the estimates of the true three-body position and velocity. The errors in these estimates are easily found. First let us write the errors in $\overline{R}_{FAI}$ and $\dot{\overline{R}}_{FAI}$ which are taken from Equations (6.60) and (6.61),

$$\delta\dot{\overline{R}}_{FAI}(t_F) = \int_I^F \left(G_{A_{FAJ}}\,\delta\overline{R}_J^{\,*} + G_{a_{IaJ}}\,\delta\overline{r}_J\right) dt_J \qquad (6.62)$$

$$\delta\bar{R}_{FAI}(t_F) = \int_I^F \int_I^K \left(G_{A_{FAJ}} \delta\bar{R}_J^* + G_{a_{IaJ}} \delta\bar{r}_J \right) dt_J dt_K$$

$$- h \int_I^F \left(G_{A_{FAJ}} \delta\bar{R}_J^* + G_{a_{IaJ}} \delta\bar{r}_J \right) dt_J \qquad (6.63)$$

Then the errors in the final position and velocity are

$$\begin{bmatrix} \delta\bar{R}_{me}(t_F) \\ \dot{\delta\bar{R}}_{me}(t_F) \end{bmatrix} = \Phi_{2B}^{A}(t_F, t_I) \begin{bmatrix} \delta\bar{R}_{FAI}(t_F) \\ \dot{\delta\bar{R}}_{FAI}(t_F) \end{bmatrix} \qquad (6.64)$$

where $\Phi_{2B}^{A}(t_F, t_I)$ is, as in Chapter 3, the state transition matrix associated with a two-body geocentric conic, which in this case is the final conic of the Moon-Earth method.

The final position and velocity errors for the Earth-Moon method may be found in a similar fashion and are given by

$$\begin{bmatrix} \delta\bar{R}_{em}(t_F) \\ \dot{\delta\bar{R}}_{em}(t_F) \end{bmatrix} = \Phi_{2B}^{a}(t_F, t_I) \begin{bmatrix} \delta\bar{r}_{FaI}(t_F) \\ \dot{\delta\bar{r}}_{FAI}(t_F) \end{bmatrix} \qquad (6.65)$$

where

$$\dot{\delta\bar{r}}_{FaI}(t_F) = \int_I^F \left(G_{A_{IAJ}} \delta\bar{R}_J + G_{a_{FaJ}} \delta\bar{r}_J^* \right) dt_J \qquad (6.66)$$

$$\delta\bar{r}_{FaI}(t_F) = \int_I^F \int_I^K \left(G_{A_{IAJ}} \delta\bar{R}_J + G_{a_{FaJ}} \delta\bar{r}_J^* \right) dt_J dt_K$$

$$- h \int_I^F \left(G_{A_{IAJ}} \delta\bar{R}_J + G_{a_{FaJ}} \delta\bar{r}_J^* \right) dt_J \qquad (6.67)$$

$$\delta\bar{r}_J^{\,*} = \bar{r}_J - \bar{r}_{FaJ} \tag{6.68}$$

and $\delta\bar{R}_J$ is defined by Equation (6.44). The matrix $\Phi^a_{2B}(t_F, t_I)$ is the two-body state transition matrix associated with the last selenocentric conic propagation of the Earth-Moon method.

This new formulation of the error functions yields approximate analytical expressions for the final position and velocity errors. They would still be approximate even if the integrals could be evaluated exactly, because the expansions, which were substituted for the unknown functions of $\bar{R}_J$ and $\bar{r}_J$, were truncated, and only the linear terms were retained. On the other hand, the Taylor series formulation derived in Appendices C and D would yield the error functions to any desired accuracy for any step size if a sufficiently large number of terms for the series were included. Of course, the effort required is prohibitive. It appears that the integral expressions for the errors, if easily calculable, yield a more accurate estimate of the errors than a truncated Taylor series, because information at both ends of the trajectory segment from t_I to t_F is included in the integral expressions, whereas in the Taylor series formulas for the errors, only information of the initial state (at t_I) is utilized.

By examining the integral formulas for the error functions, it can once again be shown (as in Appendix C) that the derivative of the position error is equal to the velocity error for the Stumpff-Weiss method but not for the Earth-Moon or Moon-Earth methods. The position and velocity errors for the Stumpff-Weiss method are given by Equations (6.54) and (6.55). Note that combining these two equations allows one to write the position error as

$$\delta\bar{R}_s(t_F) = \int_I^F \delta\dot{\bar{R}}_s(t_K)\, dt_K \tag{6.69}$$

The position error is the first integral of the velocity error, or the derivative of the position error is equal to the velocity error.

For the Moon-Earth method, if the errors in $\bar{R}_{FAI}$ and $\dot{\bar{R}}_{FAI}$ given by Equations (6.62) and (6.63) satisfy the test that the derivative of the position error is equal to the velocity error, then the errors in the final position and velocity will also satisfy the test, and the converse is also true, because the final position and velocity are found by propagating $\bar{R}_{FAI}$ and $\dot{\bar{R}}_{FAI}$ forward on a geocentric conic, and the final conic propagation will preserve either the satisfaction or non-satisfaction of the test. The above reasoning is also stated in Apprndix D. The errors in $\bar{R}_{FAI}$ and $\dot{\bar{R}}_{FAI}$ are given by Equations (6.62) and (6.63). Combining these two equations allows one to write the error in $\bar{R}_{FAI}$ as

$$\delta\bar{R}_{FAI}(t_F) = \int_I^F \delta\dot{\bar{R}}_{FAI}(t_K)\, dt_K - h\, \delta\dot{\bar{R}}_{FAI}(t_F) \qquad (6.70)$$

Taking the derivative of the above equation yields

$$\frac{d}{dt_F}\delta\bar{R}_{FAI}(t_F) = -h\frac{d}{dt_F}\delta\dot{\bar{R}}_{FAI}(t_F) \qquad (6.71)$$

The derivative of the error in $\bar{R}_{FAI}$ is not equal to the error in $\dot{\bar{R}}_{FAI}$ and therefore the derivative of the error in the final position is not equal to the error in the final velocity.

Due to the integral nature of the error functions derived in this Section, they cannot be evaluated with knowledge only of the state at t_I. That is, the errors cannot be calculated prior to taking a step. Therefore, these integral error functions are not useful as predictors of the error, so that they can not be used for internal step-size control or for switching from one multi-conic method to another. They can be used, however, to determine approximately the errors in position and velocity after a step has been taken. Adding these error estimates to the estimates of the three-body position and velocity would yield more accurate final position and velocity results. For instance, Equations (6.52) and (6.53) could be

used to define more accurate estimates of the three-body final position and velocity for the Stumpff-Weiss method, and any quadrature formulas can be used to evaluate the integrals.

For the Earth-Moon or Moon-Earth method, we may eliminate the calculation of the final position and velocity errors according to Equation (6.64) or (6.65) and simply use the integrals of Equations (6.62) and (6.63) or (6.66) and (6.67) to calculate additive corrections for the state prior to the last conic. No numerical results utilizing the integral formulations of the error functions have been generated.

CHAPTER 7
THE VARIABLE END-POINT TRAJECTORY OPTIMIZATION PROBLEM

7.1 Preliminary Remarks

The trajectory optimization problem, which was introduced in Chapter 2 and whose solution was outlined in Chapter 4, may be called the fixed end-point trajectory optimization problem. Whenever a three-impulse trajectory is optimized by iterating on the position and time of the interior impulse, the position and velocity at the final time are fixed throughout the iteration. However, a fixed final state is not consistent with certain problem statements. For instance, the criterion for all the trajectories investigated in Chapter 5 was that the final position and velocity should establish the spacecraft in a circular orbit of given altitude. Since all the trajectories of Chapter 5 lay in the plane of the Moon's orbit about the Earth, a specified inclination of zero degrees was also applied. The problem statement really was concerned with a circular orbit of desired altitude and inclination at the final time rather than with a specific position and velocity at the final time.

To fully solve the optimization problem to a circular orbit of zero inclination, a time consuming procedure was used in Chapter 5. Once a converged three-impulse trajectory was found, a new problem was defined by respecifying the final position vector while maintaining its magnitude. That is, the final position vector was varied around a circle, and the optimization problem was resolved many times to find the minimum of the converged three-impulse solutions with respect to the point of insertion into the circular orbit. Specifying the arrival angle, φ, which was arbitrarily defined as in Figure 6, fully determined the insertion point for a position vector lying in the Earth-Moon plane. Each new problem had a new fixed final position vector, and for each new final position vector the final velocity vector was chosen such that a circular orbit was established. The magnitude of the final velocity vector is of course determined from the magnitude of the position vector, and it must

also lie in the Earth-Moon plane; otherwise, the inclination of the circular orbit would not be zero.

The cumbersome procedure described above enabled the solution of the trajectory optimization problem to a circular orbit of desired altitude and zero inclination to be found with a fixed end-point trajectory optimization method. Notice that if a non-zero inclination were desired, then this procedure would become quite unwieldy since the specification of the insertion point would then require two angles, such as the longitude of the ascending node, Ω, and the argument of latitude, θ (see Figure 36). A variable end-point optimization technique is introduced in the next Section.

7.2 Variable End-Point Constraints and the Transversality Conditions

For the fixed end-point trajectory optimization problem, the position and velocity at the final time, $\bar{r}_f$ and $\bar{v}_f$, are fully specified. For the variable end-point problem, no components of the final position or velocity are specified, but they must satisfy a set of constraints. At this point the analysis will be specialized to the case for which the constraints are those which will insure a circular orbit of desired altitude and inclination at the final time.

A set of constraints satisfying the above requirements are

$$|\bar{r}_f| = r \tag{7.1}$$

$$|\bar{v}_f| = \sqrt{\frac{a}{r}} \tag{7.2}$$

$$\bar{r}_f{}^T \bar{v}_f = 0 \tag{7.3}$$

$$\bar{u}_z{}^T \bar{u}_h = \cos i \tag{7.4}$$

where $\bar{u}_z$ is a unit vector normal to the Earth-Moon plane, and $\bar{u}_h$ is a unit vector normal to the orbit plane. The quantity $\bar{u}_h$ is defined as

Fig. 36 DEFINITION OF THE LONGITUDE OF THE ASCENDING NODE AND THE ARGUMENT OF LATITUDE FOR A LUNAR ORBIT

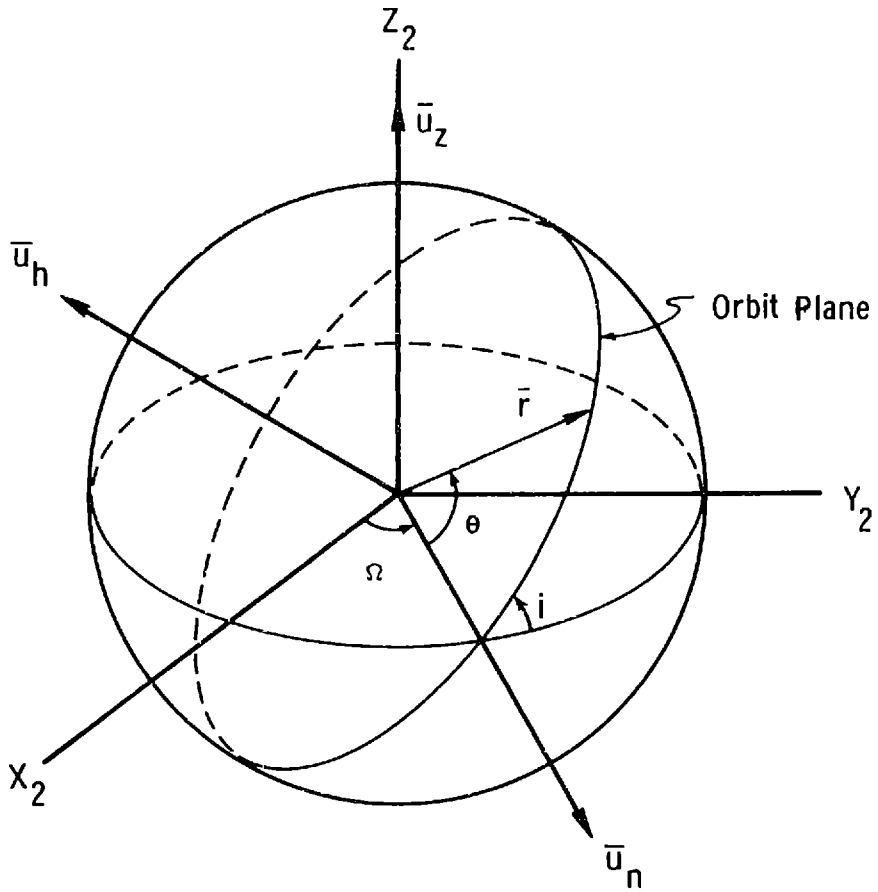

$$\bar{u}_h = \frac{\bar{h}_f}{h_f} \tag{7.5}$$

where $\bar{h}_f = \bar{r}_f \times \bar{v}_f$. The above equations refer to the case of a final lunar orbit. The altitude of the desired circular orbit determines r, the magnitude of the final position vector, and also the magnitude of the final velocity vector. The radial velocity at the final time must of course be zero for a circular orbit, and the dot product between a unit vector normal to the Earth-Moon plane and a unit vector normal to the orbit plane must be equal to the cosine of the desired inclination. Satisfying the above four constraints will insure that at the final time the spacecraft will be in a circular orbit of desired altitude and inclination.

For the fixed end-point problem, each of the six components of the final state (position and velocity) is specified. For the variable end-point problem, the final position and velocity must satisfy four scalar constraints given by Equations (7.1) to (7.4). Since there are only four scalar constraints for the variable end-point problem, two additional boundary conditions are needed to fully specify the problem. These are provided by two transversality conditions involving the adjoint variables, i.e., the primer vector and its derivative. Before deriving these transversality conditions, a few statements about the necessary conditions can be made.

Because there are only four constraints involving the state at the final time, the set of allowable end points is a manifold of dimension two. Let us assume that a variable end-point optimization problem has been solved and that the final position and velocity on the manifold which satisfied the solution are $\bar{r}_f$ and $\bar{v}_f$. Now this solution is of course also the solution to the fixed end-point optimization problem for which the specified final position and velocity are $\bar{r}_f$ and $\bar{v}_f$. Because the solution is valid for that particular fixed end point, the four necessary conditions on the primer vector (listed in Section 4.1) will be satisfied. If, in addition, a gradient search procedure was used to find the solution, then the solution is a local minimum. In order to find a solution to the fixed end-point

trajectory optimization problem, we must find the trajectory which arrives at the specified final state and which satisfies the necessary conditions on the primer vector. In order to find a solution to the variable end-point trajectory optimization problem, we must find the trajectory which satisfies the four scalar constraints on the final state, Equations (7.1) to (7.4), i.e., which arrives at the allowable end-point manifold, which satisfies the necessary conditions on the primer vector, and which also satisfies two transversality conditions. If the above trajectory is found with a gradient search procedure, the solution is a local minimum.

From optimal control theory, the two transversality conditions needed to complete the specification of the boundary conditions are given by the condition that the adjoint vector be perpendicular to the constant manifold at the final time. Let the four scalar constraints be written as

$$\psi_1 = |\bar{r}_f| - r = 0 \tag{7.6}$$

$$\psi_2 = |\bar{v}_f| - \sqrt{\frac{a}{r}} = 0 \tag{7.7}$$

$$\psi_3 = \bar{r}_f{}^T \bar{v}_f = 0 \tag{7.8}$$

$$\psi_4 = \bar{u}_z{}^T \bar{u}_h - \cos i = 0 \tag{7.9}$$

From Chapter 2, the adjoint vector for position was defined as $\bar{\mu}$, and the adjoint vector for velocity was defined as $\bar{\lambda}$, the primer vector. But $\bar{\mu} = -\dot{\bar{\lambda}}$, so that the full adjoint vector is

$$\begin{bmatrix} -\dot{\bar{\lambda}} \\ \bar{\lambda} \end{bmatrix}$$

the transversality conditions are therefore given by

$$-\dot{\bar{\lambda}}_f = \sum_{i=1}^{4} \mu_i \frac{\partial \psi_i}{\partial \bar{r}_f} \tag{7.10}$$

$$\bar{\lambda}_f = \sum_{i=1}^{4} \mu_i \frac{\partial \psi_i}{\partial \bar{v}_f} \tag{7.11}$$

where the μ_i are arbitrary constants.

A more useful form of the transversality conditions may be obtained if an orbital element formulation for the final state is employed. If the final position and velocity satisfy the four scalar constraints, Equations (7.1) to (7.4), then this is equivalent to specifying the following quantities: a, the semi-major axis of the orbit, e, the eccentricity, and i, the inclination. The time of insertion into the orbit is also known and is equal to t_f. The constraints specify a circular orbit, so that $a = r$ and $e = 0$. The orbital elements left unspecified are Ω and θ, the longitude of the ascending node and the argument of latitude. We use the argument of latitude rather than the argument of the periapse point because for a circular orbit a periapse point is undefined. In an orbital element formulation of the boundary conditions, four components of the state at the final time are specified, and two, Ω and θ, are free.

From optimal control theory, if any of the components of the final state are free, the adjoint variables associated with those components must be zero at the final time. Thus the two transversality conditions necessary to complete the specifications of the boundary conditions at the final time are

$$\lambda_\Omega(t_f) = 0 \tag{7.12}$$

$$\lambda_\theta(t_f) = 0 \tag{7.13}$$

where λ_Ω and λ_θ are the adjoint variables for the longitude of the

ascending node and the argument of latitude respectively. Equations (7.12) and (7.13) together with Equations (7.1) to (7.4), provide six boundary conditions at the final time. A trajectory which is the solution to the variable end-point optimization problem must satisfy the necessary conditions on the primer vector, the four constraints on the final state given by Equations (7.1) to (7.4), and the two transversality conditions given by Equations (7.12) and (7.13).

Since the state variables which we have been using are the components of position and velocity vectors and not the orbital elements, we have available to us the adjoint vectors associated with position and velocity, i.e., the primer vector $\overline{\lambda}$, and its derivative. Therefore, the adjoint variables associated with Ω and θ must be expressed in terms of the primer vector and its derivative. This has been done and the results[24, 25] are

$$\lambda_{\Omega} = (\overline{v} \times \overline{\lambda} + \dot{\overline{\lambda}} \times \overline{r})^{T} \overline{u}_{z} \qquad (7.14)$$

$$\lambda_{\theta} = (\overline{v} \times \overline{\lambda} + \dot{\overline{\lambda}} \times \overline{r})^{T} \overline{u}_{h} \qquad (7.15)$$

The vector quantity within the parentheses is a constant of the motion for optimal impulsive trajectories in an inverse square force field. Notice that on an optimal trajectory this vector is constant across an impulse, because $\overline{\lambda}$, $\dot{\overline{\lambda}}$, and $\overline{r}$ are everywhere continuous, and the change in $\overline{v}$ at each impulse is in the direction lf $\overline{\lambda}$. Notice also that the adjoint variable for each angle is simply the dot product of this particular vector and a unit vector normal to the plane in which the angle is measured (see Figure 36). The transversality conditions, Equations (7.12) and (7.13), may now be written in terms of the familiar primer vector and and the final position and velocity vectors:

$$(\overline{v}_{f} \times \overline{\lambda}_{f} + \dot{\overline{\lambda}}_{f} \times \overline{r}_{f})^{T} \overline{u}_{z} = 0 \qquad (7.16)$$

$$(\bar{v}_f \times \bar{\lambda}_f + \dot{\bar{\lambda}}_f \times \bar{r}_f)^T \bar{u}_h = 0 \qquad (7.17)$$

The original incentive for solving the variable end-point trajectory optimization problem came from the laborious method used to find the minimum of the converged three-impulse solutions of Chapter 5 with respect to arrival angle. The method which will be developed in the remaining part of this section will concern itself with two-impulse trajectories from the L_2 libration point to a circular orbit about the Moon for non-zero inclination. All of the trajectories studied in Chapter 5 were in the Earth-Moon plane. Many two-impulse trajectories were investigated to find candidates for which an additional impulse would decrease the cost. Then the fixed end-point trajectory optimization method was used to iterate on the position and time of the interior impulse to minimize the total cost of the three-impulse trajectory. All the two-impulse trajectories which were investigated were calculated with the modified Lambert routine of Section 3.3. The modified Lambert routine fits a trajectory between a given initial position and a given final position magnitude with no radial velocity and any desired inclination. The initial position was always that of L_2. The initial impulse was then defined as the difference between the velocity the spacecraft has at L_2 and the velocity which is a solution to the modified Lambert problem. The final impulse established the spacecraft in a circular orbit. Since the spacecraft had no radial velocity at the final time and since a zero inclination was desired the final impulse was tangential.. The point here is that all the two-impulse trajectories which were investigated in Chapter 5 were planar and utilized a tangential impulse to establish the circular orbit at the destination body.

It was noted in Section 3.3 that tangential injection minimized the magnitude of the final impulse because the greatest change in the energy of an orbit is achieved by an impulse along the velocity vector. In this Section it has been shown that an optimal injection is one which satisfies the two transversality conditions expressed by Equations (7.16) and (7.17), because the two degrees of freedom of the injection are determined by the angles Ω and θ. Now we can determine whether for planar trajectories

such as those of Chapter 5, a tangential injection does satisfy the transversality conditions. Let us define the vector quantity $\bar{c}_f$ as

$$\bar{c}_f = \bar{v}_f \times \bar{\lambda}_f + \dot{\bar{\lambda}}_f + \bar{r}_f \tag{7.18}$$

The transversality conditions are then

$$\bar{c}_f{}^T \bar{u}_z = 0 \tag{7.19}$$

$$\bar{c}_f{}^T \bar{u}_h = 0 \tag{7.20}$$

Since the final impulse is a tangential one which serves only to slow the spacecraft to circular orbit velocity, then $\bar{\lambda}_f$, which is aligned with the impulse, points in the direction opposite to that of the final velocity vector $\bar{v}_f$ (see Figure 37) and therefore

$$\bar{v}_f \times \bar{\lambda}_f = 0 \tag{7.21}$$

Therefore, we have that

$$\bar{c}_f{}^T \bar{u}_z = (\dot{\bar{\lambda}}_f \times \bar{r}_f)^T \bar{u}_z \tag{7.22}$$

But

$$(\dot{\bar{\lambda}}_f \times \bar{r}_f)^T \bar{u}_z = \dot{\bar{\lambda}}_f{}^T (\bar{r}_f \times \bar{u}_z) \tag{7.23}$$

by a vector identity for scalar triple products. Noting from Figure 37 that $\bar{\lambda}_f$ is a unit vector which points in the direction of the product $\bar{r}_f \times \bar{u}_z$, we can write

$$\dot{\bar{\lambda}}_f{}^T (\bar{r}_f \times \bar{u}_z) = r_f \dot{\bar{\lambda}}_f{}^T \lambda_f \tag{7.24}$$

But $\dot{\bar{\lambda}}_f{}^T \bar{\lambda}_f = \dot{\lambda}_f \lambda_f$ and $\lambda_f = 1$ by definition, so that

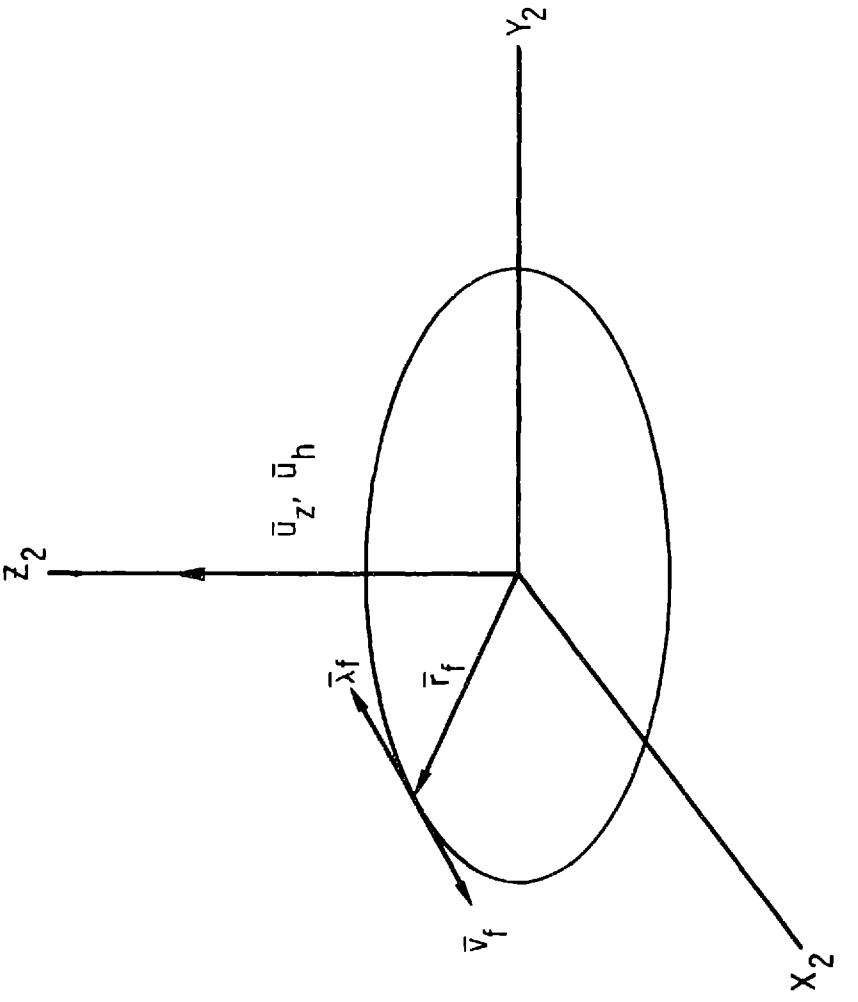

Fig. 37 ORIENTATION FOR A PLANAR TANGENTIAL INJECTION

$$\bar{c}_f{}^T \bar{u}_z = r_f \dot{\lambda}_f \tag{7.25}$$

Also since for a zero inclination orbit $\bar{u}_h = \bar{u}_z$, we have

$$\bar{c}_f{}^T \bar{u}_h = \bar{c}_f{}^T \bar{u}_z = r_f \dot{\lambda}_f \tag{7.26}$$

Unless $\dot{\lambda}_f = 0$, the two transversality conditions (which reduce to one condition for a planar trajectory) will not be satisfied, and a tangential injection is not optimal for planar transfers. As noted in Chapter 5, for time-optimal transfers, that is, for transfers which can not be improved by a coasting segment, $\dot{\lambda}_f = 0$. For the special case of time-open transfers a tangential injection will be optimal for planar trajectories. But in general tangential injection for two-impulse transfers to a zero inclination circular orbit is not optimal. The same statement can be made for non-zero inclination circular orbits. It would be interesting to apply a variable end-point trajectory optimization method to two-impulse trajectories to a circular orbit of desired altitude and various inclinations to determine what improvement the optimal injection makes over a tangential injection.

The variable end-point method may be developed as follows. From optimal control theory, it is true that if a solution satisfies the necessary conditions, the adjoint variables are influence functions for small variations in the corresponding state variables. Let us consider Ω and θ as the two variables which are being varied. Then

$$\delta J = \lambda_\Omega(t_f)\, \delta\Omega_f + \lambda_\theta(t_f)\, \delta\theta_f \tag{7.27}$$

The adjoint variables $\lambda_\Omega(t_f)$ and $\lambda_\theta(t_f)$ give estimates of the gradient of the cost with respect to small changes in Ω_f and θ_f:

$$\lambda_\Omega(t_f) \cong \frac{\partial J}{\partial \Omega_f} \tag{7.28}$$

$$\lambda_\theta(t_f) \cong \frac{\partial J}{\partial \theta_f} \tag{7.29}$$

Therefore, we can iterate on Ω_f and θ_f, the two variables which represent the two degrees of freedom of the point of insertion into the circular orbit, in order to minimize the total cost of the two-impulse trajectory. As the optimal solution is approached in the convergence procedure, $\lambda_\Omega(t_f)$ and $\lambda_\theta(t_f)$ become more accurate approximations to the true gradients, and at the solution the gradients must of course be zero:

$$\lambda_\Omega(t_f) = 0 \tag{7.30}$$

$$\lambda_\theta(t_f) = 0 \tag{7.31}$$

But these are exactly the transversality conditions which must be satisfied at the final time. Combining Equations (7.14) and (7.15) with Equations (7.28) and (7.29), the estimates of the gradients are

$$\frac{\partial J}{\partial \Omega_f} = (\bar{v}_f \times \bar{\lambda}_f + \dot{\bar{\lambda}}_f \times \bar{r}_f)^T \bar{u}_z \tag{7.32}$$

$$\frac{\partial J}{\partial \theta_f} = (\bar{v}_f \times \bar{\lambda}_f + \dot{\bar{\lambda}}_f \times \bar{r}_f)^T \bar{u}_h \tag{7.33}$$

The variable end-point trajectory optimization method which minimizes the cost with respect to the longitude of the node and the argument of latitude for a two-impulse trajectory to a circular orbit of desired altitude and inclination is summarized in the next Section.

7.3 Summary of the Variable End-Point Trajectory Optimization Method

The overall step-by-step procedure for finding fuel-optimal two-impulse trajectories to a circular orbit of desired altitude and inclination is summarized below with pertinent formulas included (this outline also gives the structure of the Fortran program used to obtain the results of the next Section):

1. Given the initial state vector, the position magnitude and inclination of the desired circular orbit, and the transfer time, solve the modified Lambert problem to find a two-impulse reference solution with a tangential injection.

2. Compute $\bar{\lambda}_o$, $\bar{\lambda}_f$, and $\dot{\bar{\lambda}}_o$ from

$$\bar{\lambda}_o = \frac{\Delta\bar{v}_o}{|\Delta\bar{v}_o|} \qquad \bar{\lambda}_f = \frac{\Delta\bar{v}_f}{|\Delta\bar{v}_f|} \tag{7.34a,b}$$

$$\dot{\bar{\lambda}}_o = \varphi_{12}^{-1}(t_f, t_o)\,[\bar{\lambda}_f - \varphi_{11}(t_f, t_o)\,\bar{\lambda}_o] \tag{7.35}$$

and generate a primer history according to

$$\bar{\lambda}(t) = \varphi_{11}(t, t_o)\,\bar{\lambda}_o + \varphi_{12}(t, t_o)\,\dot{\bar{\lambda}}_o \tag{7.36}$$

3. Evaluate the transversality conditions

$$(\bar{v}_f \times \bar{\lambda}_f + \dot{\bar{\lambda}}_f \times \bar{r}_f)^T \bar{u}_z \stackrel{?}{=} 0 \tag{7.37}$$

$$(\bar{v}_f \times \bar{\lambda}_f + \dot{\bar{\lambda}}_f \times \bar{r}_f)^T \bar{u}_h \stackrel{?}{=} 0 \tag{7.38}$$

4(a). If either of the transversality conditions is violated, use the Jacobson-Oksman algorithm to iterate on Ω_f and θ_f and minimize the cost of the two-impulse trajectory. The cost and cost gradient are found at each iteration by first solving the Lambert problem from $\bar{r}_o$ to the $\bar{r}_f$ which is calculated from the desired position magnitude, Ω_f, and θ_f, and then using the following relations:

$$J = |\Delta\bar{v}_o| + |\Delta\bar{v}_f| \tag{7.39}$$

$$\frac{\partial J}{\partial \Omega_f} = (\bar{v}_f \times \bar{\lambda}_f + \dot{\bar{\lambda}}_f \times \bar{r}_f)^T \bar{u}_z \tag{7.40}$$

$$\frac{\partial J}{\partial \theta_f} = (\bar{v}_f \times \bar{\lambda}_f + \dot{\bar{\lambda}}_f \times \bar{r}_f)^T \bar{u}_h \tag{7.41}$$

where $\bar{\lambda}_o$, $\bar{\lambda}_f$ and $\dot{\bar{\lambda}}_o$ are calculated as in Equations (7.34) and (7.35) and

$$\dot{\bar{\lambda}}_f = \varphi_{21}(t_f, t_o)\,\bar{\lambda}_o + \varphi_{22}(t_f, t_o)\,\dot{\bar{\lambda}}_o \qquad (7.42)$$

4(b). If both transversality conditions are satisfied and $|\bar{\lambda}(t)|$ does not exceed unity anywhere between the initial and final times, the two-impulse solution is locally optimal.

4(c). If both transversality conditions are satisfied but $|\bar{\lambda}(t)|$ does exceed unity then the insertion point is optimal for two-impulses but a third impulse will reduce the cost and the fixed end-point optimization procedure must be used to find a converged three-impulse trajectory.

5. Examine the primer history of the converged two-impulse trajectory by computing $\bar{\lambda}(t)$ as in Equations (7.34) to (7.36) in order to determine if $|\bar{\lambda}(t)|$ exceeds unity so that a third impulse should be added and a converged three-impulse trajectory found.

It should be noted that during the two-impulse optimization procedure outlined above (see 4(a)), the final position vector is not fixed. At each iteration, the new Ω_f and θ_f and the desired final position magnitude serve to fully define the new $\bar{r}_f$. Then a Lambert problem is solved from $\bar{r}_o$ to $\bar{r}_f$ with transfer time $t_f - t_o$. The initial impulse is the difference between the velocity vector which is a solution to the Lambert problem and the given initial velocity vector of the problem statement. The final impulse is the difference between the velocity required to establish a circular orbit at $\bar{r}_f$ of desired altitude and inclination (this velocity must be recomputed at each iteration from $\bar{r}_f$) and the velocity of arrival at $\bar{r}_f$. The final impulse is not in general tangential. Of course for the starting two-impulse solution, it is tangential by definition.

7.4 Numerical Results

The trajectories to which the variable end-point trajectory optimization method was applied were two-impulse transfers from the L_2 libration point to a 185.2 km (100 nautical mile) circular orbit about the Moon for a transfer time of 72 hours. A transfer time of 72 hours was chosen because that time was mentioned to the author as a time of flight which might be used in a real-life mission. Various inclinations between 0^o and 180^o were investigated. In order to obtain the corresponding

trajectories from the Moon to L_2, one should use either the image with respect to the xz plane or the image with respect to the x-axis. These images are explained in Section 5.1. Trajectories are displayed in the rotating barycentric coordinate system defined in Section 5.1.

As stated in the previous Section, the starting trajectory for the variable end-point optimization procedure is the two-impulse trajectory which uses a tangential impulse to establish the desired circular orbit. The 72 hour transfer from L_2 to the Moon which employ a tangential impulse at the Moon and which result in circular orbits of 0^o and 180^o inclination are shown on Figure 38. The 0^o inclination solution establishes a circular orbit whose sense of ratation is the same as that of the Earth-Moon line. The 180^o inclination solution results in a circular orbit with a sense of rotation opposite to that of the Earth-Moon line. The angular momentum vector of the circular orbit points directly out of the Earth-Moon plane toward the observer ofor the 0^o inclination orbit and away from the observer for the 180^o inclination orbit.

The 0^o inclination solution is a member of the fast family of two-impulse planar transfers between the Moon and L_2 investigated in Section 5.2. The 180^o solution is a member of the family of two-impulse planar transfers between the Moon and L_2 whose existence was noted in Section 5.2. This family was not investigated in Section 5.2 because the ΔV's were higher than those of the fast family for the same time of flight. In this Section we are not comparing trajectories of different inclinations. For any trajectory which results in an orbit with an inclination between 0^o and 180^o, the two angles Ω and θ are required to specify the final position vector, i.e., the injection point. For an orbit in the Earth-Moon plane, such as a 0^o or 180^o inclination orbit, only one angle is needed. In Chapter 5, the arrival angle was used. The arrival angle was arbitrarily defined as the angle between the direction of the final position vector and the direction of the negative x-axis in rotating barycentric coordinates. The complement of the arrival angle is equal to $\Omega + \theta$ for an orbit of 0^o inclination and $\Omega - \theta$ for an orbit of 180^o inclination. When

Fig. 38 TWO - IMPULSE TRAJECTORIES BETWEEN THE MOON AND L_2 FOR INCLINATIONS OF 0^0 AND 180^0

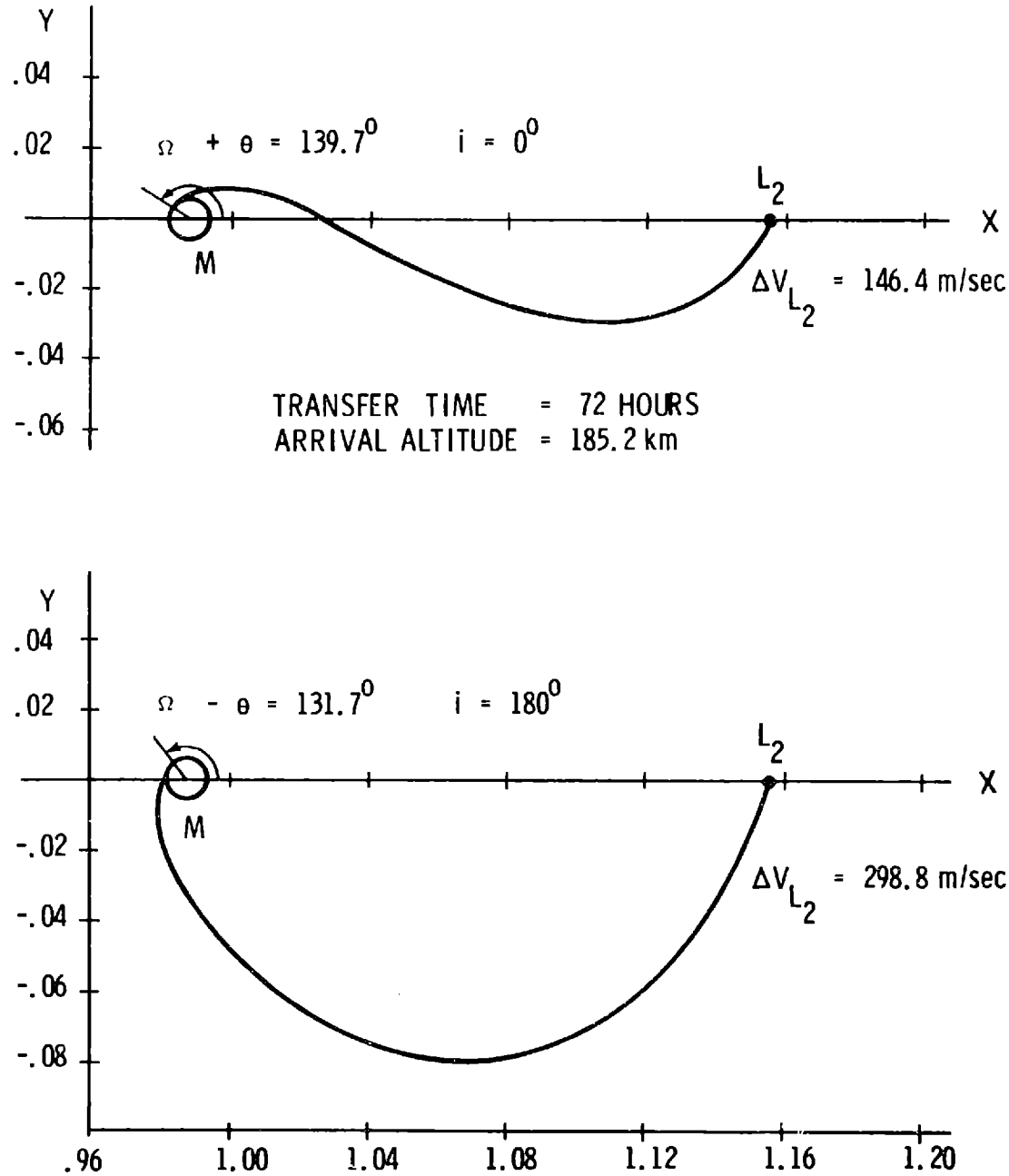

the variable end=point optimization method was applied to the 0^{o} and 180^{o} solutions, only one angle was iterated upon and that angle was $\Omega + \theta$ for 0^{o} and $\Omega - \theta$ for 180^{o}.

A family of trajectories may be defined as the two-impulse trajectories from L_2 to the Moon which (1) have the same transfer time, (2) establish circular orbits of the same altitude by means of a tangential injection, and (3) have inclinations between 0^{o} and 360^{o}. Such a family of trajectories will form a three-dimensional envelope in space. The intersection with the Earth-Moon plane of the envelope corresponding to a transfer time of 72 hours and an altitude of 185.2 km, yields the two trajectories on Figure 38. All the trajectories for orbits between 0^{o} and 180^{o} lie predominately below the Earth-Moon plane. All the trajectories for orbits between 180^{o} and 360^{o} lie predominately above the Earth-Moon plane. The projections on the xy and xz planes of the trajectory for the 90^{o} inclination orbit are shown in Figure 39. That portion of the trajectory which passes behind the Moon from the point of view of the observer is denoted by a dotted line. The longitude of the ascending node for the resulting circular orbit can be shown directly on the xy plane projection.

Trajectories in the above mentioned family having various inclinations between and including 0^{o} and 180^{o} were used as inputs for the variable end-point trajectory optimization program. All these trajectories utilize a tangential impulse to establish the circular orbit. None of them satisfied the transversality conditions. For inclination between 0^{o} and 180^{o}, the independent variables of the iteration were Ω_f and θ_f. For 0^{o} the independent variable was $\Omega_f + \theta_f$, or the angle between the position vector and the position direction of the x-axis. For 180^{o} the independent variable was $\Omega_f - \theta_f$ and has the same definition as the independent variable for 0^{o}. Recall that the two transversality conditions are identical for planar trajectories.

The results showed that a tangential injection was very close to optimal for inclinations between 0^{o} and 180^{o} and almost exactly optimal for the two planar trajectories having 0^{o} and 180^{o} inclinations. For

Fig. 39 TWO-IMPULSE TRAJECTORY BETWEEN THE MOON AND L_2 FOR INCLINATION OF 90^0

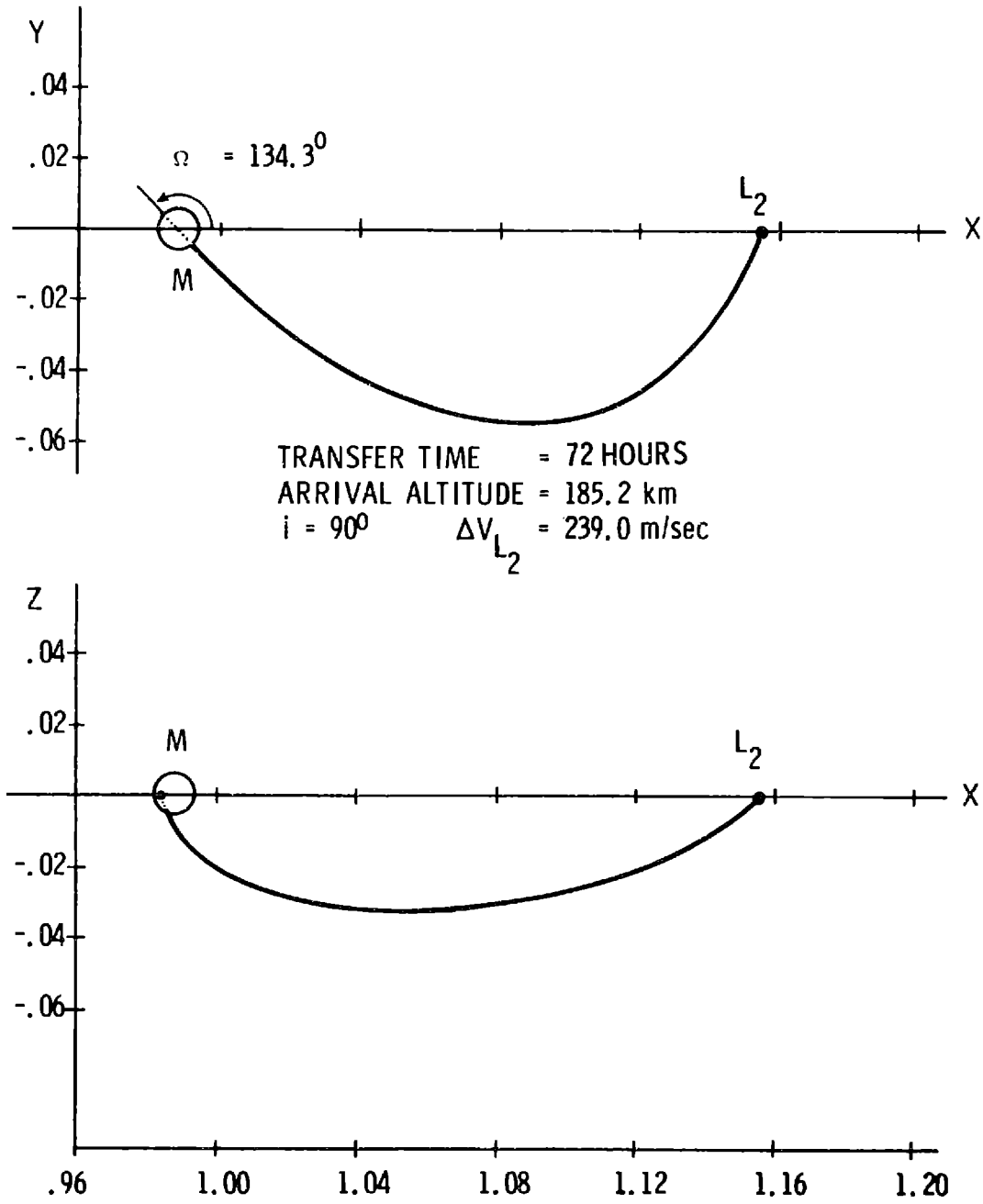

inclinations between 0^{o} and 180^{o}, the difference in the values of the longitude of the ascending node and the argument of latitude at the beginning and end of the iteration was always less than one tenth of a degree. The corresponding improvement of the optimal injection over the tangential injection was always less than one meter per second. For the two planar trajectories, the differences were several orders of magnitude less. A tangential injection is essentially optimal for planar trajectories between L_2 and the Moon for a 72 hour transfer time.

A comparison of the primer histories for the starting solutions, which used a tangential injection, and the converged solutions, for which the injection has been optimized, is given for various inclinations on Figure 40. Notice that the two planar trajectories satisfy (with a tangential impulse) the necessary condition that the primer magnitude not exceed unity. The primer histories for 45^{o}, 90^{o}, and 135^{o} violate this condition. The uppermost portion of the primer history for 90^{o} has been truncated due to space limitations. The maximum of the primer magnitude for 90^{o} is about 2.6. The surprising result is that with the very small change in the trajectory brought about by the iteration to optimize the injection, all the primer histories have become very similar and they each satisfy all the necessary conditions. An important result is that 72 hours two-impulse trajectories to circular orbits of non-zero inclination about the Moon, which have been optimized for the injection point, cannot be improved by additional impulses. They represent local minima for the variable end-point trajectory optimization problem since they satisfy both the primer necessary conditions and the transversality conditions. The violation of the primer necessary conditions evidenced by some trajectories using tangential injection for non-zero inclination seems to be caused solely by the non-optimal injection.

The total ΔV and the ΔV required at L_2 for the locally optimal converged trajectories is plotted versus inclination on Figure 41. The total cost and the ΔV at L_2 are monotonically increasing functions of the inclination for inclinations from 0^{o} to 180^{o}. The cost must be monotonically

Fig. 40 PRIMER HISTORIES FOR 72 HOUR TWO-IMPULSE TRAJECTORIES BETWEEN THE MOON AND L_2 FOR VARIOUS INCLINATIONS

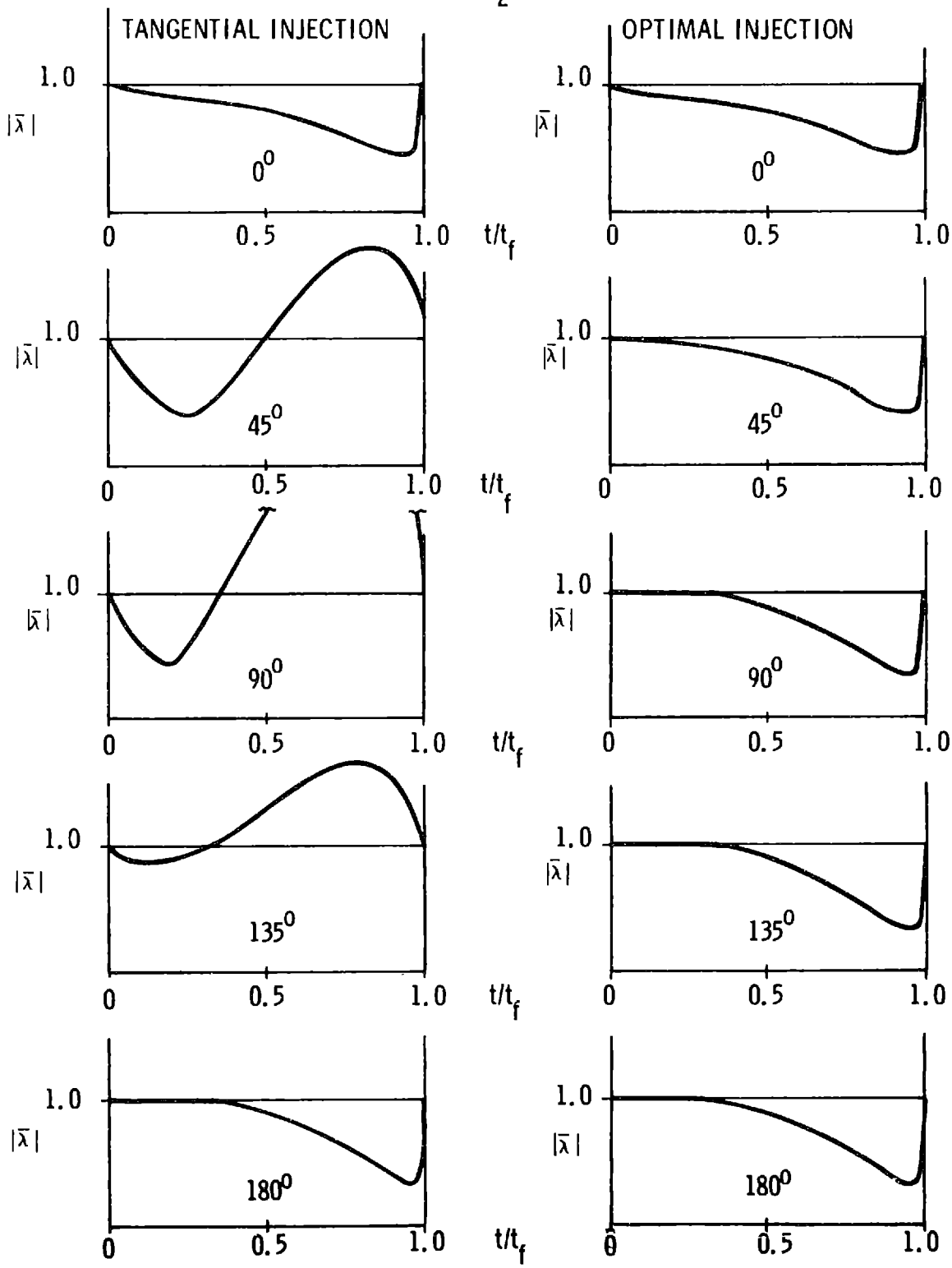

Fig. 41 TOTAL ΔV AND ΔV AT L_2 vs. INCLINATION FOR 72 HOUR TWO-IMPULSE TRAJECTORIES BETWEEN THE MOON AND L_2

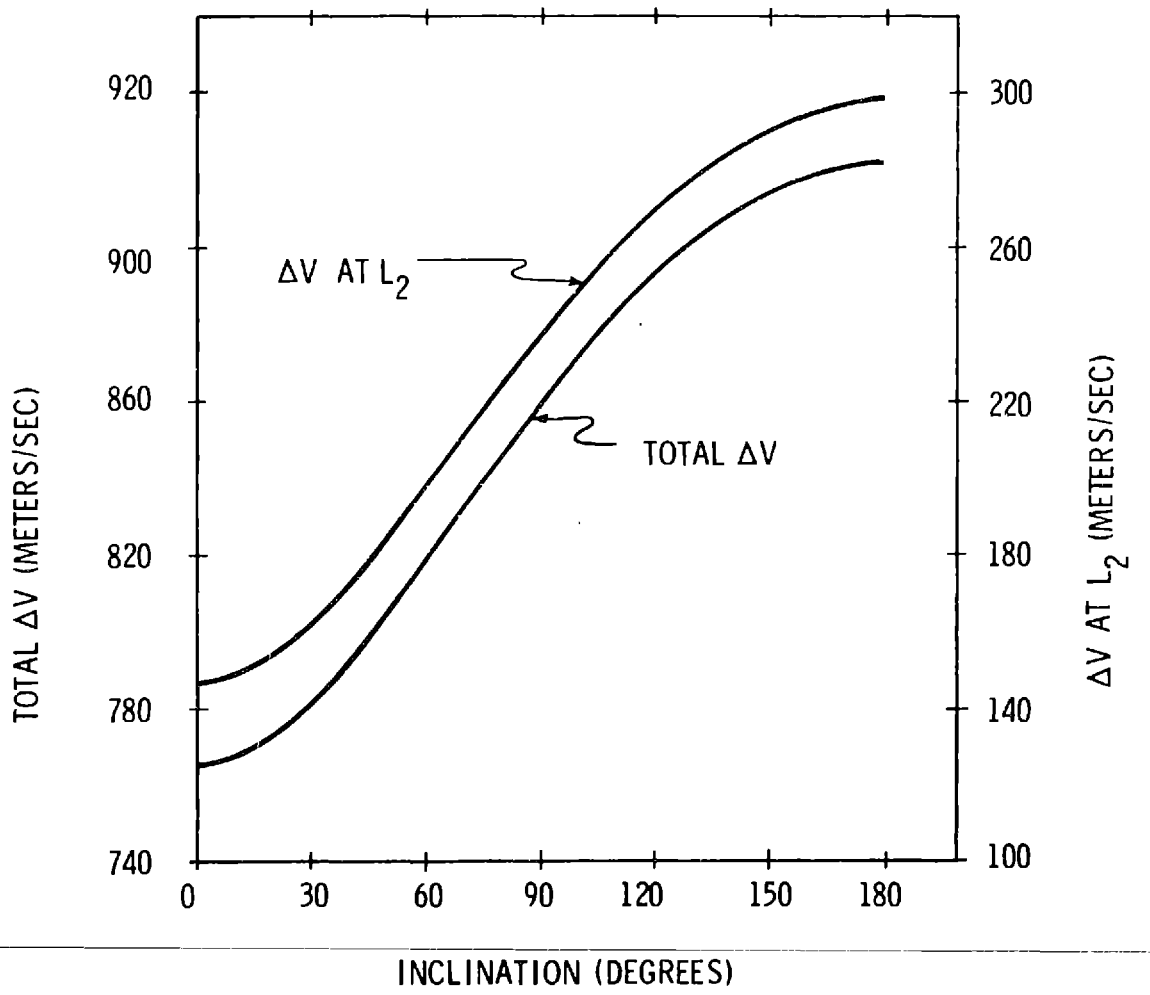

decreasing functions for inclinations between 180^{o} and 360^{o} because an inclination of 360^{o} is identical to an inclination of 0^{o}.

No other families of two-impulse trajectories were investigated with the variable end-point trajectory optimization method.

CHAPTER 8
CONCLUSIONS AND SUGGESTIONS FOR FUTURE RESEARCH

8.1 Conclusions

This thesis is the first attempt known to the author to apply the multi-conic methods of trajectory propagation to the solution of the three-body trajectory optimization problem. The method used combines a multi-conic method of trajectory integration with primer vector theory and an accelerated gradient method of functional minimization and results in a rapid and efficient method of calculating optimal three-impulse, three-body trajectories. The method also readily extends to any number of impulses or bodies.

This method has been applied to the determination of optimal two- and three-impulse planar transfers between the L_2 libration point and circular orbits about both the Earth and the Moon. The results have demonstrated that a multi-conic approach can be used for rapid and efficient calculations of optimal multiple-impulse trajectories in the three-body problem.

It has been found that there exist locally optimal families of two-impulse transfers between the L_2 libration point and both the Earth and the Moon. These families generally involve the shortest times of flight. A "slow" family of two-impulse transfers between L_2 and the Moon is not locally optimal. However, three-impulse transfers generated from this family are locally optimal. These transfers require more time but less fuel than the fast transfers.

Locally optimal three-impulse transfers between L_2 and the Earth involve close lunar swingbys which often pass below the surface of the Moon. Raising these trajectories above the surface generally causes only a small increase in fuel consumption. These locally optimal three-impulse transfers between the L_2 libration point and the Earth offer

substantial fuel savings over the corresponding locally optimal two-impulse transfers.

For the first time a general error analysis of the three basic multi-conic methods has been carried out and analytic expressions for the deviations in position and velocity of these multi-conic methods from the actual three-body trajectory for a single time step have been developed as Taylor series in powers of the time step and also in integral form.

When considering position and velocity errors at the end of a trajectory which has been propagated in a multi-step integration procedure using any of these multi-conic methods, it may be concluded that, if small step sizes are used (i.e., if accurate trajectories are being calculated), the final position and velocity errors will be of approximately the same magnitude for all three methods, because all three methods have the same per-step velocity errors, and the per-step velocity errors tend to dominate as causes of final position and velocity errors through the state transition matrix.

For the calculation of accurate trajectories, the Stumpff-Weiss method appears to be the best to use for several reasons. First, the per-step velocity errors which deminate are the same for all three methods for small steps. Secondly, the Stumpff-Weiss method is the simpliest to use. Finally, the calculations of the state transition matrix for the Stumpff-Weiss method is an additive process, while for the other two methods it is a multiplicative process, and hence the Stumpff-Weiss calculation is less susceptable to truncation errors.

When large steps are used in propagating a trajectory, the use of either the Earth-Moon or Moon-Earth method yields a definite improvement over the Stumpff-Weiss method in terms of final position errors.

It may be concluded from the shape of the constant error contours that the errors of the methods are strongly dependent on the position

relative to the Earth and Moon. The form of the terms in the error function lead to the conclusion that the shape of the contours of constant error is independent of the mass ratio of the Earth and Moon and these contours are equally valid for all three-body systems in which the mass of the third body is negligible. Furthermore, if the error functions are divided by the product of the masses of the two massive bodies, then both the direction and magnitude of the errors is independent of the masses and the mass ratio of the two massive bodies.

Using the series representation of the error for internal step-size control of the multi-conic integration procedure seems to improve the accuracy of the procedure as compared to a constant step-size rule. For increasing the accuracy of the methods by explicitly calculating a part of the error, either the series or integral representation of the error could be used although the integral representation would be more useful because it gives a better estimate of the error than a truncated Taylor series, especially for larger steps.

A variable end-point trajectory optimization method has been developed by including transversality conditions on the primer vector and its derivative. This method has been applied to the determination of locally optimal two-impulse transfers between the L_2 libration point and circular orbits of non-zero inclination about the Moon for a transfer time of 72 hours. It has been found that a simple tangential injection is very close to optimal for any inclination and essentially optimal for planar trajectories. For a transfer time of 72 hours, two-impulse trajectories satisfying the transversality conditions are locally optimal for non-zero inclinations.

In addition, some specific analytic contributions have been made in this thesis. The demonstration in Section 3.1 that the two options of Wilson's method (the Earth-Moon method and the Moon-Earth method) and the Stumpff-Weiss method may all be obtained from one derivation is original. The analytic expressions for the calculation of the state

transition matrix for the Earth-Moon and Moon-Earth methods which were derived in Section 3.2 are new results. To the author's knowledge, the formulation and method of solution of the modified Lambert problem developed in Section 3.3 has never been reported. All the analytic results for error expressions in Chapter 6 are new. Finally, the numerical solution to the variable end-point two-impulse trajectory optimization problem by the introduction of transversality conditions has never been performed before.

8.2 Suggestions for Future Research

The methods of trajectory optimization developed in this thesis are capable of determining locally optimal multiple-impulse trajectories to a fixed final state and locally optimal two-impulse trajectories which satisfy a particular set of constraints at the final time expressed in terms of orbital elements. It would be useful to extend the variable end-point solution to three or more impulses. For a three-impulse transfer to a circular orbit, the cost would be a function of the position and time of the interior impulse and also the longitude of the ascending node and argument of latitude at the final time. The solution to this problem would be in effect a combination of the methods of trajectory optimization outlined in Chapter 4 and 7.

Locally optimal three-impulse transfers between L_2 and the Earth employing a lunar swingby may pass below the surface of the Moon. A reformulation of the trajectory optimization method to allow for interior-point constraints would be one way of eliminating the problem.

It is known from the shape of the primer histories for the converged three-impulse trajectories of Chapter 5 that increasing the time of flight will result in a certain further reduction in the total cost. It would be useful to find the minimum with respect to time of flight of the converged three-impulse solutions to determine what the magnitude of the reduction is.

Also it would be desirable to investigate other possible multiple-impulse solutions with the minimum impulse program to gain experience in three-body trajectory optimization. For instance, it is believed that there exist trajectories between the Moon and L_1 and possibly L_2 which involve two intermediate approaches to the Moon before insertion into orbit and their primer histories are non-optimal, indicating multiple-impulse solutions with less cost. Also, lunar abort trajectories for which three-body efferts are significant would offer cases for application.

Finally, an investigation into the possible guidance applications of large step multi-conic approximations would be useful.

APPENDIX A
DERIVATION OF EQUATION (3.69)

The three equations which must be satisfied are:

$$|\bar{r}_{f_{n+1}}| = r_f \tag{A.1}$$

$$\bar{r}_{f_{n+1}}{}^T \bar{v}_{f_{n+1}} = 0 \tag{A.2}$$

$$\bar{u}_z{}^T \frac{\bar{h}_{n+1}}{h_{n+1}} = \cos i \tag{A.3}$$

and the final positions and velocities on successive iterations are related by

$$\bar{r}_{f_{n+1}} = \bar{r}_{f_n} + \varphi_{12}\, \Delta\bar{v}_{o_n} \tag{A.4}$$

$$\bar{v}_{f_{n+1}} = \bar{v}_{f_n} + \varphi_{22}\, \Delta\bar{v}_{o_n} \tag{A.5}$$

Taking the absolute value of both sides of Equation (A.4), one obtains

$$|\bar{r}_{f_{n+1}}| = \left[\left(\bar{r}_{f_n} + \varphi_{12}\, \Delta\bar{v}_{o_n}\right)^T \left(\bar{r}_{f_n} + \varphi_{12}\, \Delta\bar{v}_{o_n}\right)\right]^{1/2}$$

$$= \left[r_{f_n}{}^2 + 2\bar{r}_{f_n}{}^T \varphi_{12}\, \Delta\bar{v}_{o_n} + 0\,(\Delta v_o{}^2)\right]^{1/2} \tag{A.6}$$

where $0(\Delta v_o{}^2)$ denotes terms of greater than first order in $\Delta\bar{v}_{o_n}$. Simplifying Equation (A.6) further yields

$$|\bar{r}_{f_{n+1}}| = r_{f_n} + \frac{1}{\bar{r}_{f_n}}\, \bar{r}_{f_n}{}^T \varphi_{12} \Delta\bar{v}_{o_n} + 0(\Delta v_o{}^2) \tag{A.7}$$

Neglecting the higher order terms and substituting Equation (A.7) into Equation (A.1), one obtains the first scalar equation for $\Delta\bar{v}_{o_n}$:

$$\frac{1}{r_{f_n}} \bar{r}_{f_n}^T \varphi_{12} \Delta\bar{v}_{o_n} = r_f - r_{f_n} \qquad \text{(A.8)}$$

Substituting Equations (A.4) and (A.5) into Equation (A.2) yields

$$\left(\bar{r}_{f_n} + \varphi_{12} \Delta\bar{v}_{o_n}\right)^T \left(\bar{v}_{f_n} + \varphi_{22} \Delta\bar{v}_{o_n}\right) = 0 \qquad \text{(A.9)}$$

Simplifying Equation (A.9) results in

$$\bar{r}_{f_n}^T \bar{v}_{f_n} + \bar{r}_{f_n}^T \varphi_{22} \Delta\bar{v}_{o_n} + \Delta\bar{v}_{o_n}^T \varphi_{12}^T \bar{v}_{f_n} + 0(\Delta v_o^2) = 0$$

and

$$\bar{r}_{f_n}^T \bar{v}_{f_n} + \left(\bar{r}_{f_n}^T \varphi_{22} + \bar{v}_{f_n}^T \varphi_{12}\right) \Delta\bar{v}_{o_n} + 0(\Delta v_o^2) = 0 \qquad \text{(A.10)}$$

Neglecting higher order terms and rearranging Equation (A.10), one obtains the second scalar equation for $\Delta\bar{v}_{o_n}$:

$$\left(\bar{r}_{f_n}^T \varphi_{22} + \bar{v}_{f_n}^T \varphi_{12}\right) \Delta\bar{v}_{o_n} = -\bar{r}_{f_n}^T \bar{v}_{f_n} \qquad \text{(A.11)}$$

The quantity $\bar{h}_{n+1}$ is defined as

$$\bar{h}_{n+1} = \bar{r}_{f_{n+1}} \times \bar{v}_{f_{n+1}} \qquad \text{(A.12)}$$

Substituting Equations (A.4) and (A.5) into the above expression yields the following series of simplifications:

$$\bar{h}_{n+1} = \left(\bar{r}_{f_n} + \varphi_{12} \Delta\bar{v}_{o_n}\right) \times \left(\bar{v}_{f_n} + \varphi_{22} \Delta\bar{v}_{o_n}\right)$$

$$= \bar{r}_{f_n} \times \bar{v}_{f_n} + \bar{r}_{f_n} \times (\varphi_{22} \Delta\bar{v}_{o_n}) + (\varphi_{12} \Delta\bar{v}_{o_n}) \times \bar{v}_{f_n} + 0(\Delta v_o^2)$$

$$= \bar{h}_n + (\bar{r}_{f_n} \times) \varphi_{22} \Delta\bar{v}_{o_n} - (\bar{v}_{f_n} \times) \varphi_{12} \Delta\bar{v}_{o_n} + 0(\Delta v_o^2)$$

$$= \bar{h}_n + \left[\left(\bar{r}_{f_n} \times\right) \varphi_{22} - \left(\bar{v}_{f_n} \times\right) \varphi_{12}\right] \Delta\bar{v}_{o_n} + 0\,(\Delta v_o^2) \qquad \text{(A.13)}$$

where $\left(\bar{r}_{f_n} \times\right)$ and $\left(\bar{v}_{f_n} \times\right)$ denote the particular skew symmetric matrices whose non-zero elements contain the components of $\bar{r}_{f_n}$ and $\bar{v}_{f_n}$, respectively, such that if the matrix is multiplied times a vector the resulting vector is the cross product of $\bar{r}_{f_n}$ or $\bar{v}_{f_n}$ with the original vector. Defining

$$H = \left(\bar{r}_{f_n} \times\right) \varphi_{22} - \left(\bar{v}_{f_n} \times\right) \varphi_{12} \tag{A.14}$$

Equation (A.13) may be written as

$$\bar{h}_{n+1} = \bar{h}_n + H \, \Delta\bar{v}_{o_n} + 0(\Delta v_o^{\,2}) \tag{A.15}$$

Taking the absolute value of both sides of Equation (A.15) one obtains

$$\begin{aligned} h_{n+1} &= \left[\left(\bar{h}_n + H \, \Delta\bar{v}_{on} + 0(\Delta v_o^{\,2})\right)^T \left(\bar{h}_n + H \, \Delta\bar{v}_{o_n} + 0(\Delta v_o^{\,2})\right)\right]^{1/2} \\ &= \left[h_n^{\,2} + 2\bar{h}_n^{\,T} H \, \Delta\bar{v}_{o_n} + 0(\Delta v_o^{\,2})\right]^{1/2} \\ &= h_n + \frac{1}{h_n} \bar{h}_n^{\,T} H \, \Delta\bar{v}_{o_n} + 0(\Delta v_o^{\,2}) \end{aligned} \tag{A.16}$$

Forming the quotient $\bar{h}_{n+1}/h_{n+1}$ from Equations (A.15) and (A.16), one obtains

$$\frac{\bar{h}_{n+1}}{h_{n+1}} = \frac{\bar{h}_n + H \, \Delta\bar{v}_{o_n} + 0(\Delta v_o^{\,2})}{h_n + \frac{1}{h_n} \bar{h}_n^{\,T} H \, \Delta\bar{v}_{o_n} + 0(\Delta v_o^{\,2})} \tag{A.17}$$

and simplifying results in

$$\begin{aligned} \frac{\bar{h}_{n+1}}{h_{n+1}} &= \left(\bar{h}_n + H \, \Delta\bar{v}_{o_n} + 0(\Delta v_o^{\,2})\right)\left(\frac{1}{h_n} - \frac{1}{h_n^{\,3}} \bar{h}_n^{\,T} H \, \Delta\bar{v}_{o_n} + 0(\Delta v_o^{\,2})\right) \\ &= \frac{\bar{h}_n}{h_n} + \frac{1}{h_n} H \, \Delta\bar{v}_{o_n} - \frac{1}{h_n^{\,3}} \bar{h}_n \bar{h}_n^{\,T} H \, \Delta\bar{v}_{o_n} + 0(\Delta v_o^{\,2}) \end{aligned} \tag{A.18}$$

and finally

$$\frac{\bar{h}_{n+1}}{h_{n+1}} = \frac{\bar{h}_n}{h_n} + \frac{1}{h_n^3}\left(h_n^2 I - \bar{h}_n \bar{h}_n^T\right) H \Delta\bar{v}_{o_n} + 0(\Delta v_o^2) \qquad (A.19)$$

Substituting Equation (A.19) into Equation (A.3), replacing H from Equation (A.14), and neglecting higher order terms, one obtains the final equation for $\Delta\bar{v}_{o_n}$:

$$\frac{1}{h_n^3}\bar{u}_z^T\left(h_n^2 I - \bar{h}_n\bar{h}_n^T\right)\left[\left(\bar{r}_{f_n} x\right)\varphi_{22} - \left(\bar{v}_{f_n} x\right)\varphi_{12}\right]\Delta\bar{v}_{o_n} = \cos i - \cos i_n \qquad (A.20)$$

Equations (A.8), (A.11), and (A.20) may be combined into Equation (3.69).

APPENDIX B
DERIVATIVES OF THE f AND g FUNCTIONS

The f and g functions are given by

$$f = \sum_{n=0}^{\infty} a_n h^n \tag{B.1}$$

$$g = \sum_{n=0}^{\infty} b_n h^n \tag{B.2}$$

where $h = t_F - t_I$ and the coefficients a_n and b_n are functions of the position and velocity used as the initial state for the last conic, i.e., $\bar{r}_{FaI}$ and $\dot{\bar{r}}_{FaI}$ for the Earth-Moon method. The first few coefficients are

$$a_0 = 1 \tag{B.3}$$

$$a_1 = 0 \tag{B.4}$$

$$a_2 = -\frac{1}{2}\frac{a}{r^3_{FaI}} \tag{B.5}$$

$$a_3 = \frac{1}{2}\frac{a}{r^4_{FaI}}\dot{r}_{FaI} \tag{B.6}$$

$$a_4 = \frac{1}{24}\frac{a}{r^6_{FaI}}\left(-2a + 3r\left|\dot{\bar{r}}\right|^2 - 15r\dot{r}^2\right)_{FaI} \tag{B.7}$$

$$a_5 = \frac{1}{8}\frac{a}{r^7_{FaI}}\dot{r}_{FaI}\left(2a - 3r\left|\dot{\bar{r}}\right|^2 + 7r\dot{r}^2\right)_{FaI} \tag{B.8}$$

$$b_0 = 0 \tag{B.9}$$

$$b_1 = 1 \tag{B.10}$$

$$b_2 = 0 \tag{B.11}$$

$$b_3 = -\frac{1}{6}\frac{a}{r^3_{FaI}} \tag{B.12}$$

$$b_4 = \frac{1}{4}\frac{a}{r^4_{FaI}}\dot{r}_{FaI} \tag{B.13}$$

$$b_5 = \frac{1}{120}\frac{a}{r^6_{FaI}}\left(-8a + 9r\,|\dot{\bar{r}}|^2 - 45r\dot{r}^2\right)_{FaI} \tag{B.14}$$

Taking the first four derivatives of Equations (B.1) and (B.2) with respect to t_F and evaluating them at $t_F = t_I$, one obtains the following set of equations:

$$f_{t_F=t_I} = a_{0\,t_F=t_I} \tag{B.15}$$

$$\dot{f}_{t_F=t_I} = (a_1 + \dot{a}_0)_{t_F=t_I} \tag{B.16}$$

$$\ddot{f}_{t_F=t_I} = (2a_2 + 2\dot{a}_1 + \ddot{a}_0)_{t_F=t_I} \tag{B.17}$$

$$\dddot{f}_{t_F=t_I} = (6a_3 + 6\dot{a}_2 + 3\ddot{a}_1 + \dddot{a}_0)_{t_F=t_I} \tag{B.18}$$

$$\ddddot{f}_{t_F=t_I} = (24a_4 + 24\dot{a}_3 + 12\ddot{a}_2 + 4\dddot{a}_1 + \ddddot{a}_0)_{t_F=t_I} \tag{B.19}$$

$$g_{t_F=t_I} = b_{0\,t_F=t_I} \tag{B.20}$$

$$\dot{g}_{t_F=t_I} = (b_1 + \dot{b}_0)_{t_F=t_I} \tag{B.21}$$

$$\ddot{g}_{t_F=t_I} = (2b_2 + 2\dot{b}_1 + \ddot{b}_0)_{t_F=t_I} \tag{B.22}$$

$$\dddot{g}_{t_F=t_I} = (6b_3 + 6\dot{b}_2 + 6\ddot{b}_1 + \dddot{b}_0)_{t_F=t_I} \tag{B.23}$$

$$\ddddot{g}_{t_F=t_I} = (24b_4 + 24\dot{b}_3 + 12\ddot{b}_2 + 4\dddot{b}_1 + \ddddot{b}_0)_{t_F=t_I} \tag{B.24}$$

Since a_0, a_1, b_0, b_1, and b_2 are constants, all of their derivatives are zero. Therefore, we may rewrite Equations (B.15) through (B.24) as

$$f_{t_F=t_I} = a_0 \quad t_F=t_I \tag{B.25}$$

$$\dot{f}_{t_F=t_I} = a_1 \quad t_F=t_I \tag{B.26}$$

$$\ddot{f}_{t_F=t_I} = 2a_2 \quad t_F=t_I \tag{B.27}$$

$$\dddot{f}_{t_F=t_I} = (6a_3 + 6\dot{a}_2) \quad t_F=t_I \tag{B.28}$$

$$\ddddot{f}_{t_F=t_I} = (24a_4 + 24\dot{a}_3 + 12\ddot{a}_2) \quad t_F=t_I \tag{B.29}$$

$$g_{t_F=t_I} = b_0 \quad t_F=t_I \tag{B.30}$$

$$\dot{g}_{t_F=t_I} = b_1 \quad t_F=t_I \tag{B.31}$$

$$\ddot{g}_{t_F=t_I} = 2b_2 \quad t_F=t_I \tag{B.32}$$

$$\dddot{g}_{t_F=t_I} = 6b_3 \quad t_F=t_I \tag{B.33}$$

$$\ddddot{g}_{t_F=t_I} = (24b_4 + 24\dot{b}_3) \quad t_F=t_I \tag{B.34}$$

In order to evaluate the right hand side of Equations (B.25) through (B.34), the necessary derivatives of a_2, a_3, and b_3 with respect to t_F must be found and evaluated at $t_F=t_I$.

For a_2, we have from Equation (B.5)

$$a_2 = -\frac{1}{2}\frac{a}{r_{FaI}^3} \tag{B.35}$$

A derivative of the above equation with respect to t_F yields

$$\dot{a}_2 = \frac{3}{2} \frac{a}{r_{FaI}^4} \frac{d}{dt_F} r_{FaI} \tag{B.36}$$

But

$$r_{FaI}^2 = \bar{r}_{FaI}^T \bar{r}_{FaI} \tag{B.37}$$

and therefore

$$2r_{FaI} \frac{d}{dt_F} r_{FaI} = 2\bar{r}_{FaI}^T \frac{d}{dt_F} \bar{r}_{FaI} \tag{B.38}$$

or

$$\frac{d}{dt_F} r_{FaI} = \frac{1}{r_{FaI}} \bar{r}_{FaI}^T \frac{d}{dt_F} \bar{r}_{FaI} \tag{B.39}$$

Substituting Equation (B.39) into Equation (B.36) yields

$$\dot{a}_2 = \frac{3}{2} \frac{a}{r_{FaI}^5} \bar{r}_{FaI}^T \frac{d}{dt_F} \bar{r}_{FaI} \tag{B.40}$$

which, when evaluated at $t_F=t_I$, becomes

$$\dot{a}_{2_{t_F=t_I}} = \frac{3}{2} \frac{a}{r_I^5} \bar{r}_I^T \frac{d}{dt_F} \bar{r}_{FaI}\Big|_{t_F=t_I} \tag{B.41}$$

But from Equation (D.22) with n=1,

$$\frac{d}{dt_F} \bar{r}_{FaI}\Big|_{t_F=t_I} = 0 \tag{B.42}$$

and therefore, from Equation (B.41)

$$\dot{a}_{2_{t_F=t_I}} = 0 \tag{B.43}$$

Another derivative of Equation (B.40) with respect to t_F yields

$$\ddot{a}_2 = \frac{3}{2}\frac{a}{r_{FaI}^5}\left(\bar{r}_{FaI}^T \frac{d^2}{dt_F^2}\bar{r}_{FaI} + \left|\frac{d}{dt_F}\bar{r}_{FaI}\right|^2\right) - \frac{15}{2}\frac{a}{r_{FaI}^7}\left(\bar{r}_{FaI}^T \frac{d}{dt_F}\bar{r}_{FaI}\right)^2 \quad \text{(B. 44)}$$

Evaluating the above equation at $t_F=t_I$ and noting Equation (B. 42), one finds

$$\ddot{a}_{2_{t_F=t_I}} = \frac{3}{2}\frac{a}{r_I^5}\bar{r}_I^T \frac{d^2}{dt_F^2}\bar{r}_{FaI}\Big|_{t_F=t_I} \quad \text{(B. 45)}$$

Equation (D. 22) with n=2 yields

$$\frac{d^2}{dt_F^2}\bar{r}_{FaI}\Big|_{t_F=t_I} = -\frac{d}{dt_F}\dot{\bar{r}}_{FaI}\Big|_{t_F=t_I} \quad \text{(B. 46)}$$

and substituting from Equation (D. 34) into the above expression we obtain

$$\frac{d^2}{dt_F^2}\bar{r}_{FaI}\Big|_{t_F=t_I} = \left(\frac{A}{R^3}\bar{R} - \frac{A}{\rho^3}\bar{\rho}\right)_I \quad \text{(B. 47)}$$

Finally, substituting Equation (B. 47) into Equation (B. 44) results in

$$\ddot{a}_{2_{t_F=t_I}} = \frac{3Aa}{2\,(r^5 R^3 \rho^3)_I}\bar{r}_I^T\,(\rho^3\bar{R} - R^3\bar{\rho})_I \quad \text{(B. 48)}$$

For a_3, we have from Equation (B. 6)

$$a_3 = \frac{1}{2} - \frac{a}{r_{FaI}^4}\dot{r}_{FaI} \quad \text{(B. 49)}$$

A derivative of the above equation with respect to t_F yields

$$\dot{a}_3 = \frac{1}{2}\frac{a}{r_{FaI}^4}\frac{d}{dt_F}\dot{r}_{FaI} - \frac{2a}{r_{FaI}^5}\dot{r}_{FaI}\frac{d}{dt_F}r_{FaI} \quad \text{(B. 50)}$$

and substituting Equation (B. 39) into the above expression, we obtain

$$\dot{a}_3 = \frac{1}{2}\frac{a}{r_{FaI}^4}\frac{d}{dt_F}\dot{r}_{FaI} - \frac{2a}{r_{FaI}^6}\dot{r}_{FaI}\bar{r}_{FaI}^T\frac{d}{dt_F}\bar{r}_{FaI} \quad \text{(B. 51)}$$

Evaluating the above equation at $t_F=t_I$ and noting Equation (B. 42), one finds

$$\dot{a}_3\Big|_{t_F=t_I} = \frac{1}{2}\frac{a}{r_I^4}\frac{d}{dt_F}\dot{r}_{FaI}\Big|_{t_F=t_I} \tag{B.52}$$

Now

$$\dot{r}_{FaI} = \frac{1}{r_{FaI}} r_{FaI}^T \dot{\bar{r}}_{FaI} \tag{B.53}$$

and therefore

$$\frac{d}{dt_F}\dot{r}_{FaI} = \frac{1}{r_{FaI}}\left(\bar{r}_{FaI}^T \frac{d}{dt_F}\dot{\bar{r}}_{FaI} + \frac{d}{dt_F}\bar{r}_{FaI}^T \dot{\bar{r}}_{FaI}\right) - \frac{1}{r_{FaI}^2}\bar{r}_{FaI}^T \dot{\bar{r}}_{FaI}\frac{d}{dt_F} r_{FaI} \tag{B.54}$$

Substituting Equation (B. 39) into the above expression yields

$$\frac{d}{dt_F}\dot{r}_{FaI} = \frac{1}{r_{FaI}}\left(\bar{r}_{FaI}^T \frac{d}{dt_F}\dot{\bar{r}}_{FaI} + \frac{d}{dt_F}\bar{r}_{FaI}^T \dot{\bar{r}}_{FaI}\right) - \frac{1}{r_{FaI}^3}\left(\bar{r}_{FaI}^T \dot{\bar{r}}_{FaI}\right)\left(\bar{r}_{FaI}^T \frac{d}{dt_F}\bar{r}_{FaI}\right) \tag{B.55}$$

Evaluating Equation (B. 55) at $t_F=t_I$ and noting Equation (B. 42) results in

$$\frac{d}{dt_F}\dot{r}_{FaI}\Big|_{t_F=t_I} = \frac{1}{r_I}\bar{r}_I^T \frac{d}{dt_F}\dot{\bar{r}}_{FaI}\Big|_{t_F=t_I} \tag{B.56}$$

Finally, substituting Equation (D. 34) into Equation (B. 56) and substituting that result into Equation (B. 52), one finds

$$\dot{a}_3\Big|_{t_F=t_I} = -\frac{Aa}{2(r^5 R^3 \rho^3)_I}\bar{r}_I^T (\rho^3\bar{R} - R^3\bar{\rho})_I \tag{B.57}$$

Comparing Equations (B. 5) and (B. 12) one obtains

$$b_3 = \frac{1}{3}a_2 \tag{B.58}$$

Hence

$$\dot{b}_{3_{t_F=t_I}} = \frac{1}{3}\dot{a}_{2_{t_F=t_I}} = 0 \tag{B.59}$$

because of Equation (B.43).

With the results in Equations (B.43), (B.48), (B.57), and (B.59), and with the definition of Equations (B.3) through (B.14), the right hand sides of Equations (B.25) through (B.34) may now be evaluated to obtain the final desired expressions:

$$f_{t_F=t_I} = 1 \tag{B.60}$$

$$\dot{f}_{t_F=t_I} = 0 \tag{B.61}$$

$$\ddot{f}_{t_F=t_I} = -\frac{a}{r_I^3} \tag{B.62}$$

$$\dddot{f}_{t_F=t_I} = \frac{3a}{r_I^4}\dot{r}_I \tag{B.63}$$

$$\ddddot{f}_{t_F=t_I} = \frac{a}{r_I^6}(-2a + 3r|\dot{\bar{r}}|^2 - 15r\dot{r}^2)_I + \frac{6Aa}{(r^5 R^3 \rho^3)_I}\bar{r}_I^T(\rho^3\bar{R} - R^3\bar{\rho})_I \tag{B.64}$$

$$g_{t_F=t_I} = 0 \tag{B.65}$$

$$\dot{g}_{t_F=t_I} = 1 \tag{B.66}$$

$$\ddot{g}_{t_F=t_I} = 0 \tag{B.67}$$

$$\dddot{g}_{t_F=t_I} = -\frac{a}{r_I^3} \tag{B.68}$$

$$\ddddot{g}_{t_F=t_I} = \frac{6a}{r_I^4}\dot{r}_I \tag{B.69}$$

APPENDIX C

DERIVATION OF THE SINGLE-STEP POSITION AND VELOCITY ERRORS FOR THE STUMPFF-WEISS METHOD

The estimates of the final position and velocity for the Stumpff-Weiss method are given by Equations (3.34) and (3.35) and repeated here:

$$\bar{R}_F' = \bar{R}_{IAF} + \bar{r}_{IaF} - \bar{r}_I - h\dot{\bar{r}}_I + \mu\,(\bar{\rho}_F - \bar{\rho}_I - h\dot{\bar{\rho}}_I) \qquad (C.1)$$

$$\dot{\bar{R}}_F' = \dot{\bar{R}}_{IAF} + \dot{\bar{r}}_{IaF} - \dot{\bar{r}}_I + \mu\,(\dot{\bar{\rho}}_F - \dot{\bar{\rho}}_I) \qquad (C.2)$$

In order to maintain a distinction between the true final position and velocity and a multi-conic estimate of the true final position and velocity, estimates will be written as primed quantities as in the above equations. If one considers the position error first, the deviation of the Stumpff-Weiss approximation from the true position at t_F is a function of t_I and t_F and may be defined as

$$\delta\bar{R}_s(t_F, t_I) = \bar{R}_F - \bar{R}_F' \qquad (C.3)$$

Of course, since the true final position is unknown analytically, the above expression does not provide an analytic formula for the position error at t_F. However, it is possible to obtain an approximate relation for the position error by expanding the right hand side of Equation (C.3) as a Taylor series in powers of the time step (henceforth, the functional dependence of the error on the initial conditions at t_I will be suppressed):

$$\delta\bar{R}_s(t_F) = \delta\bar{R}_s(t_I) + \frac{d}{dt_F}\delta\bar{R}_s(t_F)\Big|_{t_F=t_I} h + \frac{1}{2}\frac{d^2}{dt_F^2}\delta\bar{R}_s(t_F)\Big|_{t_F=t_I} h^2 + \frac{1}{6}\frac{d^3}{dt_F^3}\delta\bar{R}_s(t_F)\Big|_{t_F=t_I} h^3 + \frac{1}{24}\frac{d^4}{dt_F^4}\delta\bar{R}_s(t_F)\Big|_{t_F=t_I} h^4 + \ldots \qquad (C.4)$$

where $h = t_F - t_I$ as usual. In order to determine the coefficients in the above power series, we must take successive derivatives of the position error function defined by Equation (C.3) and then evaluate them at the initial time.

Substituting for R_F' in Equation (C.3) from Equation (C.1) results in the following expression for the position error:

$$\delta\bar{R}_s(t_F) = \bar{R}_F - \bar{R}_{IAF} - \bar{r}_{IaF} + \bar{r}_I + h\dot{\bar{r}}_I - \mu\,(\bar{\rho}_F - \bar{\rho}_I - h\dot{\bar{\rho}}_I) \quad (C.5)$$

If one evaluates the above expression at t_I, the first term of the Taylor series expansion is obtained as

$$\delta\bar{R}_s(t_I) = 0 \quad (C.6)$$

The first derivative of Equation (C.5) is

$$\frac{d}{dt_F}\delta\bar{R}_s(t_F) = \dot{\bar{R}}_F - \dot{\bar{R}}_{IAF} - \dot{\bar{r}}_{IaF} + \dot{\bar{r}}_I - \mu\,(\dot{\bar{\rho}}_F - \dot{\bar{\rho}}_I) \quad (C.7)$$

and the coefficient of the second term in Equation (C.4) is found by evaluating Equation (C.7) at t_I:

$$\frac{d}{dt_F}\delta\bar{R}_s(t_F)\Big|_{t_F=t_I} = 0 \quad (C.8)$$

The derivative of Equation (C.7) yields

$$\frac{d^2}{dt_F^2}\delta\bar{R}_s(t_F) = \ddot{\bar{R}}_F - \ddot{\bar{R}}_{IAF} - \ddot{\bar{r}}_{IaF} - \mu\ddot{\bar{\rho}}_F \quad (C.9)$$

The true three-body acceleration, $\ddot{\bar{R}}_F$, is given by Equation (3.1)

$$\ddot{\bar{R}}_F = -A\frac{\bar{R}_F}{R_F^3} - a\frac{\bar{r}_F}{r_F^3} - a\frac{\bar{\rho}_F}{\rho_F^3} \quad (C.10)$$

and the two-body accelerations are

$$\ddot{\bar{R}}_{IAF} = -A\frac{\bar{R}_{IAF}}{R_{IAF}^3} \quad (C.11)$$

$$\ddot{\bar{r}}_{IaF} = -a\frac{\bar{r}_{IaF}}{r_{IaF}^3} \quad (C.12)$$

$$\ddot{\bar{\rho}}_F = -\alpha \frac{\bar{\rho}_F}{\rho_F^3} \tag{C.13}$$

Equation (C.9) when evaluated at the initial time becomes

$$\frac{d^2}{dt_F^2} \delta\bar{R}_s(t_F)\Big|_{t_F=t_I} = \ddot{\bar{R}}_F - \ddot{\bar{R}}_{IAF} - \ddot{\bar{r}}_{IaF} - \mu\ddot{\bar{\rho}}_F\Big|_{t_F=t_I} \tag{C.14}$$

The four terms on the right hand side of Equation (C.14) are found by evaluating Equations (C.10) to (C.13) at the initial time:

$$\ddot{\bar{R}}_F\Big|_{t_F=t_I} = -A\frac{\bar{R}_I}{R_I^3} - a\frac{\bar{r}_I}{r_I^3} - a\frac{\bar{\rho}_I}{\rho_I^3} \tag{C.15}$$

$$\ddot{\bar{R}}_{IAF}\Big|_{t_F=t_I} = -A\frac{\bar{R}_I}{R_I^3} \tag{C.16}$$

$$\ddot{\bar{r}}_{IaF}\Big|_{t_F=t_I} = -a\frac{\bar{r}_I}{r_I^3} \tag{C.17}$$

$$\ddot{\bar{\rho}}_F\Big|_{t_F=t_I} = -\alpha\frac{\bar{\rho}_I}{\rho_I^3} \tag{C.18}$$

Finally, substituting Equations (C.15) to (C.18) into Equation (C.14) and noting that $\mu\alpha = a$

$$\frac{d^2}{dt_F^2} \delta\bar{R}_s(t_F)\Big|_{t_F=t_I} = 0 \tag{C.19}$$

As one proceeds with the determination of the coefficients of Equation (C.4), one must become more and more careful to maintain the distinction between two-body derivatives and three-body derivatives. Eventually the terms will not exactly cancel and the first non-zero coefficient will appear. Differentiating Equation (C.9) now yields

$$\frac{d^3}{dt_F^3} \delta\bar{R}_s(t_F) = \dddot{\bar{R}}_F - \dddot{\bar{R}}_{IAF} - \dddot{\bar{r}}_{IaF} - \mu\dddot{\bar{\rho}}_F \tag{C.20}$$

and differentiating Equations (C.10) to (C.13) results in

$$\dddot{\bar{R}}_F = -\frac{A}{R_F^4}(R\dot{\bar{R}}-3\dot{R}\bar{R})_F - \frac{a}{r_F^4}(r\dot{\bar{r}}-3\dot{r}\bar{r})_F - \frac{a}{\rho_F^4}(\rho\dot{\bar{\rho}}-3\dot{\rho}\bar{\rho})_F \quad (C.21)$$

$$\dddot{\bar{R}}_{IAF} = -\frac{A}{R_{IAF}^4}(R\dot{\bar{R}}-3\dot{R}\bar{R})_{IAF} \quad (C.22)$$

$$\dddot{\bar{r}}_{IaF} = -\frac{a}{r_{IaF}^4}(r\dot{\bar{r}}-3\dot{r}\bar{r})_{IaF} \quad (C.23)$$

$$\dddot{\bar{\rho}}_F = -\frac{\alpha}{\rho_F^4}(\rho\dot{\bar{\rho}}-3\dot{\rho}\bar{\rho})_F \quad (C.24)$$

where $\dot{r} = \bar{r}^T\dot{\bar{r}}/r$. By evaluating Equations (C.21) to (C.24) at the initial time and substituting those results into Equation (C.20) (also evaluated at t_I), one obtains

$$\frac{d^3}{dt_F^3}\delta\bar{R}_s(t_F)\Big|_{t_F=t_I} = 0 \quad (C.25)$$

The next derivative of Equation (C.20) is

$$\frac{d^4}{dt_F^4}\delta\bar{R}_s(t_F) = \ddddot{\bar{R}}_F - \ddddot{\bar{R}}_{IAF} - \ddddot{\bar{r}}_{IaF} - \mu\ddddot{\bar{\rho}}_F \quad (C.26)$$

Taking derivatives of Equations (C.21) to (C.24) yields the following relations:

$$\begin{aligned}\ddddot{\bar{R}}_F = &-\frac{A}{R_F^5}(R^2\ddot{\bar{R}} - 6R\dot{R}\dot{\bar{R}} - 3R\ddot{R}\bar{R} + 12\dot{R}^2\bar{R})_F \\ &-\frac{a}{r_F^5}(r^2\ddot{\bar{r}} - 6r\dot{r}\dot{\bar{r}} - 3r\ddot{r}\bar{r} + 12\dot{r}^2\bar{r})_F \\ &-\frac{a}{\rho_F^5}(\rho^2\ddot{\bar{\rho}} - 6\rho\dot{\rho}\dot{\bar{\rho}} - 3\rho\ddot{\rho}\bar{\rho} + 12\dot{\rho}^2\bar{\rho})_F \end{aligned} \quad (C.27)$$

$$\ddddot{\bar{R}}_{IAF} = -\frac{A}{R_{IAF}^5}(R^2\ddot{\bar{R}} - 6R\dot{R}\dot{\bar{R}} - 3R\ddot{R}\bar{R} + 12\dot{R}^2\bar{R})_{IAF} \quad (C.28)$$

$$\ddddot{\bar{r}}_{IaF} = -\frac{a}{r_{IaF}^5}\left(r^2\ddot{\bar{r}} - 6r\dot{r}\dot{\bar{r}} - 3r\ddot{r}\bar{r} + 12\dot{r}^2\bar{r}\right)_{IaF} \tag{C.29}$$

$$\ddddot{\bar{\rho}}_F = -\frac{\alpha}{\rho_F^5}\left(\rho^2\ddot{\bar{\rho}} - 6\rho\dot{\rho}\dot{\bar{\rho}} - 3\rho\ddot{\rho}\bar{\rho} + 12\dot{\rho}^2\bar{\rho}\right)_F \tag{C.30}$$

The quantities $\ddot{R}_F$, $\ddot{r}_F$, and $\ddot{\rho}_F$ appear for the first time in Equation (C.27). Starting with the identity

$$R_F^2 = \bar{R}_F^T \bar{R}_F \tag{C.31}$$

and differentiating twice,

$$\ddot{R}_F = \frac{1}{R_F}\left(\bar{R}^T\ddot{\bar{R}} + |\dot{\bar{R}}|^2 - \dot{R}^2\right)_F \tag{C.32}$$

Exactly similar relations exist for $\ddot{r}_F$ and $\ddot{\rho}_F$:

$$\ddot{r}_F = \frac{1}{r_F}\left(\bar{r}^T\ddot{\bar{r}} + |\dot{\bar{r}}|^2 - \dot{r}^2\right)_F \tag{C.33}$$

$$\ddot{\rho}_F = \frac{1}{\rho_F}\left(\bar{\rho}^T\ddot{\bar{\rho}} + |\dot{\bar{\rho}}|^2 - \dot{\rho}^2\right)_F \tag{C.34}$$

Now if one substitutes Equations (C.32) to (C.34) into Equation (C.27),

$$\begin{aligned}\ddddot{\bar{R}}_F = &-\frac{A}{R_F^5}\left[\left(R^2 I - 3\bar{R}\bar{R}^T\right)\ddot{\bar{R}} - 6R\dot{R}\dot{\bar{R}} - 3|\dot{\bar{R}}|^2\bar{R} + 15\dot{R}^2\bar{R}\right]_F \\ &-\frac{a}{r_F^5}\left[\left(r^2 I - 3\bar{r}\bar{r}^T\right)\ddot{\bar{r}} - 6r\dot{r}\dot{\bar{r}} + 3|\dot{\bar{r}}|^2\bar{r} + 15\dot{r}^2\bar{r}\right)\Big]_F \\ &-\frac{a}{\rho_F^5}\left[\left(\rho^2 I - 3\bar{\rho}\bar{\rho}^T\right)\ddot{\bar{\rho}} - 6\rho\dot{\rho}\dot{\bar{\rho}} + 3|\dot{\bar{\rho}}|^2\bar{\rho} + 15\dot{\rho}^2\bar{\rho}\right]_F\end{aligned} \tag{C.35}$$

where I is the identity matrix. In Equations (C.28) to (C.30), $\ddot{R}_{IAF}$, $\ddot{r}_{IaF}$, and $\ddot{\rho}_F$ are needed. Equation (C.34) provides $\ddot{\rho}_F$ and Equations (C.32) and (C.33) with a change of subscript provide the other two quantities. Therefore Equations (C.28) to (C.30) become

$$\ddddot{\bar{R}}_{IAF} = -\frac{A}{R_{IAF}^5}\left[(R^2 I - 3\bar{R}\bar{R}^T)\ddot{\bar{R}} - 6R\dot{R}\dot{\bar{R}} - 3|\dot{\bar{R}}|^2\bar{R} + 15\dot{R}^2\bar{R}\right]_{IAF} \quad (C.36)$$

$$\ddddot{\bar{r}}_{IaF} = -\frac{a}{r_{IaF}^5}\left[(r^2 I - 3\bar{r}\bar{r}^T)\ddot{\bar{r}} - 6r\dot{r}\dot{\bar{r}} - 3|\dot{\bar{r}}|^2\bar{r} + 15\dot{r}^2\bar{r}\right]_{IaF} \quad (C.37)$$

$$\ddddot{\bar{\rho}}_F = -\frac{\alpha}{\rho_F^5}\left[(\rho^2 I - 3\bar{\rho}\bar{\rho}^T)\ddot{\bar{\rho}} - 6\rho\dot{\rho}\dot{\bar{\rho}} - 3|\dot{\bar{\rho}}|^2\bar{\rho} + 15\dot{\rho}^2\bar{\rho}\right]_F \quad (C.38)$$

If we substitute into Equation (C.35) $\ddot{\bar{R}}_F$ from Equation (C.10), $\ddot{\bar{r}}_F$ from Equation (3.2) and $\ddot{\bar{\rho}}_F$ from Equation (C.13),

$$\begin{aligned}\ddddot{\bar{R}}_F = &-\frac{A}{R_F^5}\left[(R^2 I - 3\bar{R}\bar{R}^T)\left(-\frac{A}{R^3}\bar{R} - \frac{a}{r^3}\bar{r} - \frac{a}{\rho^3}\bar{\rho}\right) - 6R\dot{R}\dot{\bar{R}} - 3|\dot{\bar{R}}|^2\bar{R} + 15\dot{R}^2\bar{R}\right]_F \\ &-\frac{a}{r_F^5}\left[(r^2 I - 3\bar{r}\bar{r}^T)\left(-\frac{a}{r^3}\bar{r} - \frac{A}{R^3}\bar{R} + \frac{A}{\rho^3}\bar{\rho}\right) - 6r\dot{r}\dot{\bar{r}} - 3|\dot{\bar{r}}|^2\bar{r} + 15\dot{r}^2\bar{r}\right]_F \\ &-\frac{a}{\rho_F^5}\left[(\rho^2 I - 3\bar{\rho}\bar{\rho}^T)\left(-\frac{\alpha}{\rho^3}\bar{\rho}\right) - 6\rho\dot{\rho}\dot{\bar{\rho}} - 3|\dot{\bar{\rho}}|^2\bar{\rho} + 15\dot{\rho}^2\bar{\rho}\right]_F \end{aligned} \quad (C.39)$$

Similarly, substituting into Equations (C.36) to (C.38) for $\ddot{\bar{R}}_{IAF}$, $\ddot{\bar{r}}_{IaF}$, and $\ddot{\bar{\rho}}_F$ from Equations (C.11) to (C.13) respectively, one obtains

$$\ddddot{\bar{R}}_{IAF} = -\frac{A}{R_{IAF}^5}\left[(R^2 I - 3\bar{R}\bar{R}^T)\left(-\frac{A}{R^3}\bar{R}\right) - 6R\dot{R}\dot{\bar{R}} - 3|\dot{\bar{R}}|^2\bar{R} + 15\dot{R}^2\bar{R}\right]_{IAF} \quad (C.40)$$

$$\ddddot{\bar{r}}_{IaF} = -\frac{a}{r_{IaF}^5}\left[(r^2 I - 3\bar{r}\bar{r}^T)\left(-\frac{a}{r^3}\bar{r}\right) - 6r\dot{r}\dot{\bar{r}} - 3|\dot{\bar{r}}|^2\bar{r} + 15\dot{r}^2\bar{r}\right]_{IaF} \quad (C.41)$$

$$\ddddot{\bar{\rho}}_F = -\frac{\alpha}{\rho_F^5}\left[(\rho^2 I - 3\bar{\rho}\bar{\rho}^T)\left(-\frac{\alpha}{\rho^3}\bar{\rho}\right) - 6\rho\dot{\rho}\dot{\bar{\rho}} - 3|\dot{\bar{\rho}}|^2\bar{\rho} + 15\dot{\rho}^2\bar{\rho}\right]_F \quad (C.42)$$

Finally if one evaluates Equations (C.39) to (C.42) at t_I, substitutes the results into Equation (C.26) (also evaluated at t_I), and rearranges terms, the following expression is obtained:

$$\begin{aligned}\frac{d^4}{dt_F^4}\delta\bar{R}_s(t_F)\Big|_{t_F=t_I} = &\frac{Aa}{(Rr\rho)_I^3}\left[(I - 3\bar{u}_R\bar{u}_R{}^T)(\rho^3\bar{r} + r^3\bar{\rho})\right. \\ &\left. + (I - 3\bar{u}_r\bar{u}_r{}^T)(\rho^3\bar{R} - R^3\bar{\rho})\right]_I \end{aligned} \quad (C.43)$$

where $\bar{u}_R$ and $\bar{u}_r$ are unit vectors in the directions of $\bar{R}$ and $\bar{r}$ respectively.

The first non-zero coefficient of the Taylor series expansion of the position error has been found, and it is the coefficient of the fourth order term. Noting Equations (C.6), (C.8), (C.19), (C.25), and (C.43), one may now write the position error for the Stumpff-Weiss method from Equation (C.4) as

$$\delta\bar{R}_s(h) = \frac{A\,a}{24\,(Rr\rho)_I^3}\left[(I - 3\bar{u}_R\bar{u}_R^T)(\rho^3\bar{r} + r^3\bar{\rho})\right.$$
$$\left. + (I - 3\bar{u}_r\bar{u}_r^T)(\rho^3\bar{R} - R^3\bar{\rho})\right]_I h^4 + 0\,(h^5) \qquad (C.44)$$

One could derive the velocity error in exactly the same manner that the position error was found. However there is a much simpler way to obtain the velocity error. If one takes the derivative with respect to t_F of the estimate of position given by Equation (C.1), the result is

$$\frac{d}{dt_F}\bar{R}_F' = \dot{\bar{R}}_{IAF} + \dot{\bar{r}}_{IaF} - \dot{\bar{r}}_I + \mu\,(\dot{\bar{\rho}}_F - \dot{\bar{\rho}}_I) \qquad (C.45)$$

and the above expression is identical to the velocity estimate given by Equation (C.2). The multi-conic method of Stumpff and Weiss provides rules for numerically integrating the differential equations of motion to obtain estimates of position and velocity for a given time step. The derivative of the position update equation is identical to the velocity update equation. This result may appear trivial, but it is not necessarily true for every trajectory integration scheme (see Appendix D). In any case, this result allows one to find the velocity error for the Stumpff-Weiss method by simply taking a derivative, with respect to the final time, of the position error. Thus the velocity error for the Stumpff-Weiss method is obtained from Equation (C.44):

$$\dot{\delta\bar{R}}_s(h) = \frac{A\,a}{6\,(Rr\rho)_I^3}\left[(I - 3\bar{u}_R\bar{u}_R^T)(\rho^3\bar{r} + r^3\bar{\rho})\right.$$
$$\left. + (I - 3\bar{u}_r\bar{u}_r^T)(\rho^3\bar{R} - R^3\bar{\rho})\right]_I h^3 + 0(h^4) \qquad (C.46)$$

APPENDIX D

DERIVATION OF THE SINGLE-STEP POSITION AND VELOCITY ERRORS FOR THE EARTH-MOON AND MOON-EARTH METHODS

The estimates of the final position and velocity for the Earth-Moon method are

$$\bar{r}_F' = [\bar{r}_{FaI}]_{aF} \tag{D.1}$$

$$\dot{\bar{r}}_F' = [\dot{\bar{r}}_{FaI}]_{aF} \tag{D.2}$$

where $\bar{r}_{FaI}$ and $\dot{\bar{r}}_{FaI}$ are given by Equations (3.22) and (3.23):

$$\bar{r}_{FaI} = \bar{R}_{IAF} - \bar{\rho}_F - h(\dot{\bar{R}}_{IAF} - \dot{\bar{\rho}}_F) + \mu\,(\bar{\rho}_F - \bar{\rho}_I - h\dot{\bar{\rho}}_F) \tag{D.3}$$

$$\dot{\bar{r}}_{FaI} = \dot{\bar{R}}_{IAF} - \dot{\bar{\rho}}_F + \mu\,(\dot{\bar{\rho}}_F - \dot{\bar{\rho}}_I) \tag{D.4}$$

The fact that the final position and velocity estimates are obtained in selenocentric coordinates instead of geocentric coordinates, as for the Stumpff-Weiss method, presents no difficulty since the geocentric position and velocity are immediately obtainable as

$$\bar{R}_F' = \bar{r}_F' + \bar{\rho}_F \tag{D.5}$$

$$\dot{\bar{R}}_F' = \dot{\bar{r}}_F' + \dot{\bar{\rho}}_F \tag{D.6}$$

In addition, since a small variation in $\bar{R}$ is identically equal to a small variation in $\bar{r}$, the position or velocity errors are equal in either inertial coordinate system. Thus the position error for the Earth-Moon method at t_F may be written as

$$\delta\bar{R}_{em}(t_F) = \bar{r}_F - \bar{r}_F' \tag{D.7}$$

The estimates of the final position and velocity are obtained by propagating $\bar{r}_{FaI}$ and $\dot{\bar{r}}_{FaI}$ along a selenocentric conic by an amount $h = t_F - t_I$. This final selenocentric propagation is signified by Equations (D.1) and (D.2). Another way of expressing the position and velocity resulting from a conic propagation is in terms of the familiar f and g series.[23] That is, $\bar{r}_F{}'$ and $\dot{\bar{r}}_F{}'$ can be expressed as

$$\bar{r}_F{}' = f\,\bar{r}_{FaI} + g\,\dot{\bar{r}}_{FaI} \tag{D.8}$$

$$\dot{\bar{r}}_F{}' = f_t\,\bar{r}_{FaI} + g_t\,\dot{\bar{r}}_{FaI} \tag{D.9}$$

where f, g, f_t, and g_t are given by the series

$$f = \sum_{n=0}^{\infty} a_n h^n \tag{D.10}$$

$$g = \sum_{n=0}^{\infty} b_n h^n \tag{D.11}$$

$$f_t = \sum_{n=1}^{\infty} n a_n h^{n-1} \tag{D.12}$$

$$g_t = \sum_{n=1}^{\infty} n b_n h^{n-1} \tag{D.13}$$

where $h = t_F - t_I$ and the coefficients a_n and b_n are known functions of the initial state[23], in this case, $\bar{r}_{FaI}$ and $\dot{\bar{r}}_{FaI}$. Equations (D.8) and (D.9) are not used to evaluate $\bar{r}_F{}'$ and $\dot{\bar{r}}_F{}'$; rather, they are used as analytic substitutes for Equations (D.1) and (D.2) which will enable derivatives of Equation (D.7) evaluated at the initial time to be easily found.

Once again, as for the Stumpff-Weiss method, the position error function for the Earth-Moon method, Equation (D.7), is expanded as a Taylor series in powers of the time step.

$$\delta\bar{R}_{em}(t_F) = \delta\bar{R}_{em}(t_I) + \frac{d}{dt_F}\delta\bar{R}_{em}(t_F)\Big|_{t_F=t_I} h + \frac{1}{2}\frac{d^2}{dt_F^2}\delta\bar{R}_{em}(t_F)\Big|_{t_F=t_I} h^2$$

$$+ \frac{1}{6}\frac{d^3}{dt_F^3}\delta\bar{R}_{em}(t_F)\Big|_{t_F=t_I} h^3 + \frac{1}{24}\frac{d^4}{dt_F^4}\delta\bar{R}_{em}(t_F)\Big|_{t_F=t_I} h^4 + \ldots \quad \text{(D.14)}$$

Substituting Equation (D.8) into Equation (D.7) yields for the error function

$$\delta\bar{R}_{em}(t_F) = \bar{r}_F - f\,\bar{r}_{FaI} - g\,\dot{\bar{r}}_{FaI} \quad \text{(D.15)}$$

As noted previously, $\bar{r}_{FaI}$ and $\dot{\bar{r}}_{FaI}$ are given by Equations (D.3) and (D.4). Now successive derivatives with respect to t_F of Equation (D.15) must be taken and the resulting expressions evaluated at t_I in order to determine the coefficients of the powers of h in Equation (D.14).

In the process of taking derivatives of Equation (D.15), derivatives of f and g with respect to t_F will have to be found. This becomes a very involved and tedious process because the infinite series for f and g are functions of t_F in two ways. First the series for f and g are functions of t_F through h. Secondly, they are functions of t_F through the coefficients a_n and b_n, because the a_n and b_n depend on $\bar{r}_{FaI}$ and $\dot{\bar{r}}_{FaI}$ which are functions of t_F. The results for the first four derivatives of f and g evaluated at t_I are listed below. For a detailed derivation of these results, consult Appendix B. The results are:

$$f_{t_F=t_I} = 1 \quad \text{(D.16a)}$$

$$\dot{f}_{t_F=t_I} = 0 \quad \text{(D.16b)}$$

$$\ddot{f}_{t_F=t_I} = -\frac{a}{r_I^3} \quad \text{(D.16c)}$$

$$\dddot{f}_{t_F=t_I} = 3\frac{a}{r_I^4}\dot{r}_I \quad \text{(D.16d)}$$

$$\ddddot{f}_{t_F=t_I} = \frac{a}{r_I^6}\left(-2a + 3r|\dot{\bar{r}}|^2 - 15r\dot{r}^2\right)_I + \frac{6Aa}{(r^5R^3\rho^3)_I}\,\bar{r}_I^T\,(\rho^3\bar{R} - R^3\bar{\rho})_I \qquad \text{(D.16e)}$$

$$g_{t_F=t_I} = 0 \qquad \text{(D.17a)}$$

$$\dot{g}_{t_F=t_I} = 1 \qquad \text{(D.17b)}$$

$$\ddot{g}_{t_F=t_I} = 0 \qquad \text{(D.17c)}$$

$$\dddot{g}_{t_F=t_I} = -\frac{a}{r_I^3} \qquad \text{(D.17d)}$$

$$\ddddot{g}_{t_F=t_I} = 6\frac{a}{r_I^4}\dot{r}_I \qquad \text{(D.17e)}$$

In addition to the above derivatives we will need to know the derivatives of $\bar{r}_{FaI}$ and $\dot{\bar{r}}_{FaI}$ with respect to t_F evaluated at t_I. The quantity $\dot{\bar{r}}_{FaI}$ denotes a velocity vector and not the derivative of $\bar{r}_{FaI}$ with respect to t_F. Equations (D. 3) and (D. 6) are formulas for the particular position and velocity which, if propagated forward along a selenocentric conic to the final time, will provide estimates of the true three-body position and velocity. It is not necessarily true that the derivative of the formula for this position vector (Equation (D. 3)) will yield the formula for the velocity vector (Equation (D. 4)). If it does, the last selenocentric conic propagation will provide estimates of the final three-body position and velocity which will be consistent (that is, the derivative of the position estimate will be equal to the velocity estimate), and the velocity error for the Earth-Moon method can be found by differentiating the position error. Otherwise, the velocity error must be derived separately. Differentiating Equation (D. 3) yields

$$\frac{d}{dt_F}\bar{r}_{FaI} = -h\left[\ddot{\bar{R}}_{IAF} - (1-\mu)\ddot{\bar{\rho}}_F\right] \qquad \text{(D.18)}$$

Comparing Equations (D. 18) and (D. 4), it is obvious that $d\,\bar{r}_{FaI}/dt_F$ and $\dot{\bar{r}}_{FaI}$ are not equal. Therefore, the position and velocity errors for the Earth-Moon method must be derived separately, and the derivatives of $\bar{r}_{FaI}$ and $\dot{\bar{r}}_{FaI}$, which will be needed when Equation (D. 15) is differentiated

to determine the coefficients in Equation (D.14), must be calculated independently.

Equation (D.18) gives the first derivative of $\bar{r}_{FaI}$. The nth derivative of $\bar{r}_{FaI}$ is found to be

$$\frac{d^n}{dt_F^n}\bar{r}_{FaI} = -h\left[\bar{R}_{IAF}^{(n+1)} - (1-\mu)\,\bar{\rho}_F^{(n+1)}\right] - (n-1)\left[\bar{R}_{IAF}^{(n)} - (1-\mu)\,\bar{\rho}_F^{(n)}\right] \quad n \geq 1 \tag{D.19}$$

From Equation (D.4), the nth derivative of $\dot{\bar{r}}_{FaI}$ is

$$\frac{d^n}{dt_F^n}\dot{\bar{r}}_{FaI} = \bar{R}_{IAF}^{(n+1)} - (1-\mu)\,\bar{\rho}_F^{(n+1)} \quad n \geq 1 \tag{D.20}$$

Combining Equation (D.19) and (D.20) yields the true relationship between the derivatives of $\bar{r}_{FaI}$ and $\dot{\bar{r}}_{FaI}$:

$$\frac{d^n}{dt_F^n}\bar{r}_{FaI} = -h\frac{d^n}{dt_F^n}\dot{\bar{r}}_{FaI} - (n-1)\frac{d^{n-1}}{dt_F^{n-1}}\dot{\bar{r}}_{FaI} \quad n \geq 1 \tag{D.21}$$

Evaluating Equation (D.21) at $t_F=t_I$,

$$\frac{d^n}{dt_F^n}\bar{r}_{FaI}\Big|_{t_F=t_I} = -(n-1)\frac{d^{n-1}}{dt_F^{n-1}}\dot{\bar{r}}_{FaI}\Big|_{t_F=t_I} \quad n \geq 1 \tag{D.22}$$

Now the results for all the derivatives of $\bar{r}_{FaI}$ and $\dot{\bar{r}}_{FaI}$ evaluated at t_I can be found from Equations (D.20) and (D.22). Also note from Equations (D.3) and (D.4) that

$$\bar{r}_{FaI}\Big|_{t_F=t_I} = \bar{R}_I - \bar{\rho}_I = \bar{r}_I \tag{D.23}$$

$$\dot{\bar{r}}_{FaI}\Big|_{t_F=t_I} = \dot{\bar{R}}_I - \dot{\bar{\rho}}_I = \dot{\bar{r}}_I \tag{D.24}$$

At this point all the information necessary to take successive derivatives of Equations (D.15) and evaluate them at the initial time is available.

Evaluating Equation (D.15) at t_I by using Equations (D.16a), (D.17a) (D.23), and (D.24) provides the first coefficient needed for the position error expansion (Equation (D.14)):

$$\delta\bar{R}_{em}(t_I) = 0 \tag{D.25}$$

Differentiating Equation (D.15),

$$\frac{d}{dt_F}\delta\bar{R}_{em}(t_F) = \dot{\bar{r}}_F - f\frac{d}{dt_F}\bar{r}_{FaI} - \dot{f}\,\bar{r}_{FaI} - g\frac{d}{dt_F}\dot{\bar{r}}_{FaI} - \dot{g}\,\dot{\bar{r}}_{FaI} \tag{D.26}$$

For n = 1, Equation (D.22) becomes

$$\frac{d}{dt_F}\bar{r}_{FaI}\Big|_{t_F=t_I} = 0 \tag{D.27}$$

Evaluating Equation (D.26) at t_I and using Equation (D.27) and the appropriate results from Equations (D.16) and (D.17), we obtain

$$\frac{d}{dt_F}\delta\bar{R}_{em}(t_F)\Big|_{t_F=t_I} = 0 \tag{D.28}$$

The derivative of Equation (D.26) is

$$\frac{d^2}{dt_F^2}\delta\bar{R}_{em}(t_F) = \ddot{\bar{r}}_F - f\frac{d^2}{dt_F^2}\bar{r}_{FaI} - 2\dot{f}\frac{d}{dt_F}\bar{r}_{FaI} - \ddot{f}\,\bar{r}_{FaI} - g\frac{d^2}{dt_F^2}\dot{\bar{r}}_{FaI} - 2\dot{g}\frac{d}{dt_F}\dot{\bar{r}}_{FaI} - \ddot{g}\,\dot{\bar{r}}_{FaI} \tag{D.29}$$

Equation (D.22) for n=2 yields

$$\frac{d^2}{dt_F^2}\bar{r}_{FaI}\Big|_{t_F=t_I} = -\frac{d}{dt_F}\dot{\bar{r}}_{FaI}\Big|_{t_F=t_I} \tag{D.30}$$

If one evaluates Equation (D.29) at t_I and substitutes into that expression Equations (D.27) and (D.30)

$$\frac{d^2}{dt_F^2}\delta\bar{R}_{em}(t_F)\Big|_{t_F=t_I} = \ddot{\bar{r}}_F - \ddot{f}\,\bar{r}_{FaI} - g\frac{d^2}{dt_F^2}\dot{\bar{r}}_{FaI} + (f-2\dot{g})\frac{d}{dt_F}\dot{\bar{r}}_{FaI} - \ddot{g}\,\dot{\bar{r}}_{FaI}\Big|_{t_F=t_I} \qquad (D.31)$$

Making the appropriate substitution from Equations (D.16) and (D.17) results in

$$\frac{d^2}{dt_F^2}\delta\bar{R}_{em}(t_F)\Big|_{t_F=t_I} = \ddot{\bar{r}}_F\Big|_{t_F=t_I} + \frac{a}{r_I^3}\bar{r}_I - \frac{d}{dt_F}\dot{\bar{r}}_{FaI}\Big|_{t_F=t_I} \qquad (D.32)$$

From Equation (D.20) we find that for n=1

$$\frac{d}{dt_F}\dot{\bar{r}}_{FaI} = \ddot{\bar{R}}_{IAF} - (1-\mu)\,\ddot{\bar{\rho}}_F \qquad (D.33)$$

Evaluating the above expression at t_I and substituting from Equations (C.16) and (C.18) the following result is obtained:

$$\frac{d}{dt_F}\dot{\bar{r}}_{FaI}\Big|_{t_F=t_I} = -\frac{A}{R_I^3}\bar{R}_I + \frac{A}{\rho_I^3}\bar{\rho}_I \qquad (D.34)$$

Now substituting Equation (D.34) into Equation (D.32),

$$\frac{d^2}{dt_F^2}\delta\bar{R}_{em}(t_F)\Big|_{t_F=t_I} = \ddot{\bar{r}}_F\Big|_{t_F=t_I} + \frac{a}{r_I^3}\bar{r}_I + \frac{A}{R_I^3}\bar{R}_I - \frac{A}{\rho_I^3}\bar{\rho}_I \qquad (D.35)$$

The quantity $\ddot{\bar{r}}_F$ is found from Equation (3.2):

$$\ddot{\bar{r}}_F = -\frac{a}{r_F^3}\bar{r}_F - \frac{A}{R_F^3}\bar{R}_F + \frac{A}{\rho_F^3}\bar{\rho}_F \qquad (D.36)$$

A final substitution into Equation (D.35) from Equation (D.36) yields the next coefficient

$$\frac{d^2}{dt_F^2}\delta\bar{R}_{em}(t_F)\Big|_{t_F=t_I} = 0 \qquad (D.37)$$

From Equation (D.29), the third derivative of the error function is found to be

$$\frac{d^3}{dt_F^3}\delta\bar{R}_{em}(t_F) = \dddot{\bar{r}}_F - f\frac{d^3}{dt_F^3}\bar{r}_{FaI} - 3\dot{f}\frac{d^2}{dt_F^2}\bar{r}_{FaI} - 3\ddot{f}\frac{d}{dt_F}\bar{r}_{FaI}$$
$$- \dddot{f}\,\bar{r}_{FaI} - g\frac{d^3}{dt_F^3}\dot{\bar{r}}_{FaI} - 3\dot{g}\frac{d^2}{dt_F^2}\dot{\bar{r}}_{FaI}$$
$$- 3\ddot{g}\frac{d^2}{dt_F^2}\dot{\bar{r}}_{FaI} - \dddot{g}\,\dot{\bar{r}}_{FaI} \qquad (D.38)$$

Equation (D.22) for n=3 becomes

$$\frac{d^3}{dt_F^3}\bar{r}_{FaI}\Big|_{t_F=t_I} = -2\frac{d^2}{dt_F^2}\dot{\bar{r}}_{FaI}\Big|_{t_F=t_I} \qquad (D.39)$$

Now if one evaluates Equation (D.38) at t_I and substitutes from Equations (D.27), (D.30), and (D.39),

$$\frac{d^3}{dt_F^3}\delta\bar{R}_{em}(t_F)\Big|_{t_F=t_I} = \dddot{\bar{r}}_F + (2f - 3\dot{g})\frac{d^2}{dt_F^2}\dot{\bar{r}}_{FaI} + (3\dot{f} - 3\ddot{g})\frac{d}{dt_F}\dot{\bar{r}}_{FaI}$$
$$- \dddot{f}\,\bar{r}_{FaI} - g\frac{d^3}{dt_F^3}\dot{\bar{r}}_{FaI} - \dddot{g}\,\dot{\bar{r}}_{FaI}\Big|_{t_F=t_I} \qquad (D.40)$$

The appropriate substitutions into the above expression from Equations (D.16) and (D.17) result in

$$\frac{d^3}{dt_F^3}\delta\bar{R}_{em}(t_F)\Big|_{t_F=t_I} = \dddot{\bar{r}}_F\Big|_{t_F=t_I} - \frac{d^2}{dt_F^2}\dot{\bar{r}}_{FaI}\Big|_{t_F=t_I} - \frac{3a}{r_I^4}\dot{r}_I\bar{r}_I + \frac{a}{r_I^3}\dot{\bar{r}}_I \qquad (D.41)$$

From Equation (D.20), for n=2

$$\frac{d^2}{dt_F^2}\dot{\bar{r}}_{FaI} = \dddot{\bar{R}}_{IAF} - (1-\mu)\,\dddot{\bar{\rho}}_F \qquad (D.42)$$

Evaluating the above expression at $t_F=t_I$ and substituting Equations (C.22) and (C.24) yields

$$\frac{d^2}{dt_F^2}\dot{\bar{r}}_{FaI}\Big|_{t_F=t_I} = -\frac{A}{R_I^4}(R\ddot{\bar{R}} - 3\dot{R}\dot{\bar{R}})_I + \frac{A}{\rho_I^4}(\rho\ddot{\bar{\rho}} - 3\dot{\rho}\dot{\bar{\rho}})_I \qquad (D.43)$$

A derivative of Equation (D. 36) is

$$\dddot{\bar{r}}_F = -\frac{a}{r_F^4}(r\dot{\bar{r}} - 3\dot{r}\bar{r})_F - \frac{A}{R_F^4}(R\dot{\bar{R}} - 3\dot{R}\bar{R})_F + \frac{A}{\rho_F^4}(\rho\dot{\bar{\rho}} - 3\dot{\rho}\bar{\rho})_F \quad (D.44)$$

Finally, substituting Equations (D. 43) and (D. 44) into Equation (D. 41),

$$\frac{d^3}{dt_F^3}\delta\bar{R}_{em}(t_F)\Big|_{t_F=t_I} = 0 \quad (D.45)$$

The next derivative of Equation (D. 40) is

$$\begin{aligned}\frac{d^4}{dt_F^4}\delta\bar{R}_{em}(t_F) = {} & \ddddot{\bar{r}}_F - f\frac{d^4}{dt_F^4}\bar{r}_{FaI} - 4\dot{f}\frac{d^3}{dt_F^3}\bar{r}_{FaI} - 6\ddot{f}\frac{d^2}{dt_F^2}\bar{r}_{FaI} \\ & - 4\dddot{f}\frac{d}{dt_F}\bar{r}_{FaI} - \ddddot{f}\bar{r}_{FaI} - g\frac{d^4}{dt_F^4}\dot{\bar{r}}_{FaI} - 4\dot{g}\frac{d^3}{dt_F^3}\dot{\bar{r}}_{FaI} \\ & - 6\ddot{g}\frac{d^2}{dt_F^2}\dot{\bar{r}}_{FaI} - 4\dddot{g}\frac{d}{dt_F}\dot{\bar{r}}_{FaI} - \ddddot{g}\dot{\bar{r}}_{FaI} \quad (D.46)\end{aligned}$$

Equation (D. 22) for n=4 becomes

$$\frac{d^4}{dt_F^4}\bar{r}_{FaI}\Big|_{t_F=t_I} = -3\frac{d^3}{dt_F^3}\dot{\bar{r}}_{FaI}\Big|_{t_F=t_I} \quad (D.47)$$

which, when substituted into Equation (D. 46) along with Equations (D. 27), (D. 30), and (D. 39) yields

$$\begin{aligned}\frac{d^4}{dt_F^4}\delta\bar{R}_{em}(t_F)\Big|_{t_F=t_I} = {} & \ddddot{\bar{r}}_F + (3f-4\dot{g})\frac{d^3}{dt_F^3}\dot{\bar{r}}_{FaI} + (8\dot{f}-6\ddot{g})\frac{d^2}{dt_F^2}\dot{\bar{r}}_{FaI} \\ & + (6\ddot{f}-4\dddot{g})\frac{d}{dt_F}\dot{\bar{r}}_{FaI} - \ddddot{f}\bar{r}_{FaI} - g\frac{d^4}{dt_F^4}\dot{\bar{r}}_{FaI} - \ddddot{g}\dot{\bar{r}}_{FaI}\Big|_{t_F=t_I} \\ & (D.48)\end{aligned}$$

Substituting the appropriate quantities from Equations (D. 16) and (D. 17) into the above expression,

$$\frac{d^4}{dt_F^4}\delta\bar{R}_{em}(t_F)\Big|_{t_F=t_I} = \dddot{\bar{r}}_F\Big|_{t_F=t_I} - \frac{d^3}{dt_F^3}\dot{\bar{r}}_{FaI}\Big|_{t_F=t_I} - \frac{2a}{r_I^3}\frac{d}{dt_F}\dot{\bar{r}}_{FaI}\Big|_{t_F=t_I}$$
$$- \frac{a}{r_I^6}(-2a+3r|\dot{\bar{r}}|^2-15r\dot{r}^2)_I\,\bar{r}_I - \frac{6Aa}{(r^5R^3\rho^3)_I}\bar{r}_I\bar{r}_I^T(\rho^3\bar{R}-R^3\bar{\rho})_I$$
$$- \frac{6a}{r_I^4}\dot{r}_I\dot{\bar{r}}_I \qquad (D.49)$$

Equation (D.20) with n=3 is

$$\frac{d^3}{dt_F^3}\dot{\bar{r}}_{FaI} = \dddot{\bar{R}}_{IAF} - (1-\mu)\dddot{\bar{\rho}}_F \qquad (D.50)$$

Equation (D.50) evaluated at t_I with substitutions made for $\ddddot{\bar{R}}_{IAF}$ and $\ddddot{\bar{\rho}}_F$ from Equations (C.40) and (C.42) becomes

$$\frac{d^3}{dt_F^3}\dot{\bar{r}}_{FaI}\Big|_{t_F=t_I} = -\frac{A}{R_I^5}\left[\left(R^2I-3\bar{R}\bar{R}^T\right)\left(-\frac{A}{R^3}\bar{R}\right)-6R\dot{R}\dot{\bar{R}}-3|\dot{\bar{R}}|^2\bar{R}+15\dot{R}^2\bar{R}\right]_I$$
$$+\frac{A}{\rho_I^5}\left[\left(\rho^2I-3\bar{\rho}\bar{\rho}^T\right)\left(-\frac{\alpha}{\rho^3}\bar{\rho}\right)-6\rho\dot{\rho}\dot{\bar{\rho}}-3|\dot{\bar{\rho}}|^2\bar{\rho}+15\dot{\rho}^2\bar{\rho}\right]_I \qquad (D.51)$$

If one substitutes Equations (D.34) and (D.51) into Equations (D.49),

$$\frac{d^4}{dt_F^4}\delta\bar{R}_{em}(t_F)\Big|_{t_F=t_I} = \dddot{\bar{r}}_F\Big|_{t_F=t_I} + \frac{A}{R_I^5}\left[\left(R^2I-3\bar{R}\bar{R}^T\right)\left(-\frac{A}{R^3}\bar{R}\right)-6R\dot{R}\dot{\bar{R}}-3|\dot{\bar{R}}|^2\bar{R}\right.$$
$$\left.+15\dot{R}^2\bar{R}\right]_I - \frac{A}{\rho^5}\left[\left(\rho^2I-3\bar{\rho}\bar{\rho}^T\right)\left(-\frac{\alpha}{\rho^3}\bar{\rho}\right)-6\rho\dot{\rho}\dot{\bar{\rho}}-3|\dot{\bar{\rho}}|^2\bar{\rho}+15\dot{\rho}^2\bar{\rho}\right]_I$$
$$+\frac{2Aa}{(Rr\rho)_I^3}(\rho^3\bar{R}-R^3\bar{\rho})_I - \frac{a}{r_I^6}(-2a+3r|\dot{\bar{r}}|^2-15r\dot{r}^2)_I\,\bar{r}_I$$
$$-\frac{6Aa}{(r^5R^3\rho^3)_I}\bar{r}_I\bar{r}_I^T(\rho^3\bar{R}-R^3\bar{\rho})_I - \frac{6a}{r_I^4}\dot{r}_I\dot{\bar{r}}_I \qquad (D.52)$$

Another derivative of Equation (D.44) yields

$$\dddot{\bar{r}}_F = -\frac{a}{r_F^5}\left[(r^2 I - 3\bar{r}\bar{r}^T)\left(-\frac{a}{r^3}\bar{r} - \frac{A}{R^3}\bar{R} + \frac{A}{\rho^3}\bar{\rho}\right) - 6r\dot{r}\dot{\bar{r}} - 3|\dot{\bar{r}}|^2\bar{r} + 15\dot{r}^2\bar{r}\right]_F$$

$$-\frac{A}{R_F^5}\left[(R^2 I - 3\bar{R}\bar{R}^T)\left(-\frac{A}{R^3}\bar{R} - \frac{a}{r^3}\bar{r} - \frac{a}{\rho^3}\bar{\rho}\right) - 6R\dot{R}\dot{\bar{R}} - 3|\dot{\bar{R}}|^2\bar{R} + 15\dot{R}^2\bar{R}\right]_F$$

$$-\frac{a}{\rho_F^5}\left[(\rho^2 I - 3\bar{\rho}\bar{\rho}^T)\left(-\frac{\alpha}{\rho^3}\bar{\rho}\right) - 6\rho\dot{\rho}\dot{\bar{\rho}} - 3|\dot{\bar{\rho}}|^2\bar{\rho} + 15\dot{\rho}^2\bar{\rho}\right]_F \qquad \text{(D.53)}$$

Finally, substituting Equation (D.53) into Equation (D.52) results in the first non-zero coefficient:

$$\frac{d^4}{dt_F^4}\delta\bar{R}_{em}(t_F)\Big|_{t_F=t_I} = \frac{Aa}{(Rr\rho)^3_I}[(I-3\bar{u}_R\bar{u}_R^T)(\rho^3\bar{r} + r^3\bar{\rho}) + 3(I-3\bar{u}_r\bar{u}_r^T)(\rho^3\bar{R} - R^3\bar{\rho})]_I \qquad \text{(D.54)}$$

Again, $\bar{u}_R$ and $\bar{u}_r$ are unit vectors in the direction of $\bar{R}$ and $\bar{r}$ respectively.

Noting the results of Equations (D.25), (D.28), (D.37), (D.45), and (D.54), the position error for the Earth-Moon method in Equation (D.14) may be written as

$$\delta\bar{R}_{em}(h) = \frac{Aa}{24\,(Rr\rho)^3_I}[(I-3\bar{u}_R\bar{u}_R^T)(\rho^3\bar{r} + r^3\bar{\rho}) + 3(I-3\bar{u}_r\bar{u}_r^T)(\rho^3\bar{R} - R^3\bar{\rho})]_I\, h^4 + 0(h^5) \qquad \text{(D.55)}$$

As noted earlier in this Section, due to the fact that for the Earth-Moon method the derivative of the position estimate is not the velocity estimate, the position and velocity errors must be derived separately. The procedure is the same. First, the velocity error is defined as

$$\delta\dot{\bar{R}}_{em}(t_F) = \dot{\bar{r}}_F - \dot{\bar{r}}_F' \qquad \text{(D.56)}$$

and then $\dot{\bar{r}}_F'$ is substituted from Equation (D.9) to obtain

$$\delta\dot{\bar{R}}_{em}(t_F) = \dot{\bar{r}}_F - f_t\,\bar{r}_{FaI} - g_t\,\dot{\bar{r}}_{FaI} \qquad (D.57)$$

Equation (D.57) is expanded as a Taylor series in powers of the time-step and the coefficients of the series are found by differentiating Equation (D.57) the appropriate number of times and evaluating the results at the initial time. As it turns out, the first non-zero term in the velocity error for the Earth-Moon method is exactly the same as that for the Stumpff-Weiss method, Equation (C.46).

A similar procedure is used to find the position and velocity errors for the Moon-Earth method. The result for the position error is

$$\delta\bar{R}_{me}(h) = \frac{A\,a}{24\,(Rr\rho)^3_I}\,[3(I-3\bar{u}_R\bar{u}_R{}^T)(\rho^3\bar{r} + r^3\bar{\rho}) + (I-3\bar{u}_r\bar{u}_r{}^T)(\rho^3\bar{R} - R^3\bar{\rho})]_I\,h^4 + 0(h^5) \qquad (D.58)$$

If one notes that the assumptions made to derive the Earth-Moon and Moon-Earth methods have a certain symmetry with respect to the assumptions used for the Stumpff-Weiss method, the above result could have been guessed by inspecting the form of Equations (C.44) and (D.55). The velocity error for the Moon-Earth method is also the same as the velocity error for the Stumpff-Weiss method to third order.

LIST OF REFERENCES

1. Gobetz, F. W. and J. R. Doll, "A Survey of Impulsive Trajectories", AIAA Journal, Vol. 7, No. 5, May 1969.

2. Lion, P. M. and Handelsman, M., "Primer Vector on Fixed Time Impulsive Trajectories", AIAA Journal, Vol. 6, No. 1, Jan. 1968.

3. Jezewski, D. J. and H. L. Rozendaal, "An Efficient Method for Calculating Optimal Free-Space N-Impulse Trajectories", AIAA Journal, Vol. 6, No. 11, November 1968.

4. Gobetz, F. W. and Doll, J. R., "How to Open the Heliocentric Launch Window for Earth-Mars Orbiter Missions", Journal of Spacecraft and Rockets, Vol. 6, No. 4, April, 1969.

5. Egorov, V. A., "Certain Problems of Moon Flight Dynamics", Russian Literature on Satellites, Part I, International Physical Index, Inc., New York 1958.

6. Breakwell, J. V. and Perko, L. M., "Matched Asymptotic Expansions, Patched Conics and the Computation of Interplanetary Trajectories", Progress in Astronautics and Aeronautics - Vol. 17, Academic Press, New York, 1966.

7. Lagerstrom, P. A. and Kevorkian, J., "Earth-to-Moon Trajectories in the Restricted Three-Body Problem", J. Mecanique, Vol. 2, No. 2, June 1963.

8. Lancaster, J. E. and R. A. Allemann, "Numerical Analysis of the Asymptotic Two-Point Boundary Value Solution for N-Body Trajectories", AIAA Preprint 72-49, Jan. 1972.

9. "Final Report for Lunar Libration Point Flight Dynamics Study", General Electric Co., NASA Contract NAS-5-11551, April 1969.

10. Edelbaum, T. N., "Libration Point Rendezvous", Analytical Mechanics Associates Report No. 70-12, February 1970.

11. Farquhar, R. W., "The Utilization of Halo Orbits in Advanced Lunar Operations", NASA TND-6365, July 1971.

12. Szebehely, V., Theory of Orbits, Academic Press, New York, 1967.

13. Czuchry, A. J. and Pitkin, E. T., "Regularization vs Step-Size Regulators in Optimal Trajectory Computation", Journal of Spacecraft and Rockets, Vol. 7, No. 7, July, 1970.

14. Stumpff, K. and Weiss, E. H., "Applications of an N-Body Reference Orbit", Journal of the Astronautical Sciences, Vol. 15, No. 5, Sept - Oct 1968.

15. Wilson, S. W., "A Pseudostate Theory for the Approximation of Three-Body Trajectories", AIAA Paper 70-1061, August 1970.

16. Byrnes, D. V. and Hooper, H. L., "Multiconic: A Fast and Accurate Method of Computing Space Flight Trajectories", AIAA Paper 70-1062, August, 1970.

17. Weiss, E. H., "A New Method for Computing the State Transition Matrix", Journal of the Astronautical Sciences, Vol. 16, No. 3, May - June, 1969.

18. Fang, T. C., "A Fast Method of Spacecraft Trajectory Computation in N-Body Inverse Square Force Fields", Paper presented at AAS-AIAA Astrodynamics Conference, Fort Lauderdale, August 1971.

19. Lawden, D. F., Optimal Trajectories for Space Navigation, Butterworths, London, 1963.

20. Jacobson, D. and Oksman, W., "An Algorithm that Minimizes Homogeneous Functions of N Variables in N+2 Iterations and Rapidly Minimizes General Functions", Harvard University, Div. of Engineering and Applied Physics, Tech. Report No. 618, Oct. 1970.

21. Miele, A., "Theorem of Image Trajectories in the Earth-Moon Space", Astronautica Acta, Vol. 6, 1960.

22. Lion, P. M., "Sufficient Conditions for Optimal Fixed-Time Impulsive Trajectories", presented at the 18th International Congress, Belgrade, September 1967.

23. Sconzo, P., LeSchack, A. R., and Tobey, R., "Symbolic Computation of f and g Series by Computer", The Astronomical Journal, Vol. 70, No. 4, May 1965.

24. Edelbaum, T. N. and Pines, S., "The Fifth and Sixth Integrals for Optimum Rocket Trajectories in a Central Force Field", AIAA Paper 69-904, August 1969.

25. Moyer, H. G., "Integrals for Impulsive Orbit Transfer from Noether's Theorem", Grumman Research Department Report RE-363J, March 1969.

BIOGRAPHICAL SKETCH

Louis Anthony D'Amario was born in Providence, Rhode Island on January 5, 1947. He received his early education at public schools in Providence and graduated from Classical High School in 1964. Mr. D'Amario entered Rensselaer Polytechnic Institute in 1964 as an undergraduate and received his Bachelor of Science Degree in Aeronautical Engineering in 1968. Having enrolled in the graduate school of the Massachusetts Institute of Technology in 1968, Mr. D'Amario was granted the Master of Science degree in Aeronautics and Astronautics in 1970. His Master's thesis was in the field of guidance and navigation of space vehicles. Since 1969, Mr. D'Amario has been pursuing his doctoral program in the Department of Aeronautics and Astronautics at M. I. T.

During the 1970-71 academic year, Mr. D'Amario left the Institute to travel and then worked for 8 months as a Staff Engineer at the M. I. T. Charles Stark Draper Laboratory. While attending graduate school at M. I. T., Mr. D'Amario has been a Research Assistant at the M. I. T. Measurement Systems Laboratory and the M. I. T. Charles Stark Draper Laboratory. He has also been a Summer Staff member at the Draper Laboratory. Mr. D'Amario has co-authored two papers on three-body trajectory analysis with Mr. Theodore Edelbaum of the Draper Laboratory.

Mr. D'Amario is a member of the Tau Beta Pi and Sigma Gamma Tau honorary societies and is also a student member of the American Institute of Aeronautics and Astronautics. He was awarded a Lockheed Fellowship for the academic year 1968-69.